



Elias Dias Rossi Lopes

**Advanced Estimation and Control Applied to
Vehicle Dynamic Systems**

Tese de Doutorado

Thesis presented to the Programa de Pós-graduação em Engenharia Mecânica, do Departamento de Engenharia Mecânica da PUC-Rio in partial fulfillment of the requirements for the degree of Doutor em Engenharia Mecânica.

Advisor: Prof. Helon Vicente Hultmann Ayala

Rio de Janeiro
March 2022



Elias Dias Rossi Lopes

Advanced Estimation and Control Applied to Vehicle Dynamic Systems

Thesis presented to the Programa de Pós-graduação em Engenharia Mecânica da PUC-Rio in partial fulfillment of the requirements for the degree of Doutor em Engenharia Mecânica. Approved by the Examination Committee:

Prof. Helon Vicente Hultmann Ayala

Advisor

Departamento de Engenharia Mecânica – PUC-Rio

Prof. Marco Antônio Meggiolaro

Departamento de Engenharia Mecânica – PUC-Rio

Prof. Mauro Speranza Neto

Departamento de Engenharia Mecânica – PUC-Rio

Prof. Leandro dos Santos Coelho

PUCPR / UFPR

Prof. Gustavo Simão Rodrigues

IME

Rio de Janeiro, March 9th, 2022

All rights reserved.

Elias Dias Rossi Lopes

Holds a master's degree in Mechanical Engineering (2015) and a bachelor's degree in Mechanical and Weaponry Engineering (2009), both from the Military Institute of Engineering.

Bibliographic data

Lopes, Elias Dias Rossi

Advanced Estimation and Control Applied to Vehicle Dynamic Systems / Elias Dias Rossi Lopes; advisor: Helon Vicente Hultmann Ayala. – 2022.

142 f: il. color. ; 30 cm

Tese (doutorado) - Pontifícia Universidade Católica do Rio de Janeiro, Departamento de Engenharia Mecânica, 2022.

Inclui bibliografia

1. Engenharia Mecânica – Teses. 2. Identificação de Sistemas. 3. Dinâmica de Veículos. 4. Veículos Elétricos. 5. Estimação de Estados de Horizonte Móvel. 6. Controle Preditivo baseado em Modelo. I. Ayala, Helon V. H.. II. Pontifícia Universidade Católica do Rio de Janeiro. Departamento de Engenharia Mecânica. III. Título.

CDD: 621

To my daughter Laura, who encouraged me throughout this research and arrived to illuminate its conclusion.

Acknowledgments

To God, author of life, for all the strength, health and inspiration to carry out this work.

To my beloved wife Elisa, for her company over the last 10 years and for her patience and understanding during the development of this thesis.

To my parents Mariluce and Danilo, my brother Silas and my sister Elisa, whose support and love are essential throughout my life.

To my advisor Prof. Helon Ayala, for the precise and pragmatic guidance, which was fundamental for the conclusion of this thesis under the conditions that I had to fulfill.

To the Brazilian Army, for the opportunity of this course and to my colleagues at the Military Institute of Engineering, for their friendship over these years.

To PUC-Rio and the Department of Mechanical Engineering, for all administrative and technical support.

This study was financed in part by the Coordenação de Aperfeiçoamento de Pessoal de Nível Superior - Brasil (CAPES) - Finance Code 001

Abstract

Lopes, Elias Dias Rossi; Ayala, Helon V. H. (Advisor). **Advanced Estimation and Control Applied to Vehicle Dynamic Systems**. Rio de Janeiro, 2022. 142p. Tese de Doutorado – Departamento de Engenharia Mecânica, Pontifícia Universidade Católica do Rio de Janeiro.

The rising demand of autonomous and intelligent transportation systems requires the development of advanced control and estimation techniques, aiming to ensure safety and efficient operations. Due to the nonlinear nature of vehicle dynamics and its characteristic phenomena, classical estimation and control methods may not achieve adequate results, which encourages the research of novel algorithms. By some contributions, the first part of this work deals with estimation algorithms, both for identification of time invariant parameters and for estimation of states and time varying parameters. Special emphasis is given to Moving-Horizon State Estimation (MHSE), which is presented to be robust and accurate, due to the constrained optimization problem on which it is based. This algorithm is evaluated in vehicle longitudinal dynamics, for slip and tire-road friction estimation. Despite its efficiency, the high computational cost makes it necessary to search for suboptimal alternatives, and the employ of a Neural Networks that maps the optimization results is a promising solution, which is treated as Neural Networks Moving-Horizon Estimation (NNMHE). The NNMHE is evaluated on a state-of-charge (SOC) estimation of batteries for electric vehicles, demonstrating, through experimental data, that the NNMHE emulates accurately the optimization problem, and the literature indicates its effectively application on embedded hardware. Finally, a contribution about Nonlinear Model-based Predictive Control (NMPC) is presented. It is proposed and evaluated its use compounding a novel hierarchical control framework for electric vehicles with independent in-wheel motors, through which it is possible to adequately control the vehicle on velocity and path tracking tasks, with reduced computational effort. The control is evaluated using experimental obtained tire data, which approaches the simulation to real situations.

Keywords

System Identification; Vehicle Dynamics; Electric Vehicles; Moving-Horizon State Estimation; Model-based Predictive Control.

Resumo

Lopes, Elias Dias Rossi; Ayala, Helon V. H.. **Estimação e Controle Avançados Aplicados a Sistemas Dinâmicos Veiculares**. Rio de Janeiro, 2022. 142p. Tese de Doutorado – Departamento de Engenharia Mecânica, Pontifícia Universidade Católica do Rio de Janeiro.

A crescente demanda por sistemas de transporte autônomos e inteligentes exige o desenvolvimento de técnicas avançadas de controle e estimativa, visando garantir operações seguras e eficientes. Devido à natureza não linear da dinâmica veicular e seus fenômenos característicos, os métodos clássicos de estimativa e controle podem não alcançar resultados adequados, o que incentiva a pesquisa de novos algoritmos. Por algumas contribuições, a primeira parte deste trabalho trata de algoritmos de estimação, tanto para identificação de parâmetros invariantes no tempo, quanto para estimação de estados e parâmetros variantes no tempo. Especial destaque é dado aos algoritmos de Estimação de Estados por Horizonte Móvel (MHSE), que se apresenta como robusto e preciso, devido ao problema de otimização com restrição em que se baseia. Este algoritmo é avaliado em dinâmica longitudinal de veículos, para estimativa de deslizamento longitudinal e coeficiente de atrito pneu-estrada. Apesar de sua eficiência, o alto custo computacional torna necessária a busca por alternativas sub-ótimas, e o emprego de Redes Neurais que mapeiam os resultados da otimização é uma solução promissora, que é tratada como Estimação por Horizonte Móvel com Redes Neurais (NNMHE). O NNMHE é avaliado em uma estimativa do estado de carga (SOC) de baterias para veículos elétricos, demonstrando, através de dados experimentais, que o NNMHE emula com precisão o problema de otimização e a literatura indica sua aplicação efetiva em *hardwares* embarcados. Por fim, é apresentada uma contribuição sobre o controle preditivo baseado em modelo não linear (NMPC). É proposto e avaliado seu uso compondo uma nova estrutura de controle hierárquica para veículos elétricos com motores independentes nas rodas, através do qual é possível controlar adequadamente o veículo em tarefas de rastreamento de velocidade e trajetória, com reduzido esforço computacional. O controle é avaliado usando dados experimentais de pneus obtidos, que aproximam a simulação de situações reais.

Palavras-chave

Identificação de Sistemas; Dinâmica de Veículos; Veículos Elétricos; Estimação de Estados de Horizonte Móvel; Controle Preditivo baseado em Modelo.

Table of Contents

I	Preliminaries	16
1	Introduction	17
1.1	Objectives	21
1.2	Document Organization	22
2	Related Works and Originality Claims	23
2.1	Critical Literature Review	23
2.2	Contributions	37
II	Theoretical Background	41
3	Dynamic Models	42
3.1	Tire Efforts on Planar Vehicle Dynamics	42
3.2	Planar Vehicle Dynamics	44
3.3	Quarter-car Model - Longitudinal Dynamics	46
3.4	Single-Track Model - Coupled Longitudinal and Lateral Dynamics	47
3.5	Equivalent Battery Model	48
3.6	Landing Gear System	50
4	Estimation Methods	52
4.1	Grey-box Time Invariant Parameters Estimation Algorithm	52
4.2	Kalman Filter Nonlinear Estimation Methods	54
4.3	Moving-Horizon State Estimation	57
4.4	Neural Network Moving-Horizon Estimation	59
4.5	Evaluation Metrics	60
5	Model-based Predictive Control	62
5.1	MPC formulation	62
5.2	Constrained Optimization Problems	64
5.3	Computational Algorithm	66
III	Contributions	67
6	Nonlinear Grey-box Identification of a Landing Gear based on Drop Test Data	68
6.1	Problem Definition	68
6.2	Drop Test Simulations	69
6.3	Results	69
6.4	Discussion	73
7	Comparison of Nonlinear Receding-Horizon and Kalman Filter Strategies for Ground Vehicles Longitudinal Slip Estimation	75

7.1	Problem Definition	75
7.2	Simulation and Results	76
7.3	Discussion	79
8	Tire-road Friction Coefficient Estimation Using Nonlinear Receding-Horizon and Kalman Filter Strategies	81
8.1	Problem Definition	81
8.2	Dataset Description	82
8.3	Proposed Approach	83
8.4	Results	84
9	Nonlinear Receding-horizon Filter Approximation with Neural Networks for Fast State of Charge Estimation of Lithium-Ion Batteries	93
9.1	Problem Definition	93
9.2	Dataset Description	94
9.3	Proposed Approach	94
9.4	Results	96
9.5	Discussion	102
10	Hierarchical Nonlinear Model Predictive Control for Path Tracking of In-Wheel Motor Drive Electric Vehicles	103
10.1	Dataset Description and Parameters Estimation	103
10.2	Hierarchical Framework for EV Control	104
10.3	Results	107
10.4	Discussion	112
IV	Final Remarks	115
11	Conclusions	116
12	Future Works	118
	Bibliography	121

List of Figures

Figure 1.1	In-Wheel Motor Drive Electric Vehicle Model.	19
Figure 3.1	Tire frame and angles.	43
Figure 3.2	IWMD-EV dynamics.	45
Figure 3.3	Quarter-car Model.	46
Figure 3.4	Single-Track Model.	47
Figure 3.5	Equivalent circuit model of lithium-ion battery.	48
Figure 3.6	Landing gear model.	50
Figure 4.1	MHSE strategy.	57
Figure 5.1	MPC strategy.	62
Figure 6.1	Vertical displacement of the sprung mass.	70
Figure 6.2	Vertical velocity of the sprung mass.	70
Figure 6.3	Angle of the structure of landing gear.	71
Figure 6.4	Comparison between measured and estimated angle.	74
Figure 7.1	Estimated wheel rotation (rad/s).	77
Figure 7.2	Estimated longitudinal slip.	78
Figure 7.3	Estimated longitudinal slip, in detail.	78
Figure 7.4	RMSE(t) for measurement noise of 0.1%.	79
Figure 7.5	RMSE(t) for measurement noise of 5%.	80
Figure 8.1	Schematic Model of the Vehicle.	82
Figure 8.2	Longitudinal velocity of the vehicle (m/s).	83
Figure 8.3	Current at electric motors (A).	83
Figure 8.4	Peak value of coefficient of adherence (μ_p , dimensionless).	86
Figure 8.5	Longitudinal slip of the wheel 4.	87
Figure 8.6	RMSE(t) of estimation of longitudinal velocity (dB).	90
Figure 8.7	RMSE(t) of estimation of angular velocity (dB).	91
Figure 8.8	Estimated value of coefficient of adherence.	91
Figure 9.1	Electrical current measured on battery, in A.	94
Figure 9.2	Voltage on battery terminals, in V.	95
Figure 9.3	Polynomial fitting of OCV-SOC.	96
Figure 9.4	Flowchart of NNMHE.	100
Figure 9.5	Estimation of the SOC, with experimental data.	101
Figure 9.6	R^2 for SOC estimated by NNMHE.	101
Figure 10.1	Available experimental data about longitudinal force.	104
Figure 10.2	Fitted curve for longitudinal friction coefficient.	105
Figure 10.3	Proposed Hierarchical Framework.	106
Figure 10.4	Stable and unstable regions of tire curve.	107
Figure 10.5	Vehicle velocity for NMPC and HMPC.	108
Figure 10.6	Vehicle velocity for NMPC and HMPC.	109
Figure 10.7	Longitudinal slip for NMPC and HMPC.	109

Figure 10.8 Processing Times, in seconds, for NMPC and HMPC.	110
Figure 10.9 Torque defined by NMPC and HMPC.	110
Figure 10.10 Path tracking results comparison.	111
Figure 10.11 Longitudinal velocity of the vehicle.	112
Figure 10.12 Yaw angle of the vehicle.	112
Figure 10.13 Reference and real wheel angular velocities.	113
Figure 10.14 Reference and real steering angles.	113

List of Tables

Table 6.1	Estimation results without measurement noise.	72
Table 6.2	Estimation results with measurement noise of 0.1%.	73
Table 6.3	Estimation results with measurement noise of 1.0%.	73
Table 7.1	RMSE results with well-known initial conditions.	77
Table 7.2	ARMSE analysis for longitudinal slip (λ) estimation.	79
Table 7.3	Mean time for simulation (s).	80
Table 8.1	Vehicle Parameters.	84
Table 8.2	ARMSE results for simulated data, considering no noise.	87
Table 8.3	ARMSE analysis for friction coefficient (μ_p) estimation.	88
Table 8.4	Mean time for sample on simulations (s).	88
Table 9.1	Parameters for polynomial fitting of OCV-SOC.	96
Table 9.2	Results for simulated data.	98
Table 9.3	ARMSE analysis results.	99
Table 9.4	Validation results of the ANN trained with MHSE.	101
Table 10.1	Identified tire parameters.	105
Table 10.2	Description of the symbols used on the framework.	106

List of Abbreviations

ANN – Artificial Neural Network
ARMSE – Asymptotic Root Mean Square Error
AV – Autonomous Vehicles
BMS – Battery Management System
CKF – Cubature Kalman Filter
DOF – Degrees of Freedom
ECM – Equivalent Circuit Model
EKF – Extended Kalman Filter
EV – Electric Vehicles
FPGA – Field Programmable Gate Array
GA – Genetic Algorithm
GNSS – Global Navigation Satellite System
HEV – Hybrid Electric Vehicles
HIL – Hardware-in-the-loop
ICE – Internal Combustion Engine
IMU – Inertial Measurement Unit
IWMD-EV – In-Wheel Motor Drive Electric Vehicle
KF – Kalman Filter
LQR – Linear Quadratic Regulator
LS – Least Squares
LSTM – Long Short-Term Memory
MHE – Moving Horizon Estimation
MHSE – Moving Horizon State Estimation
MPC – Model-based Predictive Control
NARX – Nonlinear Auto-Regressive with Exogenous Inputs

NMPC – Nonlinear Model-based Predictive Control
NN – Neural Network
NNMHE – Neural Network Moving-Horizon Estimation
OCV – Open-Circuit Voltage
PEV – Pure Electric Vehicles
PID – Proportional–Integral–Derivative
PSO – Particle Swarm Optimization
R2 – Coefficient of Determination
RLS – Recursive Least Squares
RMSE – Root Mean Square Error
RNN – Recursive Neural Network
SOC – State of Charge
SOH – State of Health
SVM – Support Vector Machine
UKF – Unscented Kalman Filter

*For I know the thoughts that I think toward
you, says the Lord, thoughts of peace and not
of evil, to give you a future and a hope.*

Jeremiah, 29:11.

Part I

Preliminaries

1 Introduction

There is a growing interest from researchers in Electric Vehicles (EV). This research trend has increased more than 10 times in the last decade [1]. The main objective of this broad subject is to develop technologies aiming at decreasing emissions of greenhouse gases and air pollution, and the reduction of the use of fossil fuels, in favor of renewable sources of energy [2]. Research has many themes, from charging infrastructure to psychological aspects, including, evidently, vehicle design and technology. This trend is relevant both for passenger and commercial vehicles [3], about its high possible demand and actual employment in European Union.

There are different configurations of EV [2], and we may, firstly, distinguish hybrid and pure electric ones. In pure electric vehicles (PEV), batteries are the only source of energy, and they are characterized by fast and smooth acceleration and no emission of polluting gases. In most of these vehicles, known as Plug-in EV, batteries may be recharged by external power sources, which constitutes a challenge in future infrastructure projects [4, 5]. Alternative energy sources for pure electric vehicles are fuel cells, photovoltaic cells and regenerative braking systems [4].

Hybrid electric vehicles (HEV) present both internal combustion engines (ICE) and electric motors and these sources may be mounted in series, parallel or combined configurations. In Series HEV, the vehicle is powered mainly by the electric motor and fuel energy is used to move the motor, recharge the battery pack and drive an electric generator, so that the ICE works at optimum speed, reducing emissions and fuel consumption. Parallel HEVs are powered both by an electric motor and an internal combustion engine, and each one may be individually triggered, depending on the operation mode and conditions. Among Parallel HEVs, there is, also, a combined version, in which the electric motor, the ICE, the electric generator and the wheels are linked by mechanical devices, such as planetary gear sets, so that both work simultaneously. HEV may have as an energy source only the fuel or, may be plug-in vehicles. In these cases, they are called Plug-in HEV or Extended-Range EV.

All EV kinds are hardly dependent on an efficient Battery Management System (BMS), which is one of the most challenging research themes in this

field, since it is critically related to the autonomy of EVs and, therefore, to the practical use of these vehicles. One of the tasks performed by the BMS is the estimation of the State of Charge (SOC) of the batteries, which must be done using filtering algorithms, since it is not directly measurable [6]. This variable is important to indicate the status of the battery for the sole purpose of monitoring, but it may also be used as input for the traction controller or charging stations in the context of smart grids [7]. For example, it is possible to define control laws with optimized SOC preservation or recharging using economical model predictive control [8, 9]. As SOC is nonlinearly related to current input and must be indirectly estimated on an unknown time-varying battery, it is nontrivial to operate even a single one in charging/discharging scenarios [10]. The case of many EV batteries and varying electricity prices are even a bigger challenge to solve from both user and utility service points of view [11, 12]. SOC estimation is thus an important issue and doing that accurately and online using limited computational resources is difficult.

It is important to remark that most versions of previous kinds of EV, are equipped with central power sources, so that axles, inter-axle differentials and Ackermann steering mechanisms are needed. In recent developments, In-Wheel Motor Drive Electric Vehicles (IWMD-EV) are proposed for vehicle motion and steering. In this configuration, two or more wheels have torque and steering angle independently controlled. Each motion wheel has a motor in its hub, so that all driveshafts, differentials, gearboxes and gear sets are expendables.

Murata [13] remarks that IWMD-EV has faster response, precise torque generation, the capability of both forward and reverse torque generation and is not affected by limitations imposed by low natural frequencies of driveshafts. Besides that, it may be used in driving, turning, stopping and other driving conditions. Consequently, a vehicle with IWMD-EV (details in Figure 1.1) presents more control possibilities, since it has more degrees of freedom (DOF), when compared with conventional designs. This is important to achieve better results, even under many requirements and constraints to control law.

Some researches on EV also comprise autonomous vehicles (AV) subject, which is a fertile field of research [14, 15], and may include estimation and control tasks.

Nonlinear observers are usually implemented on many vehicular applications, especially those related to tire dynamics, such as traction, braking, and stability control systems. Some tire states are non directly measurable, such as longitudinal slip and side-slip angle, as well as model parameters, such as friction coefficient and cornering stiffness, which are difficult to be accurately

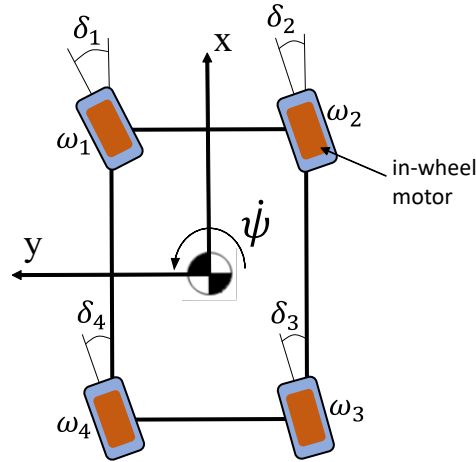


Figure 1.1: In-Wheel Motor Drive Electric Vehicle Model. This vehicle has more degrees of freedom, since the wheels have independent angular velocities (ω_i) and steering angles (δ_i).

defined and may change due to road conditions. Moreover, correctly inferring the friction-related parameters linked to tire and soil interaction is necessary for optimal and safe performance of ground vehicles. Such issue is important for lateral and longitudinal dynamics for agile and critical operation, as well as with yaw and roll rates.

For intelligent and autonomous vehicles, the accurate determination of these parameters also affects the efficiency of control laws, specially Model-based Predictive Control (MPC) ones, since tasks such as path tracking and controlled anti-lock braking depend on accurate system models. In these and other MPC applications for autonomous navigation, it is useful to estimate friction parameters in each sample, so that a current value is used on the MPC optimization algorithm. In these cases, the use of state and parameter nonlinear observers becomes necessary. The authors of [16] remark the importance of the peak value of the adherence coefficient between tire and road for controlling motion, path planning, and path tracking of intelligent vehicles, as they are related to the maximum adhesion operating envelope.

The implementation of nonlinear observers is the focus of many studies, but their effectiveness depends on the specificities of each nonlinear dynamic model and there are many classical techniques already defined [17]. Using the state-space formalism, Kalman Filter (KF) is among the most known and used, such as appointed by [18]. For nonlinear estimation, two approaches are remarked [17]: the Extended Kalman Filter (EKF) and the Unscented Kalman Filter (UKF), which are comprehensively studied in the literature, especially the first algorithm [19–21].

Recently, optimization-based methods have been developed, looking for robustness and accuracy [22], namely, Moving Horizon State Estimation (MHSE), in which states are estimated using a constrained optimization problem, that takes into account the model dynamic equations and a defined horizon of recent information and output measures. This algorithm is cited in the literature as robust and powerful, even for systems with model uncertainties, numerical errors, and noisy measures [22]. The author of [23] evaluates this algorithm in many applications so that it is possible to understand its capacities and robustness. It is also demonstrated that MHSE may provide flexibility for the estimator design, through alternative versions of the algorithm [24]. Despite such features, MHSE has been little explored in the context of friction estimation. We are therefore motivated to use it here, as we shall describe next after the state-of-the-art review.

Estimation methods are also important for BMS, especially for SOC monitoring. As batteries dynamics are commonly defined by Equivalent Circuit Models (ECM), SOC estimation usually also requires parameter identification, which many works treat as a separate task in the estimation process [25–33]. For this purpose, many algorithms and techniques have been proposed, among which the KF and Least Squares (LS) are the most widely adopted for this application [6]. As well as the previous case, the EKF is largely explored for SOC estimation, due to its simpler implementation and reduced processing time [34–41].

However, many advanced techniques, such as MHSE, have the potential to be applied to this task, even for simultaneous estimation of states and parameters, through an augmented states formulation of the dynamical model. Despite presenting optimal results, the MHSE computational effort is considerably higher when compared to Kalman-based approaches, as it involves the resolution of a nonlinear optimization problem at each sampling step. Nonetheless, approximate solutions obtained by offline trained Artificial Neural Networks (ANN) may provide adequate results with low processing time [42], showing that machine learning may be employed to approximate the state estimation task with a Neural Network Moving-Horizon Estimation (NNMHE). In the literature review presented in the following chapter, it is evidenced that the receding-horizon algorithms are not evaluated for simultaneous estimations of states and parameters on battery systems for electric vehicles.

Regarding advanced control, optimal control techniques, among which the Model-based Predictive Control (MPC), or its nonlinear version (NMPC), are potentially evaluated, as a response to the increasing demand of different levels of automation on vehicles. As a dual of MHSE, the MPC is a constrained

optimization problem and, consequently, is characterized as flexible, robust and accurate [43], since we may consider many states and situations on the cost function. Besides that, as it is predictive, its answer trends to be faster than reactive techniques.

In vehicle control, many objectives may be achieved with MPC, such as slip control [44, 45], path tracking [44, 46, 47], stability [44, 47, 48], feasible regions [46] and safety [45, 47, 48], which denotes the flexibility of this control technique. Even though, MPC applications are not always feasible, due to the high processing time that may be required. As a possible solution, hierarchical frameworks may be used [49, 50], which may be designed properly to enable online applications.

1.1 Objectives

The general objective of this thesis is to present five contributions regarding advanced control and estimation of ground and aircraft vehicle systems. The specific objectives of the presented contributions are:

- Contribution 1: Present a nonlinear identification methodology for a four degree of freedom landing gear model that includes the gear walk phenomenon;
- Contribution 2: Evaluate the performance of EKF, UKF and MHSE for state estimation of nonlinear systems, which is analyzed on slip estimation of a ground vehicle during traction and braking processes, which is characterized by nonlinear and discontinuity efforts. Moreover, their limitations and advantages are presented, aiming at future control applications on autonomous vehicles;
- Contribution 3: Compare three nonlinear observers, namely EKF, UKF and MHSE, for simultaneous states and friction coefficient estimation of an EV with independent in-wheel motors. These observers are studied to be used on MPC algorithms for EV path tracking and handling control, in which a correct and current value of friction coefficient is essential for optimizing the vehicle performance. The observers are evaluated with simulated and experimental data;
- Contribution 4: Present receding-horizon observers for SOC estimation of lithium-ion batteries. The first strategy presented is the MHSE, which is presented to be powerful enough to estimate states and parameters of an equivalent circuit model through an augmented states formulation. Its results are proposed to be used in the training of the NNMHE,

which employs the receding-horizon information to predict the SOC of the battery;

- Contribution 5: Evaluate a novel framework, in which the MPC is performed using only the rigid-body dynamics of the vehicle chassis, aiming to define the reference forces on the body frame, which are used to establish references to wheel angular velocities and steering angles through mathematical models of the tire forces.

1.2

Document Organization

The remainder of this thesis document is organized as follows. The first part is dedicated to exposing the context, motivation, literature review and contributions of the thesis. In the second part, the theoretical background is presented, in which we describe the vehicle dynamic systems models employed in the proposed contributions. Besides that, the algorithms for states and parameters estimation and the MPC optimization problem are described, with details for their implementation, as used in this work. In the third part, the contributions of the thesis are exposed, with the details inherent to each one, such as the specific problem definition, the results and a discussion about them. In the last part, the conclusions of the thesis are discussed, as well as the possible future research that may be executed using the knowledge developed in this work.

2

Related Works and Originality Claims

This chapter is dedicated to presenting and discussing recent research related to this work. For each objective mentioned in section 1.1, a literature review is presented, with a critical analysis of the research gaps and the relevance of the issue in the related field. Afterward, the original contributions of this thesis are presented in the later section, respecting each of the objectives.

2.1

Critical Literature Review

The critical literature review is divided according to the objectives listed in Section 1.1 and at the end of each subsection, a critical analysis is presented.

2.1.1

Grey-box Identification of Time Invariant Parameters

For a robust design for antiskid control of aircraft brake systems, the gear walk phenomenon must be considered, since the estimation of braking force depends on the angular velocity of the wheel and the velocity of the wheel hub. Pritchard [51] remarks on the relevance of the study of the dynamics of landing gear, mainly due to the effects of vibration and shimmy induced by braking, highlighting its criticality on aircraft safety. Krüger et al. [52] give a complete review of landing gear requirements and operational conditions. They describe the drop test and remark on its importance to analyze the stiffness and inertial of each element, to evaluate the behavior of the shock absorber and of the wheel and tire. Sinou et al. [53] study an experimental approach of friction-induced vibration on aircraft brake, remarking the number of researches on this subject. Luo and Zhao [54] propose a spatial landing gear mechanism to achieve higher stiffness and higher strength, demonstrating that these properties are closely dependent on the geometry and the constraints between the bodies.

We may observe many studies that are dedicated to understanding the dynamics of landing gears and improving their performance, since it is a critical system for aircraft security [52]. Moreover, the physical phenomena involving the tires have important effects on the system dynamics and they must be considered in developed models. Van Slagmaat [55] develops a nonlinear model

for landing gear simulation, using the magic formula for tire dynamics. Yadav and Singh [56] present an optimal anti-skid braking control based on a one-step-ahead prediction of the braking force required, aiming to reduce the landing run. Gualdi et al. [57] feature a multi-body landing gear model, demonstrating the effect of gear walk, to be employed as a design tool for anti-skid landing gear braking control. D'Avico et al. [58] presents a control-oriented model of landing gear, using the Burckhardt tire model for determining the braking forces. This model is validated experimentally, as presented in [59]. The suppression of gear walk phenomenon is studied by Yin et al. [60], who propose an anti-skid control that minimizes the maximum gear walk angle, satisfying other constraints. Jiao et al. [61] propose an anti-skid brake control with the identification of the runway characteristics and the tire conditions, so that it is possible to estimate the maximum friction force. They obtain, as result, a considerable improvement in the braking efficiency when compared to algorithms based only on wheel deceleration. Chen et al. [62] present an improved braking control algorithm, which considers both the wheel deceleration and longitudinal slip, to enhance the robustness and the efficiency of the braking process. Tourajizadeh and Zare [63] propose a robust and optimal nonlinear control of shimmy vibration, remarking on the importance of minimizing this vibration on aircraft performance and security. Somakumar and Chandrasekhar [64] propose an intelligent anti-skid brake controller based on a neural network, with learning, nonlinear mapping and pattern-recognition abilities. It defines the brake torque after analyzing the runway condition, so that the braking is optimum.

The design of a landing gear is evaluated on many tests, among which there is the drop test. It consists in lifting the landing gear in a specific testbed and dropping it from a height that will cause a desired impact velocity. Among the measurements commonly made, the horizontal force is very important as it affects directly the gear walk phenomenon [65]. Xue et al. [66] present a method of optimizing the damper coefficient of an amphibious landing gear by means of simulation and drop test, which illustrates the large application of this test on aircraft design. Shixing et al. [67] study a drop test of a landing gear with a magneto-rheological (MR) fluid damper, assessing the influence of this component on the dynamics and performance of the landing gear. This kind of damper is also the focus of Li et al. [68], who present a MR damper structure for landing gear, commenting on its main advantages, such as adjustable damping force, simple structure and independence of external energy. Wei et al. [69] develop a more complex model for landing gear fall dynamics. The model presented has two degrees of freedom and adds viscous friction and grip effects to the Coulomb friction model.

The drop test may also be used for evaluating the gear walk and predicting the structural stiffness and damping of the landing gear, by identification techniques. Fallah et al. [70] demonstrate the importance and influence of structural parameters in the design and control of vibrations on aircraft landing gears. This phenomenon is not considered on ground vehicles, because the braking forces are not of the same scale. The drop test measurement system is also the focus of some recent research, as presented by Pytka et al. [71]. They feature a dynamometer wheel for landing gear tests. The measurement system is designed for obtaining the vertical load and longitudinal forces acting in the wheel, as well as the moments around all the axes.

Batill and Bacarro [72] feature a nonlinear identification of a single degree of freedom of landing gear system, applying Newtonian Iteration. It considers the suspension and structure both linear and nonlinear, when is used the hydropneumatic damper on the airplane. The identification process of mechanisms is most explored in robotic systems. These methods are well explored by Wu et al. [73], who give an overview of dynamic parameter identification of serial and parallel robots, summarizing the main methods used and the advantages and disadvantages of each one. Oliviers and Campion [74] propose a methodology for parameters identification in a nonlinear model of a robot with flexible arms. So, both inertial and elastic parameters are estimated, and the kinematics must consider the displacements due to the flexibility of the bodies.

Díaz-Rodríguez et al. [75] present a methodology for dynamic parameters identification of a 3 degree of freedom (DOF) parallel robot. They explain that not all the parameters may be properly identified, and they apply the weighted least squares method for determining the relevant ones. This method is also used by Bahloul et al. [76] on an identified model for a 6-DOF industrial robot, based on the inverse dynamic equations. Gao et al. [77] present a parameter identification method based on Denavit-Hartenberg model, validated on a 6-DOF industrial robot. They suggest a modified least-squares algorithm, designed to minimize the residual movement uncertainties and the application of singular value decomposition for determining the parameters most relevant.

2.1.2

State Estimation of Vehicle and Tire Dynamics

In the context of state estimation on vehicle systems, the authors of [19] propose the use of EKF associated with Recursive Least Squares and Neural Networks in a methodology of estimation of road friction coefficient, which is a hardly obtaining parameter. Kayacan et al. [78] present a control strategy

for tracked field robots with receding horizon estimation and control (RHEC). The estimation algorithm is used to estimate states and parameters, and the receding horizon control is based on an adaptive system whose model is time-varying. Li et al. [79] present an EKF based estimator for sideslip angle for a vehicle stability control and the authors remark that its measure is complex and expensive, which justifies the estimation process. Sun et al. [80] apply a nonlinear observer for state estimation on an ABS, due to the nonlinearity of the friction force during brake.

Boada et al. [81] develop a new method for estimation of different states and parameters of a vehicle, using a constrained version of Kalman Filter to consider the physical limitations of the parameters. It is demonstrated by experimental results that the constraints are important to improve the accuracy of the algorithm. The authors of [82] present two torque estimation methods for vehicle engines, using a proper dynamical model and air mass flow rate and engine speed, which are measurable. In [83] a road slope and position estimator is presented, which inputs are GPS data and vehicle onboard sensors. The estimator proposed presents more accurate and reliable results, which is proven by experiments. Hsiao [84] proposes an observer-based control scheme for traction force, robust to variations in road conditions and uncertainties on tire models.

Nilsson et al. [85] study the problem of estimating the position and direction of a vehicle with a single camera since it is hardly dependent on image quality. So, the authors propose an estimator which combines onboard vehicle sensors and adjusted camera images, with a single-track model. Chen and Wang [86] remark on the importance of tire-road friction coefficient estimation for autonomous vehicle applications and present an observer which does not depend on longitudinal motion information and is properly associated with adaptive speed control. Singh et al. [87] remark that simpler stability control performs well in many situations, but it is improved when a tire-road friction estimator is associated with the control scheme. In this way, the authors present a method, in which is used frequency response of tire vibrations in the estimation algorithm. Hsu et al. [88] remark on the importance of knowledge of physical limits of parameters used on vehicle control, such as tire slip angle and maximum lateral force and propose a model-based estimation algorithm that estimates them using information from the applied steering torque.

Du et al. [89] construct a side-slip estimator based on a fuzzy system for lateral dynamics and the nonlinear Dugoff tire model, using measured yaw rate and estimated states. Li et al. [90] use the same tire model to propose a side-slip estimation algorithm robust to inaccurate tire parameters.

Recent research in vehicle control point to the increased use of electric in-wheel motors, which allows many control strategies and simpler configurations of electric vehicles. These devices allow to reduce mass and simplify transmission systems, which is favorable in electric and autonomous vehicles. Zhao and Liu [91] present a four degree-of-freedom nonlinear dynamical model of a four independent wheel electric vehicle, considering the measurements provided by modern sensors used on vehicles. An observer is associated with this model to estimate vehicle velocity and roll angle, since these variables must be controlled on stability control system. Feng et al. [92] present two estimation algorithms based on moving horizon methods. The observer is applied on a four wheels electric robotic platform under different friction conditions.

Jeon et al. [93] propose a real-time constrained Kalman filter algorithm for estimation of the three tire forces on vehicle tires, namely, vertical, longitudinal and lateral forces in mobile robots equipped with wheel encoders and navigation sensors. Tire forces in the estimation process are modeled by Magic Formula, an empirical model developed by Pacejka and Bakker [94]. Hong et al. [20] present an application of the Unscented Kalman Filter to the estimation of inertial parameters of vehicles, which may be not accurately determined in the design phase. Heidfeld et al. [21] applied the same algorithm in a state and tire slip estimation for an electric vehicle with four independent wheels.

Estimation algorithms are used also in path-tracking applications for autonomous vehicles. Brembeck [23] remarks that state-estimators for autonomous vehicles are even more challenging, since the complexity of models and applications rises over time. In this way, he presents a vehicle state observer to estimate position, yaw angle and their rates, with a focus on path following and he discusses the balance between model complexity and estimator performance. The author uses constrained versions of EKF and MHSE to better approximate the results to real data. Jalali et al. [95] present a model predictive control scheme for tracking yaw rate with small lateral velocity and tire slips. The proposed method controls lateral velocity by adjusting the reference yaw rate, which reduces the size of the model and computational complexity. They also present an estimation algorithm by means of vehicle kinematics and tire model.

The state estimation is possible only if the system is fully observable. The condition of observability of a system is characterized by the possibility of observing all state variables by means of the measurement variables, or yet, if two different sets of states are related to two different sets of measured variables [96]. The authors explore the observability of nonlinear systems,

presenting two sufficient conditions to prove it. Katriniok et al. [97] present an EKF estimation for longitudinal and lateral velocities and yaw rate. They also present an approach for evaluating local observability online and a virtual measurement variable for instants in which local observability is lost.

2.1.3

Friction Coefficient Estimation using MHSE

Vehicle state and parameter estimation has been the focus of much research currently and in the past, as it enables better control [98]. Adequate handling, in turn, is of great importance as it is related to safety and performance. This fact is even more prominent in autonomous vehicles [16, 99], as automation implies to aim toward an optimal operation. In [100], it is remarked that safety issues are a challenge for autonomous vehicle integration into roads, which makes important the surveillance of some variables which are not measurable, as the sideslip and roll angle of vehicles.

In this context, we provide a brief state-of-the-art review, focusing on the most recent content in the scope of vehicle state and parameter estimation found in the specialized literature. As the mathematical abstractions vary greatly concerning the type of maneuver, we try to elucidate the importance of each application of estimation theory case by case.

In the context of vehicle control and autonomous navigation, the authors of [18] present a comprehensive literature review about state estimation on tires and vehicles, denoting the importance that this subject gained in the last years research and remarking that LS and KF algorithms are most employed. In [101], the authors compare many different estimation algorithms, using EKF, NN, and Sliding Mode Observer, for different tire models, comparing their advantages and disadvantages. We may note that both studies do not present comparisons with MHSE, concluding that it is a novel approach to be evaluated.

The researches about the EKF have addressed both its classical formulation and adapted versions. The authors in [102] propose the use of a nonlinear state-space model with augmented states to estimate translation velocity and yaw rate together with vehicle inertial parameters based on a gyroscope and an accelerometer. The goal of the paper was to estimate the vehicle state and parameters in lateral motion, and thus longitudinal slip was not included in the formulation. The observability of the resulting system was proven with Lie derivatives and the augmented states formulation was validated with the application of a standard EKF in a simulation environment with double lane change and path following maneuvers.

In [103], the authors comment that treating some vehicle model parameters as time-invariant may lead to sub-optimal control since they are not exactly known. Therefore, they propose the application of EKF for simultaneous estimation of states and tire cornering stiffness and, then, remark that other nonlinear approaches may achieve better results. The authors of [104] use high fidelity simulations to tune and validate Kalman-based state estimation methods used for evaluating inertial parameters and road profiles.

The authors of [105] present a sideslip angle estimator employing a combination of NN and nonlinear KF approaches so that KF is fed by a previous estimation obtained by the first one. The purpose of this arrangement is to obtain also the uncertainty of the estimation, which is used for an adaptive definition of the measurement covariance matrix. In [106], the authors propose a sideslip angle estimator based on a kinematic model, using fused information from an inertial measurement unit (IMU) and global navigation satellite system (GNSS). In this case, an adaptive KF approach is used to estimate errors and, then, reduce noise influence on the obtained data.

A constraint version of KF is presented in [81], which considers the physical limitations of the parameters, demonstrating experimentally that it improves the accuracy of the algorithm. A novel KF approach is presented in [19], in which are associated EKF, RLS, and NN for tire-road friction coefficient estimation. In [107], a robust framework is proposed, based on Unknown Input Observer for tire-road friction estimation using indirect measurements for application on vehicle control. The obtained results are, then, better than those presented by the EKF estimator.

The authors in [108] remark on the challenges in the implementation of lane guidance control for heavy vehicles, due to uncertainties. The authors present an adaptive state and parameters estimator, developed from EKF so that it is possible to estimate time-varying parameters. For the control task, an H_∞ regulator is proposed, ensuring robustness, even under external disturbances.

The UKF has been also evaluated as an option for some kinds of nonlinear systems, especially when the unscented transformations may be more useful and applicable than the linearization. In [21], the authors present an UKF-based adaptive algorithm for vehicle and tire states estimation, for application on an electrical vehicle under variable road conditions. In their study, they apply the concept of local observability for ensuring the effectiveness of the observer. The authors of [109] evaluate in a simulation environment the application of an EKF/UKF based solution for estimating vehicle velocities, as well as uncertain parameters such as mass and friction using the TMeasy

model [110].

Among the reviewed papers, the MHSE is the less explored and presents a broad range of possible applications. The authors of [78] propose a control strategy for tracked field robots with receding horizon estimation and control. The estimation algorithm is used for estimating states and traction parameters, and the receding horizon control is based on an adaptive system whose model is time-varying. The model used is kinematic-based, and the estimated parameters are related to the effective velocity and yaw rate. In [111], moving horizon approaches are compared to UKF and the authors investigate the advantages of each one in states estimation tasks for longitudinal and lateral velocities, yaw rate, and yaw angle of a vehicle.

Some other techniques are also the focus of research. In [112], the authors propose a friction estimator based on load sensing bearing measurements and employing a combined slip tire model. The authors of [113] present a nonlinear reduced observer for estimation of road conditions and side-slip, which is applied to traction control and validated by simulations. Some studies also demonstrate the effective use of Fuzzy Systems [114] and ANN [115] for estimation of road conditions and vehicle states.

The authors of [116] present an algorithm for friction coefficient estimation based on tire efforts and kinematics measurements, which is experimentally validated. Its measured data is freely available so that other algorithms may be evaluated.

Based on the literature review, we may note that MHSE is not broadly studied in augmented states approaches for nonlinear estimation [18, 23, 101], with a few exceptions, such as [23, 111], that employ this approach for estimating states and [78] that use a kinematic model for estimation of the parameters that indicate effective velocity and yaw rate. So, any of them are focused on friction coefficient estimation.

Among the proposed estimation algorithms, EKF is the most studied for nonlinear systems [19, 102, 103, 108]. Meantime, as it is based on derivatives, we note that its application on friction effort systems may have its performance degraded since these systems are characterized by discontinuities on state equations and hence their Jacobians which should be evaluated at each state trajectory evolution on time.

The use of unscented transformations rather than Jacobians on UKF is an attempt of avoiding such discontinuities, but the literature review denotes that this approach is less explored on states and parameters estimation for vehicle control. The UKF application presented on [21] is limited to state estimation and the authors of [109] use a dual Kalman Filter framework for

states and friction coefficient estimation, indicating that its performance may be improved. We may also observe in the previous subsection that moving-horizon approaches are studied in a few researches, but it is also demonstrated its flexibility and the broad range of possible applications, which may lead us to understand that it may achieve good results for the estimation of vehicle dynamics states.

2.1.4

Receding-horizon Strategies for State of Charge Estimation of Lithium-ion Batteries

Due to growing interest in EV, SOC estimation on lithium-ion batteries has been the focus of many recent researches, aiming at higher effectiveness of the BMS. This is of great importance to improve the autonomy of EVs and the design of traction control laws with optimized energy consumption. Many papers present an equivalent Thévenin's model as a suitable solution for first principles modeling, since it has a simple structure and low complexity [6]. Despite its simplicity, ECM is proved to be an efficient approximation of many kinds of batteries [117], but it requires the identification of model parameters, in addition to SOC estimation, which may be performed offline or simultaneously.

The authors of [118] use a physics-based battery model, whose parameters must be calibrated before the application of an adaptive Cubature Kalman Filter (CKF) for SOC estimation. In [34] a lumped parameters model of the battery is proposed, considering the influence of ambient temperature, which can improve EKF based SOC estimation when compared to Thévenin's model. In [119] a fractional-order ECM is proposed for lithium-ion batteries and the authors demonstrate that it can improve SOC estimation. These works remark that a reliable mathematical model is important to ensure the overall accuracy of a BMS. To improve the reliability, the authors of [120] propose a modeling of the degradation of Li-ion batteries, which is evaluated by experimental tests.

Machine learning techniques have been also evaluated as solutions for black-box modeling of batteries, as presented in [121], whose research demonstrates the effectiveness of different machine learning models for both electrical and thermal effects on Li-ion batteries. The thermal effects on batteries are also the focus of the modeling presented in [122], which estimates and evaluates the heat dissipation of batteries.

The estimation of SOC is evaluated in some researches, which comprise improved versions of classical methods, namely LS [123], EKF [34], and UKF [124]. Specifically about EKF, some published papers focus on modified

versions, in order to overcome its shortcomings, such as tedious trial and error calibration and fine tune required by the method, by means of approaches with adaptive features [36, 37, 41], reduced parameters [38], fractional-order approaches [35, 40] or combined with other methods, such as UKF [125], CKF [126] and Support Vector Machines (SVM) [127].

Many researches employ KF-based improvements for state estimation combined with other algorithms for model parameters identification, such as RLS [25, 28], Particle Swarm Optimization (PSO) [29, 30], Lagrange multipliers [31] and Genetic Algorithms (GA) [32]. Another approach employed is the augmented states formulation, which allows simultaneous estimation of states and parameters. In this case, the identifiability of the parameters is defined by an observability analysis of the augmented system [128]. Not fully observable augmented systems may present unreliable results for parameters estimation, which is avoided with the methodology proposed by the authors of [129].

The authors of [130] propose an intelligent adaptive EKF approach for SOC estimation as an improved version of adaptive EKF, and both are validated employing freely available experimental data [131], which is also used in this paper. Parameter estimation is online, performed by a forgetting factor RLS. The authors demonstrated that the intelligent approach improves estimation accuracy, reducing considerably the errors without significantly increasing the computational efforts.

Other algorithms are also evaluated for SOC estimation. An adaptive fuzzy system is proposed in [132] for SOC estimation in series-connected battery packs. According to the authors, the fuzzy system is designed for improving accuracy even under cell inconsistencies, which is proved to be effective by simulation and experimental analysis.

A machine learning approach is proposed in [133], in which the authors use a linear regression model and Gaussian process regression. They conclude that the method may be used in BMS, since the presented error is acceptable. In [134], it is proposed a weighted LS-SVM to State of Health (SOH) estimation on lithium-ion batteries, remarking that this task is a challenge on retired ones, in which dynamics is highly nonlinear.

Many other observer designs are based on Particle Filter, such as proposed in [135]. The same algorithm is the base of the research presented in [136], which proposes an adaptive version for simultaneous parameters and states estimation.

A robust estimation is proposed in [137] to solve ill-conditioned observability points, avoiding unreliable SOC estimation. The authors of [138] present

a scheme for robust estimation, which is designed to consider model uncertainties and time-varying parameters. A robust algorithm is also proposed in [139], applying H_∞ filter with bias compensation.

The interest in NN for SOC estimation increased significantly in recent years, as we review next. The authors of [140] employ NN in two different tasks for SOC estimation of lithium-ion batteries. The first one has the purpose of filtering measured data, extracting the main features and reducing noise. These data are used as inputs for the latter one, which performs the SOC estimation. In [141], the authors present a Recursive Neural Network (RNN) for modeling battery dynamics under varying temperatures and SOC estimation, using voltage, current and temperature measures. Results demonstrate that the algorithm may estimate SOC in different temperatures and even in temperatures in which the NN was not trained.

A bidirectional Long Short Term Memory (LSTM) network is proposed in [142], so that past and future battery information are considered, improving accuracy and enabling the characterization of nonlinear dynamics of the battery. A similar structure of a deep NN is proposed in [143], which is experimentally evaluated, demonstrating that it is accurate at different ambient temperatures.

In [144], the authors propose a framework of estimation, in which an approximate estimation is performed using a LSTM in the first step and refined in a latter one that employs an adaptive H_∞ filter, improving accuracy. The authors of [145] propose wavelet NN, optimized by the Levenberg-Marquardt algorithm and PSO, for SOC estimation, which is proved to have good performance, in comparison with EKF and a back-propagation NN.

The authors in [146] propose the application of a Nonlinear Autoregressive with Exogenous Inputs (NARX) RNN with a moving window to establish an adequate model and to perform state estimation. The authors remark that the moving window allows the use of a small amount of data, accelerating the NN training process and avoiding the loss of information needed for estimation.

Recently, receding-horizon estimation algorithms have been evaluated for SOC estimation. In [147] the authors propose a moving-horizon approach for SOC and input current estimation, through a constrained optimization problem. This approach is useful even when there is no current measure available, but it requires the model parameters to be defined beforehand. A noise adaptive Moving-Horizon Estimation (MHE) algorithm is proposed by the authors of [148] to improve efficiency even under unknown noisy measurements. In this paper, model parameters are defined by a polynomial fitting, in function of SOC at each sample.

The authors of [149] present a combination of auto-regressive LSTM network and MHE for SOC estimation, so that the results of each one are combined to obtain the desired estimation. In the algorithm proposed, model parameters are defined by a two-dimensional polynomial fitting, which has as arguments the SOC and the input current.

The literature review allows us to observe that different versions of KF and LS are broadly explored on BMS tasks [34, 123, 124, 130, 150, 151]. Adapted versions of EKF are proposed by many researchers, in order to bypass the main disadvantages of this algorithm, such as calibration difficulties and variable efficiency according to state variables [35–38, 40, 41, 125–127].

Concerning MHSE, we may note that it is not broadly studied for SOC estimation with augmented states formulation. Very few papers have explored this technique [147–149], but not for simultaneous state and parameters estimation. Additionally, none of the aforementioned papers has explored the approximate version of the MHSE using the NN proposed in [22, 42], which embedded solutions for BMS may greatly benefit. Results indicate that, due to its predictive power and robustness, MHSE may achieve better results than its Kalman-based counterparts even for a system with augmented states formulation [22], which makes evident the need of testing receding-horizon solutions for SOC estimation.

Recent developments on NN methods indicate that they may be successfully applied to SOC estimation, due to their robustness and adaptability, which is evaluated by some researchers for black-box state estimation [140, 141, 146]. We herein adopt a fundamentally different approach, which takes advantage of the physical model of the system. As the physical meaning of the variables is preserved by the model-based state estimation structure of MHSE and this method is presented as accurate and robust [22], we evaluate the possibility of using MHSE results for training an ANN which defines faster the SOC using the information available on the receding-horizon defined, that is defined as NNMHE. In summary, this methodology associates the accuracy and interpretability of the results of MHSE, with the reduced computational cost that NNMHE may demand [42]. This machine learning approach arises as relevant, since reliable measured data of SOC for training the NN are hardly obtained and not always available. Besides that, ANN can be conveniently embedded on hardware [152], enabling its online application.

2.1.5 Hierarchical Framework for IWMD-EV Control

Many recent researches propose the use of MPC for vehicle control. The authors of [153] employ MPC on adaptive cruise control for vehicles, comparing its performance with a Linear Quadratic Regulator (LQR) controller, concluding that the first one performs well even when in unstable situations. In [154], the researchers propose a MPC for longitudinal control of a vehicle with ICE, in which the weights inside the cost function are defined through a fuzzy inference system, in order to improve performance and fuel consumption on road slopes. In comparison to a controller that keeps velocity constant, the proposed MPC presents lower fuel consumption and emissions.

The authors of [155] apply a linear MPC algorithm [155] for autonomous navigation at low speeds, such as crossing obstacles with known profiles. In [156], the authors propose a novel modeling framework and a hybrid MPC strategy for velocity regulation of an intelligent vehicle with ICE and automatic transmission. The control can define the longitudinal working modes (acceleration or braking) and the continuous control inputs for throttle opening and braking pressure.

The authors of [157] remark that the wheel slip control and estimation is a critical issue in driving control of EV, improving power consumption and safety, as the loss of traction is prevented. So, the authors present a sliding mode based method for control and estimation of wheel slip of an electric tractor, using a Burckhardt tire model. In [158] a novel strategy for EV control is proposed, that integrates state estimation performed with a Particle Filter and a NMPC for driving and handling of IWMD-EV.

The authors of [159] present a MPC for path tracking and stability control for highly automated vehicles, with a linearized model, in which is supposed that tires operate next to friction limits. In [160], a path tracking NMPC is proposed. The 2-DOF model supposes that longitudinal slip and sideslip angle are small enough that tire forces are defined by linear formulations.

In [161], the authors apply MPC for stability control, with a combined tire model LuGre and conclude that this model is more accurate than the pure slip models. The authors of [162] use MPC and NMPC for braking in straight paths with variable friction. Due to this uncertainty, an estimation algorithm for longitudinal velocity is developed, based on wheel speed and linear accelerations.

The authors of [163] evaluate fidelity levels and execution time of many dynamical models of autonomous vehicles for a MPC application for obstacle avoidance at high speeds. The results are applied on a nonlinear MPC for-

mulation in unstructured environments, ensuring safe and smooth operations [164]. In this research, safety is defined as the constant contact between tire and soil.

A controller for an EV is presented in [44], with many objectives, such as slip control, lateral stability, handling and rollover prevention. The authors use a MPC algorithm, which defines the torque on each independent wheel. The authors of [45] propose a nonlinear MPC for slip control, considering safety conditions as constraints of the cost function, which is employed on an IWMD-EV model with four independent wheels. A path tracking MPC-based is proposed on [46], in which vehicle shape and feasible road region are used as constraints of the optimization problem. In [47], a MPC algorithm, associated with a 2 DOF model, is proposed for path tracking and lateral stabilization, considering stable handling and safe navigation as constraints.

Collision avoidance and stability in highways applications are also possible to be reached by MPC algorithms, such validated by hardware-in-the-loop in [48]. With the same objective, MPC is used in [165], for decision making and control, with a combined tire model and controlling the vehicle by means of active steering and independent wheels.

Nonetheless, as MPC is based on an optimization problem, its application in complex systems, as vehicle controls, may be compromised due to the high processing times required. Aiming to address this issue, some researches have proposed as a solution the adoption of hierarchical frameworks, in which the control task is divided into two or more layers, so that the output of one layer is used as the reference for the subsequent one.

In this context, the authors of [166] present a hierarchical strategy for longitudinal control of a vehicle with ICE, using a linear tire model. They propose a Lyapunov function on the outer layer, which defines the wheel torque reference, while the inner one defines the throttle opening, through a PI controller.

In [167], the authors propose a three-layer strategy for longitudinal control of an automated vehicle with ICE, especially for traveling on low friction roads. Then, the purpose of the control is to ensure that the longitudinal slip is kept in stable region of the traction force curve.

The authors of [168] propose a three-layer control with compensators on the upper and lower layers and an optimization problem on the middle one. The purpose of this layer is to define the wheel angular velocity that minimizes the power required on the motor. The model employs a linearized approach of longitudinal force.

Specifically associating with MPC, the authors of [169] propose a hierar-

chical strategy for coordinating braking performance and steering in IWMD-EV with two layers. In each time step, in the outer layer, references longitudinal and lateral forces and yaw moment are defined by a NMPC based on a PSO algorithm. So, the inner layer defines the optimal torque allocation and brake actuator regulation, in order to achieve those efforts, ensuring stability and energy recovery.

In [49], the authors propose a framework for path tracking of intermediate or advanced automated vehicles, in highway situations. In the framework, the path planning layer defines the optimal trajectory and the tracking layer defines the best control variables by a linearized time-varying MPC.

The authors of [50] propose a control strategy with two NMPC layers, which define, respectively, kinematics and dynamics conditions for path tracking in handling limits conditions. In [170] a MPC structure is proposed for yaw stability in a 8-DOF model of an IWMD-EV, by means of motor torque distribution and active steering on the front axle.

We may observe in the literature review, that MPC has been used for EV path tracking tasks [44, 47, 158–160]. Meanwhile, due to the complexity of vehicle systems, the use of MPC for the determination of torque inputs of IWMD-EV may harm the processing time, especially due to nonlinearities and discontinuities on tire models. Aiming to improve the performance of autonomous EV on path tracking, the use of hierarchical frameworks is evaluated, in which the control task is divided into many layers, so that the output of one is the input or the reference of the subsequent [49, 50, 169, 170].

2.2

Contributions

Based on the critical analysis of the literature, presented at the end of each subsection of the previous section, we may establish the contributions of this thesis, which may be divided into five groups, as follows:

- Grey-box identification of time invariant parameters (presented in Chapter 6):
 - Present a grey-box identification methodology on an enhanced complexity analytical model of a landing gear, aiming to be able to precisely identify parameters on a real drop test data;
 - Evaluate batch and recursive approaches for time-invariant parameters of a multi-body system.

This chapter has been published in:

LOPES, E. D. R.; AYALA, H. V. H. **Nonlinear grey-box identification of a landing gear based on drop test data.** In: CONGRESSO BRASILEIRO DE AUTOMÁTICA-CBA, 2020.

- State Estimation of Vehicle and Tire Dynamics (presented in Chapter 7):
 - Present a comparative analysis between EKF, UKF and MHSE algorithms for estimation of longitudinal slip in ground vehicle control applications, which is applicable to other systems characterized by nonlinear and discontinuity efforts;
 - Demonstrate that MHSE presents superior results, even under measurement noise, since it does not depend on the linearization processes of the system.

This chapter has been published in:

LOPES, E. D. R.; RODRIGUES, G.S.; AYALA, H. V. H. **Comparison of Nonlinear Receding-Horizon and Extended Kalman Filter Strategies for Ground Vehicles Longitudinal Slip Estimation.** In: CONGRESSO BRASILEIRO DE AUTOMÁTICA-CBA, 2020.

- Friction coefficient estimation using MHSE (presented in Chapter 8):
 - Propose nonlinear observers for vehicle dynamics and control, analyzing the particularities of their application for friction efforts systems;
 - Evaluate EKF, UKF and MHSE performance for friction coefficient estimation, with augmented states, considering that this phenomenon is present on nonlinear systems and that it is characterized by discontinuities on Jacobians and derivatives;
 - Present MHSE as a suitable nonlinear observer for friction coefficient estimation, commenting about its advantages and disadvantages and demonstrating its robustness and capacity for correctly estimating states and parameters even under noisy measures.

This chapter has been submitted for review:

LOPES, E. D. R.; RODRIGUES, G.S.; AYALA, H. V. H. **Tire-road Friction Coefficient Estimation Using Nonlinear Receding-Horizon and Kalman Filter Strategies.** Under Review, 2022.

- Receding-horizon strategies for state of charge estimation of lithium-ion batteries (presented in Chapter 9):

- Propose the original application of MHSE for simultaneous SOC and model parameters estimation, which is not explored in previous papers, comparing their results with the classical formulation of EKF showing overall better results for the receding-horizon approaches;
- Prove that the augmented states and parameters are not observable in the original Kalman definition, while they become observable by increasing the window size in the moving-horizon approach. This is of great importance as it enables asymptotic stability of the filter without adding more sensors and thus avoiding costs by improving the estimation algorithm;
- Evaluate an augmented states formulation for state-space equations used on proposed estimators, verifying influences of the higher number of variables on estimation. This shows that it is possible to perform accurate and simultaneous estimation, with reduced complexity of the algorithms;
- Evaluate the effectiveness of the use of states observed by MHSE on the training of the NNMHE, that can estimate SOC accurately, in a reduced time, using recent information measured on the batteries. This receding-horizon approach is validated with experimental data.

This chapter has been submitted for review:

LOPES, E. D. R.; AYALA, H. V. H. **Nonlinear Receding-horizon Filter Approximation with Neural Networks for Fast State of Charge Estimation of Lithium-Ion Batteries**. Under Review, 2022.

- Hierarchical Framework for IWMD-EV Control (presented in Chapter 10):
 - Propose a novel hierarchical framework for driving and path-tracking control of an IWMD-EV, using a NMPC algorithm for defining reference forces on the vehicle body;
 - Demonstrate that the proposed control framework is efficient about safety and driveability, ensuring that the tire longitudinal slip is kept into the stable region of the tire-road friction curve;
 - Demonstrate that the hierarchical framework reduces considerably the computational effort;
 - Evaluate the use of different sample times for the plant and the NMPC algorithm, enlarging the prediction horizon in time and reducing processing times.

This chapter has been submitted for review:

LOPES, E. D. R.; AYALA, H. V. H. **Hierarchical Nonlinear Model Predictive Control for Path Tracking of In-Wheel Motor Drive Electric Vehicles**. Under Review, 2022.

Part II

Theoretical Background

3 Dynamic Models

In this chapter, the dynamic models used on the contributions are presented. Firstly, the mathematical models for tire efforts on planar motion are described, which are the forces and moments produced during the traction, braking and steering processes. Subsequently, a planar dynamic model of a vehicle is presented, derived from the Newton-Euler equations and the efforts developed on tires. It is used to obtain the quarter-car and the single-track models, which are presented in the last sections.

3.1 Tire Efforts on Planar Vehicle Dynamics

The tires are the vehicular components in contact with the road, and they have as functions supporting the weight of the vehicle, dampening road irregularities and interacting with the road, which produces the main forces and moments that act on vehicle motion, such as longitudinal and lateral forces and yaw moment.

The longitudinal force developed on wheels during traction and braking is defined as proportional to normal load, according to a friction coefficient μ_x , which depends on the longitudinal slip λ [171].

$$F_{x_w} = \mu_x F_{z_w} \quad (3-1)$$

$$\lambda = \frac{\omega r - v_{w_x}}{v_{w_x}} = \frac{\omega r}{v_{w_x}} - 1 \quad (3-2)$$

We may note that during acceleration, slip is positive, and during braking, it is negative and equation (3-2) demonstrate that λ must be on $[-1, \infty[$. There are many formulations for the relationship between μ_x and λ , as the Julien Theory [172], the Burckhardt model [173] and the Magic Formula, proposed by Pacejka [174]. All of them depend on many parameters, which are empirically obtained. The last one has the advantage of being continuous in the whole domain of slip, which does not happen in the others, reducing the elapsed time of simulations and estimation processes. Besides that, other models are applicable only to longitudinal forces, while Pacejka model may be applied to all tire forces and moments. So, according to the Magic Formula model, μ may

be written as:

$$\mu_x(\lambda) = A_x \sin(B_x \arctan(C_x \lambda^* - D_x(C_x \lambda^* - \arctan(C_x \lambda^*)))) + S_{V_x} \quad (3-3)$$

In which:

$$\lambda^* = \lambda + S_{H_x} \quad (3-4)$$

The parameters A_x , B_x , C_x and D_x depends on road conditions on which the vehicle moves. The shift parameters S_{H_x} and S_{V_x} are used with experimental data, to include in the results the effects of rolling resistance and energy lost on the longitudinal force.

The lateral forces may also be defined by another version of Magic Formula. The frames and angles used on tire dynamics and equations below are presented in Figure 3.1, for the i -th tire of the vehicle. In this case, the argument for Magic Formula equation is the sideslip angle (α), defined by Eq (3-5), in which β_i is the attack angle (Eq. (3-6)) of the wheel, δ_i is the steering angle and δ_ϕ is the steering angle due to rolling angle ϕ [171].

$$\alpha_i = \beta_i - \delta_i - \delta_\phi \quad (3-5)$$

$$\beta_i = \arctan\left(\frac{v_{wy}}{v_{wx}}\right) \quad (3-6)$$

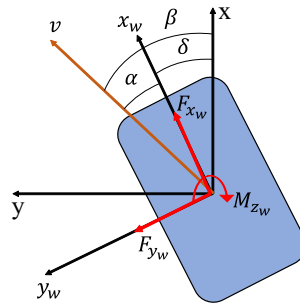


Figure 3.1: Tire frame and angles.

In this case, the lateral force may be calculated by:

$$F_{y_w} = \mu_y F_{z_w} \quad (3-7)$$

In which, μ_y may be defined with a similar magic formula model, such as presented on Eq. (3-3). For small values of the sideslip angle and neglecting Camber angle and roll angle (planar motion), the lateral force, written on the tire frame, may be defined by Eq. (3-8).

$$F_{y_w} = -C_\alpha \alpha = -C_\alpha^* F_{z_w} \alpha \quad (3-8)$$

The parameter C_α is called cornering stiffness and its dimensionless value C_α^* may be calculated from μ_y :

$$C_\alpha^* = - \lim_{\alpha \rightarrow 0} \frac{\partial \mu_y}{\partial \alpha} \quad (3-9)$$

Analogously to longitudinal force formulation, we adopt horizontal and vertical shifts to lateral force, in order to fit properly the experimental data. In this case, these shifts are necessary to include ply steer and tire conicity effects. So, a more complete model for the lateral force may be defined as:

$$F_{y_w} = -(C_\alpha^*(\alpha + S_{H_y}) + S_{V_y})F_{z_w} \quad (3-10)$$

The main moments we consider acting on tires in planar dynamics models are the overturning and the aligning ones. The first one (M_{y_w}) is produced by the rolling resistance force, which is due to non-uniform normal stress distribution on tireprints and it is usually calculated as proportional to the vertical load (equation (3-11)), according to rolling resistance coefficient f_R .

$$M_{y_w} = f_R r F_{z_w} \quad (3-11)$$

The aligning moment is due to the non-uniform distribution of lateral force and its calculated by means of the distance a_y between the centerline of the tireprint and the virtual point in which this force is applied, that is:

$$M_{z_w} = a_y F_{y_w} \quad (3-12)$$

So, noting that δ_i is the rotation angle of the tire around the axle z_w and ω its angular speed around y_w , the equations of motion of the wheels may be defined by:

$$\ddot{\delta} = \frac{T_{steer} - M_{z_w}}{I_{w_z}} \quad (3-13)$$

$$\dot{\omega} = \frac{T_{trac} - M_{y_w} - r F_{x_w}}{I_{w_y}} \quad (3-14)$$

3.2 Planar Vehicle Dynamics

The forces acting on a vehicle and its generalized coordinates are easier understood on vehicle frame (body frame) $B(x, y)$ than on fixed frame $F(X, Y)$ (details in Figure 3.2). Because this, the equations of motion are better defined by Newton-Euler equations:

$$\begin{bmatrix} \dot{v} \\ \dot{\omega} \end{bmatrix} = I^{-1} \begin{bmatrix} F - \omega \times I v \\ M - \omega \times I \omega \end{bmatrix} \quad (3-15)$$

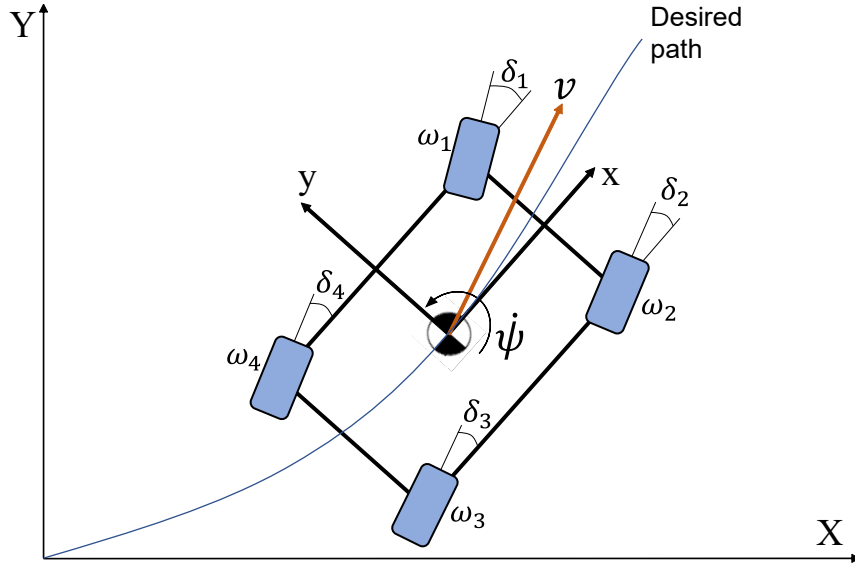


Figure 3.2: IWMD-EV dynamics.

Besides the tire forces transmitted to the vehicle chassis, there is acting on its CG the aerodynamic resistance R_{aer} , that we assume proportional to the square of velocity norm by c_{aer} . For passenger vehicles traveling on level roads, we may neglect the vertical displacement of the chassis and pitch and roll rotations, so that the equations of motion are written as:

$$\begin{bmatrix} \dot{v}_x \\ \dot{v}_y \\ \ddot{\psi} \end{bmatrix} = \begin{bmatrix} m & 0 & 0 \\ 0 & m & 0 \\ 0 & 0 & I_z \end{bmatrix}^{-1} \begin{bmatrix} F_x + \dot{\psi} m v_y - R_{aer_x} \\ F_y - \dot{\psi} m v_x - R_{aer_y} \\ M_z \end{bmatrix} \quad (3-16)$$

$$\begin{bmatrix} \dot{v}_x \\ \dot{v}_y \\ \ddot{\psi} \end{bmatrix} = \begin{bmatrix} (F_x - R_{aer_x} + m\dot{\psi}v_y)/m \\ (F_y - R_{aer_y} - m\dot{\psi}v_x)/m \\ M_z/I_z \end{bmatrix} \quad (3-17)$$

In equation (3-17), the forces F_x and F_y and moment M_z transmitted to the chassis by the n_t tires considered on the model are defined as:

$$F_x = \sum_{i=1}^{n_t} F_{x_{w_i}} \cos \delta_i - F_{y_{w_i}} \sin \delta_i \quad (3-18)$$

$$F_y = \sum_{i=1}^{n_t} F_{x_{w_i}} \sin \delta_i + F_{y_{w_i}} \cos \delta_i \quad (3-19)$$

$$M_z = \sum_{i=1}^{n_t} M_{z_{w_i}} + \tilde{r}_i T_z(\delta_i) \begin{bmatrix} F_{x_{w_i}} \\ F_{y_{w_i}} \\ 0 \end{bmatrix} \quad (3-20)$$

where T_z indicates a rotation matrix (equation (3-21)), r_i is the position of each wheel in relation to vehicle center of gravity and \tilde{r} an anti-symmetric matrix which may calculate a cross product (Equation (3-22)).

$$T_z(\delta_i) = \begin{bmatrix} \cos \delta_i & -\sin \delta_i & 0 \\ \sin \delta_i & \cos \delta_i & 0 \\ 0 & 0 & 1 \end{bmatrix} \quad (3-21)$$

$$\tilde{r} = \begin{bmatrix} 0 & -r_z & r_y \\ r_z & 0 & -r_x \\ -r_y & r_x & 0 \end{bmatrix} \quad (3-22)$$

3.3

Quarter-car Model - Longitudinal Dynamics

A quarter-car model may be effectively used for the study of nonlinear estimation of longitudinal slip and velocity reference tracking. In this model, the vehicle is understood as a concentrated mass (with mass m) over a single wheel (with the moment of inertia I_{wy}), and there are no effects related to vertical or lateral dynamics. Are considered also the rolling resistance momentum and aerodynamic resistance as presented in Figure 3.3.

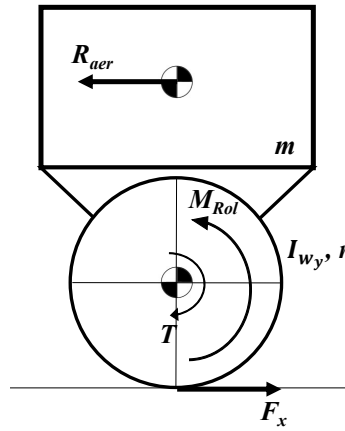


Figure 3.3: Quarter-car Model.

As only the longitudinal displacement DOF is considered and treating the $c = c_{aer}/m$, the dynamical model may be obtained from (3-14) and (3-17) with the proper simplifications:

$$\dot{v}_x = \mu_x(\lambda)g - cv_x^2 \quad (3-23)$$

$$\dot{\omega} = \frac{T}{I_{wy}} - (\mu_x(\lambda) + f_R) \frac{mgr}{I_{wy}} \quad (3-24)$$

The friction coefficient μ_x depends on the longitudinal slip λ , which may be define, in this case, as:

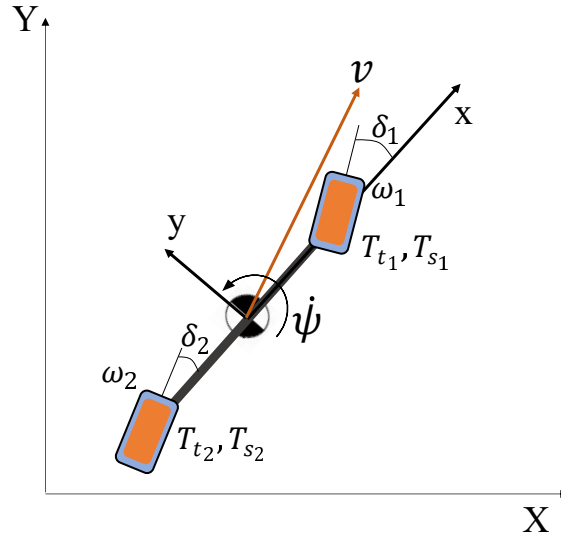


Figure 3.4: Single-Track Model.

$$\lambda = \frac{\omega r - v_x}{v_x} = \frac{\omega r}{v_x} - 1 \quad (3-25)$$

If we define that an electric in-wheel motor is responsible for traction and braking of the vehicle, the input torque T may be written as proportional to electrical current according to the torque constant K_t .

3.4

Single-Track Model - Coupled Longitudinal and Lateral Dynamics

As the full vehicle longitudinal and lateral dynamic model is complex, the evaluation of MPC application on vehicles may be more efficient in reduced systems, such as the bicycle one, also known as single-track model. This model treats the vehicle as a body with negligible width, with only one wheel on each axle, such as demonstrated in Figure 3.4.

As we study and research MPC applications for IWMD-EV, in the model we consider that front and rear wheels are independently controlled for traction and steering. The equations of motion of the vehicle may be obtained from Eq. (3-17), but as the single-track model considers single wheels on each axle, the positions of each wheel related to the vehicle center of gravity (CG) are only the distances between the CG and, respectively, the front and rear axles.

From the rigid body equation of the vehicle and dynamic equations of each wheel (Eqs. (3-13) and (3-14)), we may obtain the state-space model of the single-track model, as described below.

$$\mathbf{x} = [v_x \ v_y \ \omega_z \ \omega_1 \ \delta_1 \ \dot{\delta}_1 \ \omega_2 \ \delta_2 \ \dot{\delta}_2 \ X \ Y \ \psi]^T \quad (3-26)$$

$$\mathbf{u} = [T_{t_1} \quad T_{s_1} \quad T_{t_2} \quad T_{s_2}]^T \quad (3-27)$$

$$\dot{\mathbf{x}} = f(\mathbf{x}, \mathbf{u}) = \begin{bmatrix} (F_x - R_{aer_x} + m\omega_z v_y)/m \\ (F_y - R_{aer_y} - m\omega_z v_x)/m \\ M_z/I_z \\ (T_{t_1} - M_{y_{w_1}} - rF_{x_{w_1}})/I_{w_y} \\ \dot{\delta}_1 \\ (T_{s_1} - M_{z_{w_1}})/I_{w_z} \\ (T_{t_2} - M_{y_{w_2}} - rF_{x_{w_2}})/I_{w_y} \\ \dot{\delta}_2 \\ (T_{s_2} - M_{z_{w_2}})/I_{w_z} \\ v_x \cos \psi - v_y \sin \psi \\ v_x \sin \psi + v_y \cos \psi \\ \omega_z \end{bmatrix} \quad (3-28)$$

Note that the input of the system may also be defined as the electrical currents on traction and steering motors, since the torques are proportional to them according to their torque constant. Besides that, the terms F_x , F_y and M_y are defined as described in Eqs. (3-18), (3-19) and (3-20), with $n_t = 2$.

3.5 Equivalent Battery Model

Based on Thévenin's theorem [130], the battery may be modeled by a simplified ECM, with an open-circuit voltage (OCV) as a source U_{OC} , in series with a resistor R_s and a parallel-connected RC network, composed by a resistor R_p and a capacitor C_p . It is a lumped-parameters model commonly used for battery modeling for SOC estimation [6, 130]. The scheme of the equivalent circuit is presented in Fig. 3.5.

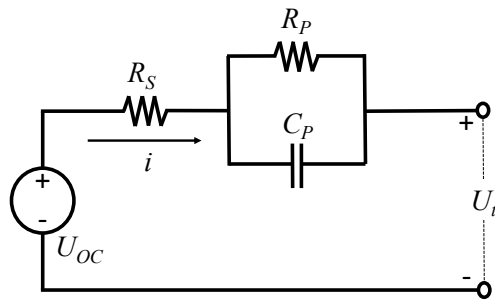


Figure 3.5: Equivalent circuit model of lithium-ion battery, based on Thévenin's theorem.

Based on Kirchhoff laws, the continuous-time equations of the circuit given in Fig. 3.5 are

$$\dot{U}_p = \frac{i}{C_p} - \frac{U_p}{R_p C_p} \quad (3-29)$$

$$U_t = U_{OC} - U_p - iR_s \quad (3-30)$$

where U_p is the voltage on RC network, U_t is the measured voltage on battery terminals, and i is the electrical current, which is the system input. Note that a positive current indicates a discharging phase, while a negative one a charging phase.

The SOC time-derivative is defined by equation (3-31) [30, 32], which is applied on Coulomb Counting method for SOC definition. Despite being used in most of the researches, the accuracy of this equation may be severally affected by some factors, such as ambient temperature, discharge current and the history and cycle life of the battery [175].

$$S\dot{OC} = -\frac{\eta i}{C_n} \quad (3-31)$$

where C_n is the nominal capacity of the battery and η is the efficiency of the charging and discharging process. Note that the SOC is related to the current state. According to the equation, the SOC decreases while the current increases.

The U_{OC} depends on SOC and this relation may be established by means of a low current discharge test. The reason to use a low current discharge test is that the effects of the dynamics of other components are minimized and the open-circuit voltage is approximately equal to the terminal voltage [176]. In this ECM, we adopt a polynomial fit to relate U_{OC} and SOC, as in [130]. To this end let

$$U_{OC} = p(SOC) = \sum_{i=0}^{n_p} K_i SOC^i \quad (3-32)$$

where n_p is the order of the polynomial of coefficients $K_i, i \in [0, n_p]$.

Applying a discretization with sampling time T_s on equations (3-29), (3-30) and (3-31) [17], we may define the discrete-time equations for the equivalent circuit model:

$$U_{p,k} = U_{p,k-1} \exp\left(-\frac{T_s}{C_p R_p}\right) + i_{k-1} R_p \left[1 - \exp\left(-\frac{T_s}{C_p R_p}\right)\right] \quad (3-33)$$

$$SOC_k = SOC_{k-1} - \frac{\eta i_{k-1} T_s}{C_n} \quad (3-34)$$

$$U_{t,k} = U_{OC,k} - U_{p,k} - i_k R_s \quad (3-35)$$

3.6 Landing Gear System

The landing gear is modeled, in this work, as a planar mechanism, with concentrated inertia. The stiffness and damping of its structure and suspension system are considered a rotational spring and damper, which represents the stiffness and damping of the structure. In the system, there are three bodies: a concentrated mass representing the airplane with coordinates (x, z) , a bar with length L representing the structure of the landing gear, with coordinates $[x_b, z_b, \theta]$, and the wheel with coordinates $[x_w, z_w, \phi]$, radius R , and an applied braking torque T , as shown in Figure 3.6.

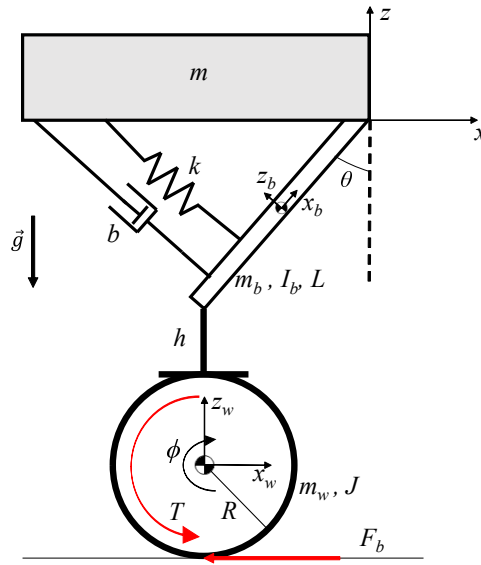


Figure 3.6: Landing gear model.

We use the Lagrange formulation in order to obtain the dynamic equations of motion for the landing gear. To this end, the kinematic relations between the generalized coordinators are presented as

$$\dot{x}_b = \dot{x} - \frac{L}{2} \dot{\theta} \cos \theta \quad (3-36a)$$

$$\dot{z}_b = \dot{z} + \frac{L}{2} \dot{\theta} \sin \theta \quad (3-36b)$$

$$\dot{x}_w = \dot{x} - L \dot{\theta} \cos \theta \quad (3-36c)$$

$$\dot{z}_w = \dot{z} + L \dot{\theta} \sin \theta \quad (3-36d)$$

We may rewrite some parameters, for simplifying equations, as follows:

$$M_1 = m + m_b + m_w \quad (3-37)$$

$$M_2 = I_b + \left(\frac{m_b}{4} + m_w\right)L^2 \quad (3-38)$$

$$M_3 = (m_b + 2m_w)L \quad (3-39)$$

So, the kinetic energy E_k and potential energy E_p of the system may be described as:

$$E_k = \frac{1}{2}M_1(\dot{x}^2 + \dot{z}^2) + \frac{1}{2}M_2\dot{\theta}^2 + \frac{1}{2}M_3(-\dot{x}\dot{\theta}\cos\theta + \dot{z}\dot{\theta}\sin\theta) + \frac{1}{2}J\dot{\phi}^2 \quad (3-40)$$

$$E_p = M_1gz - M_3g\cos\theta - m_wgh + \frac{k}{2}(\theta - \theta_0)^2 \quad (3-41)$$

The Lagrange Equation is defined at Eq. (3-42), where q_i indicates each generalized coordinate and Q_i the external forces or moments related to q_i .

$$\frac{d}{dt} \frac{\partial}{\partial \dot{q}_i} (E_k - E_p) - \frac{\partial}{\partial q_i} (E_k - E_p) = Q_i \quad (3-42)$$

Applying the Lagrange Equation for each generalized coordinate, namely x , z , θ and ϕ , it is possible to obtain the system dynamic equations.

$$M_1\ddot{x} - M_3\ddot{\theta}\cos\theta + M_3\dot{\theta}^2\sin\theta = 0 \quad (3-43a)$$

$$M_1\ddot{z} + M_3\ddot{\theta}\sin\theta + M_3\dot{\theta}^2\cos\theta + M_1g = 0 \quad (3-43b)$$

$$-M_3\ddot{x}\cos\theta + M_3\ddot{z}\sin\theta + M_2\ddot{\theta} + M_3g\sin\theta + k(\theta - \theta_0) + b\dot{\theta} = F_zL\sin\theta + F_bL\cos\theta \quad (3-43c)$$

$$J\ddot{\phi} + c\dot{\phi} = F_bR - T \quad (3-43d)$$

The braking force is not considered in the first equation, because the prototype on test is confined. So, this force is balanced by the kinematic constraint imposed by the apparatus. The braking force is considered proportional to the vertical load, which is due to the elastic condition of the tire. So, it may be written as:

The parameter μ depends on the slip (λ), which relates the wheel hub velocity and the wheel angular velocity as

$$\lambda = \frac{\dot{x}_w - \dot{\phi}R}{\dot{x}_w} \quad (3-44)$$

There are many models relating the coefficient μ and the slip λ , among which, one of the most widespread on braking systems is the Burckhardt model, described in [177].

$$\mu(\lambda) = \vartheta_1(1 - e^{-\lambda\vartheta_2}) - \lambda\vartheta_3 \quad (3-45)$$

4

Estimation Methods

This chapter deals with the estimation methods employed on the contributions presented in Part III. Except for the first one, which treats of time-invariant parameters estimation, all methods are described for discrete-time nonlinear state-space model. If only the continuous-time model is available, it must be discretized by any analytic or numeric integration. In this thesis, the discretization is usually performed with a 4th-order Runge-Kutta algorithm.

Generally, a discrete-time nonlinear state space model may be defined as:

$$\begin{cases} x(k+1) = f(x(k), u(k)) \\ z(k+1) = h(x(k+1), u(k+1)) + \xi_n \end{cases} \quad (4-1)$$

where the index k denotes discrete-time dependence, $x(k)$ is the state vector, $u(k)$ is the input vector of the system, and $z(k)$ is the output vector, that is, the measured variables which are functions of the states and inputs. Functions $f(\cdot)$ and $h(\cdot)$ are called state and measurement equations, respectively, and are in general nonlinear mappings. They relate states and inputs to state transitions and measurements, respectively.

4.1

Grey-box Time Invariant Parameters Estimation Algorithm

The grey-box identification has as an objective the determination of unknown parameters, through measured or estimated states. When the ne dynamic equations of a multi-body system are known, it is possible to identify np linearly independent parameters that allow rewriting the equations as matrix multiplication, for each sample j :

$$\varphi(j)\Theta = f(j) \quad (4-2)$$

where $\Theta \in R^{np}$ is a vector with the smallest set of linear independent parameters of the model, $\varphi(j) \in R^{ne \times np}$ is a matrix with only known terms, as measured or estimated positions, velocities and accelerations. The vector $f(j) \in R^{ne}$ is composed of independent terms, which include external forces and moments and others that are not related to unknown parameters.

Since the measured or estimated states may be affected by noise, it is important that Φ and F are as large as possible, considering all points available. So, concatenating the matrix equations, the system may be described as

$$\begin{bmatrix} \varphi(1) \\ \vdots \\ \varphi(j) \\ \vdots \\ \varphi(N) \end{bmatrix} \Theta = \begin{bmatrix} f(1) \\ \vdots \\ f(j) \\ \vdots \\ f(N) \end{bmatrix} \quad (4-3)$$

Generally, the Equation (4-3) may be written as

$$\Phi \Theta = F \quad (4-4)$$

which may be then treated effectively. The identification problem resembles obtaining the vector of parameters Θ with measurements made in Φ and F . For the grey-box identification, many methods may be used for estimating the vector of parameters Θ . The simplest is the Batch Least Squares (LS) algorithm, or the Penrose-Moore pseudo-inverse. So, the estimated vector is:

$$\hat{\Theta} = (\Phi^T \Phi)^{-1} \Phi^T F \quad (4-5)$$

The recursive approach of Least Squares may already be used in this grey-box identification, with suitable precision. With some modifications, this method converges to the Kalman Filter (KF) for parameter estimation, which may be employed for online or offline identification [178]. This algorithm is recursive and described in these equations, for each sample j

$$\epsilon(j) = F(j) - \hat{F}(j) = F(j) - \Phi(j) \hat{\Theta}(j-1) \quad (4-6)$$

$$K(j) = \frac{P(j-1) \Phi(j)^T}{I + \Phi(j) P(j-1) \Phi(j)^T} \quad (4-7)$$

$$P(j) = P(j-1) - K(j) \Phi(j) P(j-1) + R_1 \quad (4-8)$$

$$\hat{\Theta}(j) = \hat{\Theta}(j-1) + K(j) \epsilon(j) \quad (4-9)$$

where P is the covariance matrix, ϵ is the prediction error and K is the gain. In each iteration, the vector of parameters is corrected with a factor proportional to the error between the actual and the estimated vector F . In order to execute the identification procedure given by the Equations (4-6)-(4-9), the matrix $P(0)$ and the vector $\hat{\Theta}(0)$ must be initiated at iteration $j = 0$. In most cases, $P(0)$ is properly defined as a diagonal matrix with large entries and the initial estimation of vector $\hat{\Theta}(0)$ may be defined as zero, so that the estimator does not converge to a local minimum [179].

It is important to note that the trace of P decreases along with the iterations and tends to zero if R_1 is not considered. So, when the system is time-varying or in online applications, it is important to define a matrix R_1 with large entries, so that the trace of P remains in a large value. In offline applications or time-invariant systems, R_1 may be defined as zero.

4.2

Kalman Filter Nonlinear Estimation Methods

In most control applications, not all controlled state variables are measurable, which leads to the development of estimators, to observe these non-measurable variables that must be used on control laws. The existence and efficiency of the estimator are conditioned to the observability of the system, which indicates that all states may be observed through the output variables.

In this section, two Kalman-based methods for nonlinear state estimation are presented: the EKF and UKF.

4.2.1

Extended Kalman Filter

The EKF is applied to a discrete-time system, such as described by Eq. (4-1). The algorithm is presented below, in which $\hat{x}(i|j)$ means the state at sample i , estimated on sample j , matrices P , R and Q are, respectively, state prediction covariance, the covariance of a supposed gaussian white-noise on the process model and the covariance of a gaussian white-noise on measures. For improving accuracy, predicted and updated states on Equations (4-15) and (4-18) must be constrained to their physical bounds.

1. Obtain function Jacobians:

$$F(k-1) = \frac{\partial f}{\partial x_{x=\hat{x}(k-1|k-1)}} \quad (4-10)$$

$$H(k-1) = \frac{\partial h}{\partial x_{x=\hat{x}(k-1|k-1)}} \quad (4-11)$$

2. Calculate state prediction covariance:

$$P(k|k-1) = F(k-1)P(k-1|k-1)F(k-1)^T + Q(k-1) \quad (4-12)$$

3. Calculate residual covariance:

$$S(k) = R(k-1) + H(k-1)P(k|k-1)H(k-1)^T \quad (4-13)$$

4. Obtain filter gain:

$$W(k) = P(k|k-1)H(k-1)^T S(k)^{-1} \quad (4-14)$$

5. Obtain predicted states:

$$\hat{x}(k|k-1) = f(\hat{x}(k-1|k-1), u(k-1)) \quad (4-15)$$

6. Calculate measurement prediction:

$$\hat{z}(k|k-1) = h(\hat{x}(k|k-1)) \quad (4-16)$$

7. Calculate measurement residual:

$$\nu(k) = z(k) - \hat{z}(k|k-1) \quad (4-17)$$

8. Update state estimate:

$$\hat{x}(k|k) = \hat{x}(k|k-1) + W(k)\nu(k) \quad (4-18)$$

9. Update state covariance:

$$P(k|k) = P(k|k-1) - W(k)S(k)W(k)^T \quad (4-19)$$

4.2.2

Unscented Kalman Filter

The first step of EKF is a linearization of the system, using the Jacobians. However, for highly nonlinear systems or when the Jacobians F and H are discontinuous, this linearization may harm the estimation process, leading to non-accurate results. UKF has been developed for this kind of system, since it applies unscented transformations [17], instead of linearization, for the prediction and update of estimated states. These transformations are part of the algorithm, which is presented on Equations (4-20) to (4-35). As UKF does not depend on derivatives and Jacobians, its results are better, even with discontinuities and nonlinearities. It is important to remark that matrices P , Q and R have the same sense described for EKF, as well as the physical bounds that must be imposed on predict and update steps.

1. Choose $2n$ sigma points near to states estimated for previous step:

$$\check{x}^{(i)}(k-1) = \hat{x}(k-1) + \tilde{x}^{(i)}, i = 1, \dots, 2n \quad (4-20)$$

$$\tilde{x}^{(i)} = (\sqrt{nP(k-1)})_i^T, i = 1, \dots, n \quad (4-21)$$

$$\tilde{x}^{(n+i)} = -(\sqrt{nP(k-1)})_i^T, i = 1, \dots, n \quad (4-22)$$

In these equations, $\sqrt{nP(k-1)}$ is the Cholesky transformation of $nP(k-1)$

2. Use state equation of the system to transform sigma points:

$$\check{x}^{(i)}(k) = f(\check{x}^{(i)}(k-1), u(k-1)), i = 1, \dots, 2n \quad (4-23)$$

3. Combine transformed sigma points to obtain a prediction of state estimation:

$$\bar{x}(k) = \frac{1}{2n} \sum_{i=1}^{2n} \check{x}^{(i)}(k) \quad (4-24)$$

4. Estimate a prediction of error covariance:

$$\bar{P}(k) = \frac{1}{2n} \sum_{i=1}^{2n} (\check{x}^{(i)}(k) - \bar{x}(k))(\check{x}^{(i)}(k) - \bar{x}(k))^T + Q \quad (4-25)$$

5. Choose n sigma points near to predicted states:

$$\check{x}^{(i)}(k) = \hat{x}(k) + \tilde{x}^{(i)}, i = 1, \dots, 2n \quad (4-26)$$

$$\tilde{x}^{(i)} = (\sqrt{n\bar{P}(k)})_i^T, i = 1, \dots, n \quad (4-27)$$

$$\tilde{x}^{(n+i)} = -(\sqrt{n\bar{P}(k)})_i^T, i = 1, \dots, n \quad (4-28)$$

6. Use output equation to transform sigma points into predicted measurements:

$$\check{z}^{(i)}(k) = f(\check{x}^{(i)}(k), u(k)), i = 1, \dots, 2n \quad (4-29)$$

7. Combine the predicted measurements related to sigma points to obtain estimated measurement at time k :

$$\hat{z}(k) = \frac{1}{2n} \sum_{i=1}^{2n} \check{z}^{(i)}(k) \quad (4-30)$$

8. Estimate the covariance of predicted measurement:

$$\bar{P}_z = \frac{1}{2n} \sum_{i=1}^{2n} (\check{z}^{(i)}(k) - \hat{z}(k))(\check{z}^{(i)}(k) - \hat{z}(k))^T + R \quad (4-31)$$

9. Estimate cross covariance between predicted states and estimated measurement:

$$\bar{P}_{xz} = \frac{1}{2n} \sum_{i=1}^{2n} (\check{x}^{(i)}(k) - \bar{x}(k))(\check{z}^{(i)}(k) - \hat{z}(k))^T \quad (4-32)$$

10. Calculate Kalman Filter gain:

$$W(k) = P_{xz}P_z^{-1} \quad (4-33)$$

11. Update state estimate:

$$\hat{x}(k) = \bar{x}(k) + W(k)(z(k) - \hat{z}(k)) \quad (4-34)$$

12. Update state covariance:

$$P(k) = \bar{P}(k) - W(k)P_yW(k)^T \quad (4-35)$$

4.3 Moving-Horizon State Estimation

Among studied estimators, the MHSE is the most recent and has been developed in the context of Model-based Predictive Control (MPC), due to the duality between control and observer algorithms. The main purpose of the MHSE is to estimate the states at the current time, using the recent information about the measured inputs and outputs of the system, as illustrated in Figure 4.1.

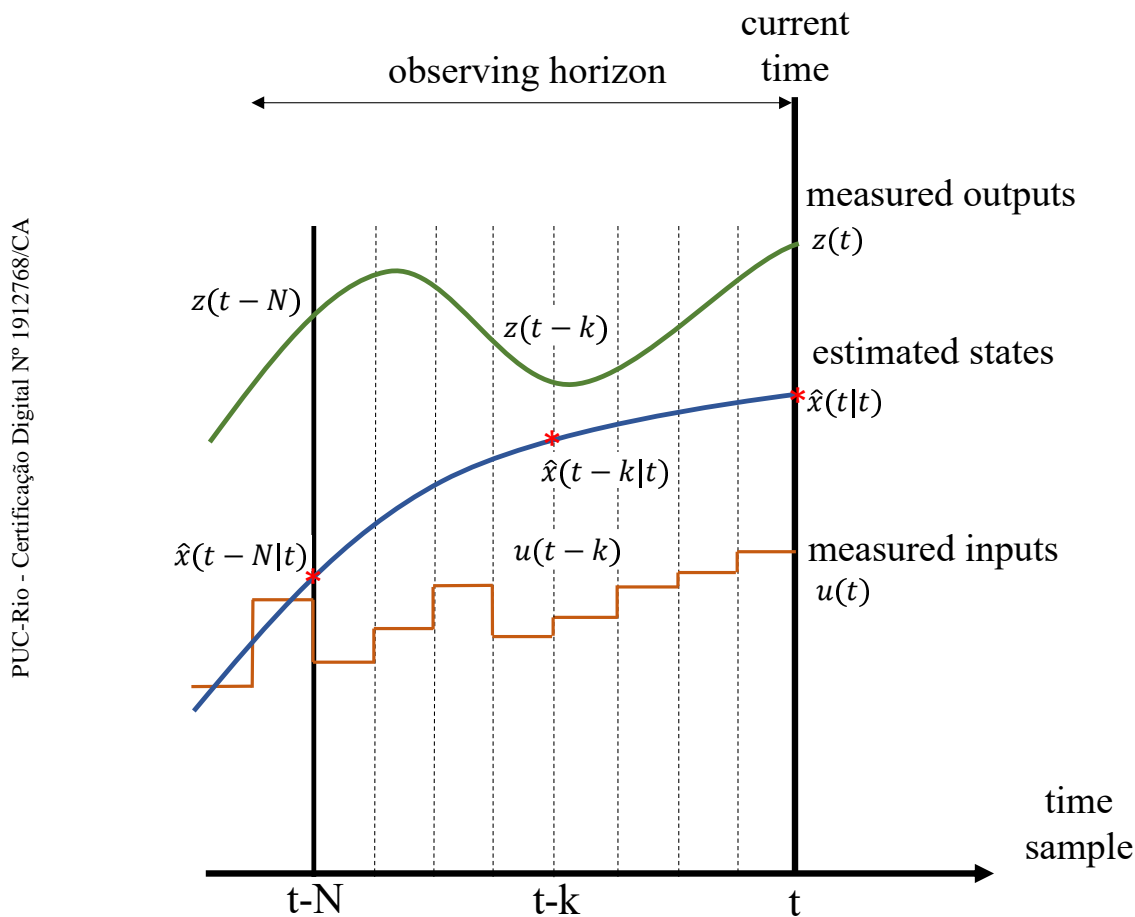


Figure 4.1: MHSE strategy.

The MHSE is performed through a constrained optimization problem, whose cost function depends on the estimated states and the measured inputs and outputs along the observing horizon of size N . This cost function may be defined as:

$$J(\hat{x}(\cdot), u(\cdot), z(\cdot)) = \rho \|\hat{x}_{k-N|k} - x_{k-N|k}^+\|^2 + \sum_{i=k-N}^k \|h(\hat{x}_{i|k}, u_i) - z_i\|^2 \quad (4-36)$$

In this formulation, N is the receding-horizon window size and ρ is the weight factor, which is a parameter to associate different relevance for measured data and dynamic model prediction. Note that $\hat{x}_{j|k}$ is the estimation of states at sample j , performed at sample k and $x_{k-N|k}^+$ is a prediction of the states at the beginning of the horizon, which is based on the dynamic model, so that:

$$x_{k-N|k}^+ = f(\hat{x}_{k-N-1|k-1}, u_{k-N-1}) \quad (4-37)$$

The cost function may also be defined with higher complexity, as described as follows:

$$J(\hat{x}(\cdot), u(\cdot), z(\cdot)) = \|\hat{x}_{k-N|k} - x_{k-N|k}^+\|_P^2 + \sum_{i=k-N}^k \|z_i - \hat{z}_i\|_Q^2 \quad (4-38)$$

In the Eq. (4-38), P and Q are weighting matrices, which may associate different contributions to the prediction of each state variable and experimental data, which may be interesting

The state estimation may be performed using different arguments. In a first approach, the argument of the optimization problem is the set of states on the beginning of the horizon, as presented in the Eq. (4-39).

$$\begin{aligned} \hat{x}_{k-N|k} &= \arg \min J(\hat{x}(\cdot), u(\cdot), z(\cdot)) \\ \text{where } \hat{x}_{i+1|k} &= f(\hat{x}_{i|k}, u_i) \\ \hat{z}_{i+1|k} &= h(\hat{x}_{i+1|k}, u_{i+1}) \end{aligned} \quad (4-39)$$

Once defined the states estimation on the beginning of the horizon $\hat{x}_{k-N|k}$, the state estimation the current sample must be defined through the dynamic model:

$$\hat{x}_{i+1|k} = f(\hat{x}_{i|k}, u_i), \quad i = k - N, \dots, k - 1 \quad (4-40)$$

A second approach, which is more efficient but with higher computational cost, considers as the argument of the cost function all the states along the observing horizon. In this formulation, the optimization problem is defined as:

$$\begin{aligned} [\hat{x}_{k-N|k} : \hat{x}_{k|k}] &= \arg \min J(\hat{x}(\cdot), u(\cdot), z(\cdot)) \\ \text{s.t. } \hat{x}_{i+1|k} &= f(\hat{x}_{i|k}, u_i) \\ \hat{z}_{i+1|k} &= h(\hat{x}_{i+1|k}, u_{i+1}) \\ x_{min} &\leq \hat{x}_{i|k} \leq x_{max} \end{aligned} \quad (4-41)$$

In this last case, the state estimation $\hat{x}(k|k)$ is defined on the problem itself, eliminating the later step of the first approach.

One of the advantages of the MHSE is to improve the observability of the system, through a larger observing window, while the Kalman filter approaches are based on only one sample. For observability analysis in receding-horizon strategies, let us consider the following observation mapping F_N and its Jacobian J_N related to the state vector:

$$F_N = \begin{bmatrix} h(x(t-N)) \\ h \circ f(x(t-N), u(t-N)) \\ h \circ f(x(t-1), u(t-1)) \circ \dots \circ f(x(t-N), u(t-N)) \end{bmatrix} \quad (4-42)$$

$$J_N = \frac{\partial F_N}{\partial x} \quad (4-43)$$

A system is observable if $\exists N > 0$, $\forall x \in X$ and $\forall u \in U$, so that $\text{rank}(J_N) = n$, that is, the Jacobian is full column rank. For a given system, this property may be proved by means of software and symbolic calculation [180].

The solution of the MHSE optimization problem may be performed through software toolboxes, as available on MATLAB[®], or CasADi symbolic toolbox [181], which presents many solvers for efficient optimization solutions.

4.4 Neural Network Moving-Horizon Estimation

The operation made in Eqs. (4-39) and (4-41) can be viewed as function mappings from input and output measurements to state estimates. Being so, it may be performed using any universal approximation function, as it has been proposed in [22] and shown in greater detail in [42], where it is proposed the use of ANN for this purpose. Naturally, the NN will produce approximate results when compared to the resolution of the online optimization problem, but with significantly reduced processing time. In other words, a feed-forward NN may be used to obtain the estimation of states ($\hat{x}(k)$) using measured inputs and outputs along a receding horizon and the predicted states at the beginning of the window, so that, larger information is used, improving the accuracy of estimation. In this way, the NNMHE may be defined as:

$$\hat{x}_k = NN(I_v) \quad (4-44)$$

where the information vector I_v contains the measured inputs and outputs along the observing horizon, as well as the state predicted on the beginning of the window x_{k-N}^+ :

$$I_v = [x_{k-N}^+ \quad z_{k-N} \quad \dots \quad z_k \quad u_{k-N} \quad \dots \quad u_k]^T \quad (4-45)$$

Note that the NN proposed may be used to estimate all states or only those that might be used for control or monitoring tasks. Once demonstrated that MHSE results are accurate and reliable, they may be used for NN training, so that the latter, as defined on (4-44) is proposed to be a faster approximation of the optimization and estimation process of MHSE, enabling the NNMHE for online applications with less computational cost and processing times. The methodology of NNMHE is illustrated in Fig. 9.4, for the case study presented in Chapter 9.

4.5

Evaluation Metrics

The evaluation of these methods may be done with some metrics [22]. One of them is the RMSE based metrics to quantitatively evaluate different filters estimation accuracy. It is defined as

$$RMSE_k = \sqrt{\frac{\sum_{j=1}^{n_{sim}} \|e_{k,j}\|^2}{n_{sim}}}, \quad (4-46)$$

where $e_{k,j}$ is the error of the state estimate at the j -th estimation process of a total of n_{sim} realizations. Thus, for smaller values of RMSE at a given time instant, the better the estimation is. Note that there is a time dependency for this metric, so that it is possible to track the error on time with different initial conditions and noise realizations. The RMSE of all evaluated period may be calculated as the mean of the RMSE of all samples.

The ARMSE metric is defined as

$$ARMSE = \sum_{k=T-S}^T \frac{1}{S+1} \sqrt{\frac{\sum_{j=1}^{n_{sim}} \|e_{k,j}\|^2}{n_{sim}}}, \quad (4-47)$$

where T is the final estimation procedure time and S is the final window being considered to calculate the metric. As it calculates the RMSE solely in the last time samples of the estimation procedure, it measures the error after enough time for convergence of the estimation method and denotes better asymptotic state tracking capability.

Both RMSE and ARMSE are dimensional, so that their value may present difficulties to understand, according to the magnitude of the variables. So, a dimensionless quantitative evaluation may be done with the R^2 , which range varies between 0 and 1, and is defined as:

$$R^2 = 1 - \frac{\sum_{k=1}^n \|e_k\|^2}{\sum_{k=1}^n \|x_k - \bar{x}\|^2} \quad (4-48)$$

The closer to 1 the R^2 , the more accurate is the estimation, enabling easier the evaluation of variables of different magnitudes.

5 Model-based Predictive Control

This chapter deals with the MPC theory and implementation. In the first section, we present its concept and the different formulations of the optimization problem on which it is based. The second one is about the computational algorithm and some remarks about its application.

5.1 MPC formulation

The MPC is based on an optimization process. Different to feedback control techniques, MPC aims to define control actions based on predicted future states or outputs of the systems, instead of previous output measures. The prediction is related to a moving horizon window of time or samples, with a predefined size (Figure 5.1).

There are many definitions for MPC optimization problem, for both

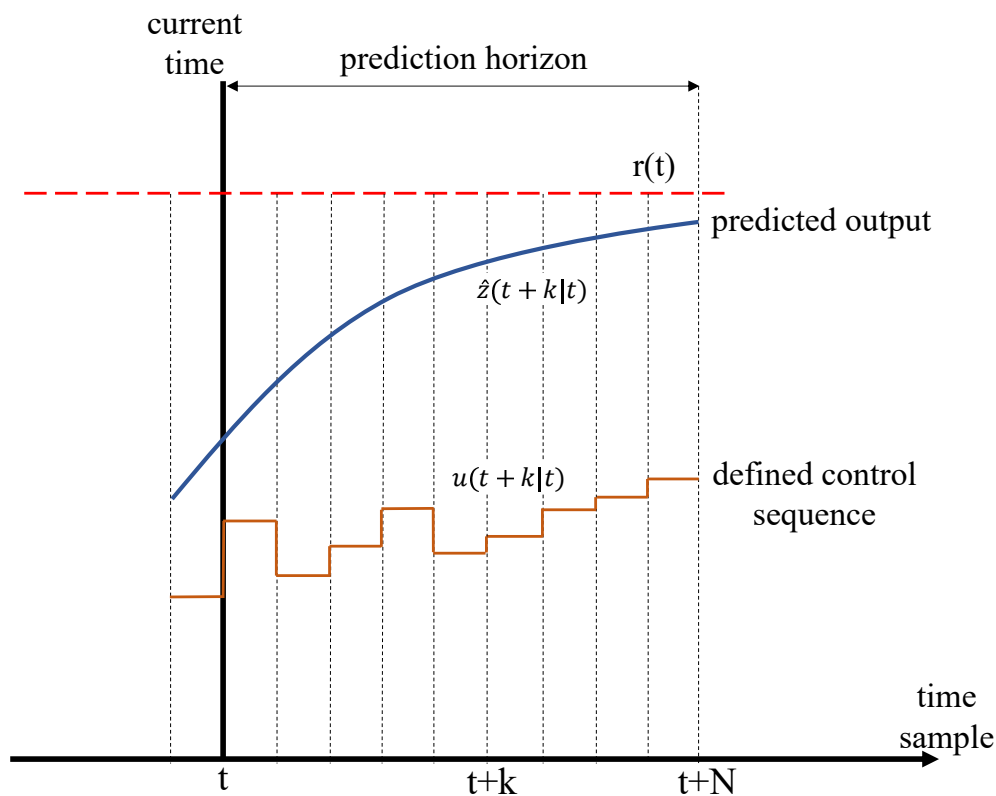


Figure 5.1: MPC strategy.

continuous and discrete-time systems. Considering a nonlinear discrete system described by equation (4-1), the cost function may be defined as:

$$J(\mathbf{u}(\cdot), \mathbf{x}(\cdot)) = \sum_{i=k}^{k+N} \|(z(i) - r(i))\|_Q^2 + \|(u(i) - u_r(i))\|_R^2 + \|(\Delta u(i))\|_S^2 \quad (5-1)$$

where, $r(i)$ and $u_r(i)$ are references for, respectively, outputs and control inputs. Each portion of cost function is weighted by diagonal matrices Q , R and S , so that one may be considered more relevant than others, besides variable dimensions must be equalized. The last term is important to ensure that there are no high shifts on control sequence, which is unfeasible on most dynamic systems. It is important to remark that this cost function definition may be adapted according to different requirements of the controlled system, so that it is not a definitive formulation.

For the solution of the MPC optimization problem, two main strategies are presented, namely the single and multiple shooting ones. In the first one, the argument of the cost function is only the sequence of control inputs within the prediction window, that is, from sample $k + 1$ to $k + N$, as presented on Equation (5-2).

$$\begin{aligned} u(\cdot) = \arg \min \quad & J(\mathbf{u}, \mathbf{x}) \\ \text{s.t.} \quad & x(i+1) = f(x(i), u(i)) \\ & z(i+1) = h(x(i+1)) \\ & u_{min} \leq u(i) \leq u_{max} \end{aligned} \quad (5-2)$$

In the multiple shooting solution [182], the argument is composed of the sequence of control inputs and the states of the system within the prediction window. Despite the higher computational cost, the multiple shooting method is more accurate and allows to include states boundaries on the cost function [183]. Due to these advantages, we explore the multiple-shooting method (Eq. (5-3)) in this work.

$$\begin{aligned} [u(\cdot); x(\cdot)] = \arg \min \quad & J(\mathbf{u}, \mathbf{x}) \\ \text{s.t.} \quad & x(i+1) = f(x(i), u(i)) \\ & z(i+1) = h(x(i+1)) \\ & x(k) = x_0 \\ & u_{min} \leq u(i) \leq u_{max} \\ & x_{min} \leq x(i) \leq x_{max} \end{aligned} \quad (5-3)$$

The implementation may be realized by some toolboxes, as, for example, MATLAB [184] and CasADi [181], which is an open-source software for optimization. This symbolic framework can be used to solve high flexible

optimization problems, especially optimal control ones, and, consequently, MPC, that are constrained by differential equations.

Specifically related to nonlinear systems, the NMPC algorithms solution may be obtained using CasADi, which includes some solver plugins for defining the local minimum of constrained optimization problems. The solution to NMPC optimization problems using CasADi is performed through a nonlinear program (NLP) and in this work is used the plugin Interior Point Optimization (IPOPT), which may be used on higher dimension problems, such MPC, with faster local convergence [181]. The NLP is solved through symbolic variables, using the Lagrange Multipliers method and the Karush-Kuhn-Tucker (KKT) conditions [43]. The implementation of the optimization problems used on NMPC and MHSE solutions is presented in detail in [43] and the complete information about the usage of CasADi for this purpose is available in [181].

5.2

Constrained Optimization Problems

Generally, a constrained optimization problem, as the presented for MHSE and MPC applications, may be formulated as:

$$\begin{aligned} \arg \min \quad & f(x) \\ \text{s.t.} \quad & g_i(x) = 0, \quad i = 1, \dots, p \\ & h_j(x) \geq 0, \quad j = 1, \dots, q \end{aligned} \quad (5-4)$$

The function $f(x)$ is called the cost or objective function, whose argument is the n^{th} -order vector x . The problem is constrained for p equality constraints $g_i(x)$ and q inequality constraints $h_j(x)$.

For the resolution of the optimization problem, a Lagrangian function must be defined, so that:

$$\mathcal{L}(x, \lambda, \mu) = f(x) - \sum_{i=1}^p \lambda_i g_i(x) - \sum_{j=1}^q \mu_j h_j(x) \quad (5-5)$$

in which λ_i and μ_j are called the Lagrange multipliers related, respectively, to equality and inequality constraints [185]. The feasible set Ω of the optimization problem is:

$$\Omega = \{x \mid g_i(x) = 0, \quad i = 1, \dots, p; \quad h_j(x) \geq 0, \quad j = 1, \dots, q\} \quad (5-6)$$

The first-order conditions, also known as Karush-Kuhn-Tucker (KKT) conditions, are presented in the following. These conditions are necessary, but not sufficient, for the existence of a local solution to the optimization problem.

Supposing that f , g_i , h_j are continuously differentiable, for a local solution $x^* \in \Omega$ of the Eq. (5-4), there is a set of Lagrange multipliers (λ^*, μ^*) so that the following conditions are satisfied:

$$\nabla_x \mathcal{L}(x^*, \lambda^*, \mu^*) = 0 \quad (5-7a)$$

$$g_i(x^*) = 0, \quad \text{for } i = 1, \dots, p \quad (5-7b)$$

$$h_j(x^*) = 0, \quad \text{for } j = 1, \dots, q \quad (5-7c)$$

$$\mu_j^* \geq 0, \quad \text{for } j = 1, \dots, q \quad (5-7d)$$

$$\lambda_i^* g_i(x^*) = 0, \quad \text{for } i = 1, \dots, p \quad (5-7e)$$

$$\mu_j^* h_j(x^*) = 0, \quad \text{for } j = 1, \dots, q \quad (5-7f)$$

The two last ones are known as complementarity conditions, which indicates that if the condition is active, that is equal to zero, the relative Lagrange multiplier is positive. If the condition is inactive, its Lagrange multiplier is zero. In summary, the value of each multiplier indicates the application of the condition [185].

The second-order conditions are the sufficient ones and are related to second derivatives of the Lagrangian. It may be proved that a feasible point x^* , for which a set of Lagrange multipliers (λ^*, μ^*) satisfy the KKT conditions, is a strict local solution for the optimization problem if:

$$w^T \nabla_{xx}^2 \mathcal{L}(x^*, \lambda^*, \mu^*) w > 0, \quad \forall w \in \mathcal{C}(x^*, \lambda^*, \mu^*), w \neq 0 \quad (5-8)$$

in which the set $\mathcal{C}(x^*, \lambda^*, \mu^*)$ (critical cone) contains the critical directions w for which it is not possible to define the direction of $\nabla f(x^*)$. Or:

$$w \in \mathcal{C}(x^*, \lambda^*, \mu^*) \Rightarrow w^T \nabla f(x^*) = \sum_{i=1}^p \lambda_i w^T \nabla g_i(x) + \sum_{j=1}^q \mu_j w^T \nabla h_j(x) = 0 \quad (5-9)$$

In summary, the sufficient condition is that the Hessian of the Lagrangian function must be positive-definite for all critical directions [185].

In this work, the main algorithm used for numerical solving of the constrained optimization problem is the Interior-Point Optimizer (IPOPT), which employs a point inside the feasible region to approximate the solution. The cost function is, then, replaced by a barrier function, which takes into account the inequality constraints, so that:

$$P(x, \rho) = f(x) - \rho \sum_{j=1}^q \log(h_j(x)) \quad (5-10)$$

Because of the barrier function definition, the closer the iterate solution

of the boundaries of feasible sets, the higher its value, tending to infinity. This prevents the iterate point to leave the feasible region. Besides that, as the solution is searched inside the feasible region, in which any constraint is active, the problem may be solved using unconstrained optimization methods [185].

5.3 Computational Algorithm

The algorithm for MPC implementation for control of dynamic systems is presented below:

- (i) Define the prediction window N and the weighting matrices Q , R and S ;
- (ii) Initialize the sample counting $k = 0$;
- (iii) Read the system states x_k at the current sample;
- (iv) Obtain the optimization problem solution, according to Single-shooting (Eq. (5-2)) or Multiple-shooting (Eq. (5-3)) formulations;
- (v) Apply the control action u_k on the open-loop system;
- (vi) Increment the sample counting $k = k + 1$;
- (vii) Return to step (iii).

Some comments must complement the information about the algorithm. Regarding the initialization parameters (item (i)), it is evident that the larger the prediction window, the higher the computational effort required for each sample. So, this parameter must be designed so that it corresponds to a prediction time proper for the dynamic system in question. The weighting matrices may be used for equalizing the dimensions of the variables, but also to prioritize or penalizes one or some of them. The higher the weight value of a variable, the higher its relevance to cost function.

In the third step (item (iii)), the system states must be completely defined, either through measurements or estimation. If not all states may be measured, one of the estimation methods presented in Chapter 4 must be applied. This set of states must be used on the first one-step prediction of the single-shooting method or as a constrain of the multiple-shooting one.

Regarding the control action (item (v)), it is important to remark that for both single-shooting and multiple-shooting formulation, only the control action related to the current sample is used. The remainder variables of the argument are used for the initialization of the algorithm in its next iteration.

Part III

Contributions

6

Nonlinear Grey-box Identification of a Landing Gear based on Drop Test Data

In many aircraft applications, especially on an antiskid control design, it is important to understand and consider the gear walk phenomenon, which is characterized by the deflection on the landing gear structure due to the high braking force acting at the tire contact with the ground. This phenomenon is observed on drop tests, and its prediction on landing gear design depends on an adequate evaluation of the equivalent stiffness and damping of the structure, which is difficult, since they depend on the mechanism configuration. In this paper, it is presented a grey-box identification methodology for estimating these parameters of the landing gear, based on simulated data of a drop test. As the drop tests are mandatory obligatory for certifying modern aircraft according to e.g. Federal Aviation Regulations (FARs) by the Federal Aviation Administration (FAA), we hope to introduce a method based on measurements that are available at the design phase. The method will be useful to decrease men/hour costs and increase reliability by enabling better and more accurate anti-skid design.

6.1

Problem Definition

Landing gears are critical parts of the hydromechanical subsystem of an aircraft. During braking, their purpose is to dissipate kinetic energy efficiently to ensure proper aircraft performance. The anti-skid system orchestrates braking given the inputs by the pilot. Its primary purpose is to avoid wheels to block and thus maximize brake efficiency. However, landing gears have rich nonlinear dynamics, which makes difficult the design of anti-skid control laws [186]. Torsional and translational vibrations are observed when the mechanical dynamics of such complex multi-body systems is measured. Shimmy happens when the torsional structural dynamics is poorly damped [187], while the gear walk phenomenon is observed when translational deflection amplitude in the landing gear is relatively high due to the braking force acting at the tire contact with the ground [57]. In aircraft braking simulations, we must efficiently evaluate or predict the gear walk phenomenon. The deflection observed during

gear walk is limited by the stiffness and damping of the ensemble composed of suspension and structure of the landing gear. In this context, it is of utmost importance to be able to model and simulate efficiently the aforementioned phenomena so that the design meets specified requirements.

6.2 Drop Test Simulations

For obtaining the data used on identification, the complete dynamics of the landing gear mechanism is simulated, such explained previously in the previous section. The simulation aims to reproduce the drop test. This test consists of simulating the moment the aircraft landing gear touches the ground, only with vertical movement. The initial conditions are set to be equal to the real test. So, the wheel receives an initial angular velocity, so that there is braking force and the ensemble is released from a certain height.

The dynamical equations are, then, numerically solved so that the generalized coordinates and their first derivatives are found. The accelerations associated with each coordinate must be estimated as:

$$\ddot{q}_k = \frac{\dot{q}_{k+1} - \dot{q}_{k-1}}{2\Delta t} \quad (6-1)$$

The tires are considered elastic elements, with internal damping. So, in the simulation, the vertical load is calculated as proportional to its vertical deformation and deformation rate. However, since the normal force on the ground is measured on drop tests, its value is computed in the simulation. Beyond that, the set of measured variables on the drop test includes also the vertical acceleration of the sprung mass and the vertical displacement of the wheel hub, which may lead to the angle between the suspension and the sprung mass, and its derivatives.

The simulations are performed considering dry asphalt as ground, for which the Burckhardt parameters ϑ_1 , ϑ_2 and ϑ_3 are, respectively, 1.2801, 23.99 and 0.52 [177].

The results of the simulation of the drop test, with the actual parameters are presented in the following section.

6.3 Results

In the present section, we describe the results of applying the grey-box estimation procedure for the landing gear case with simulated drop-test data. The present grey-box identification is based on simulated data from a landing gear drop test. The main goal is to determine the unknown parameters from the

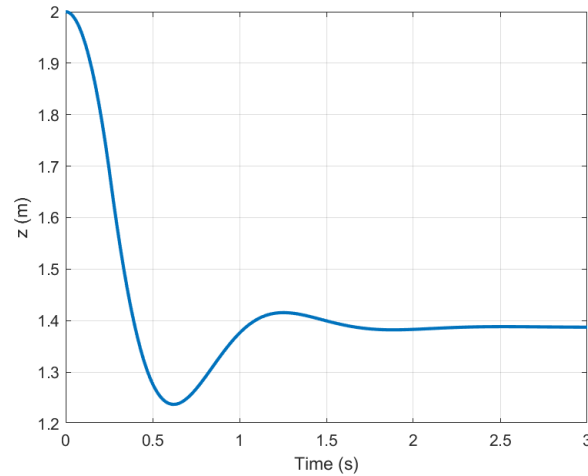


Figure 6.1: Vertical displacement of the sprung mass.

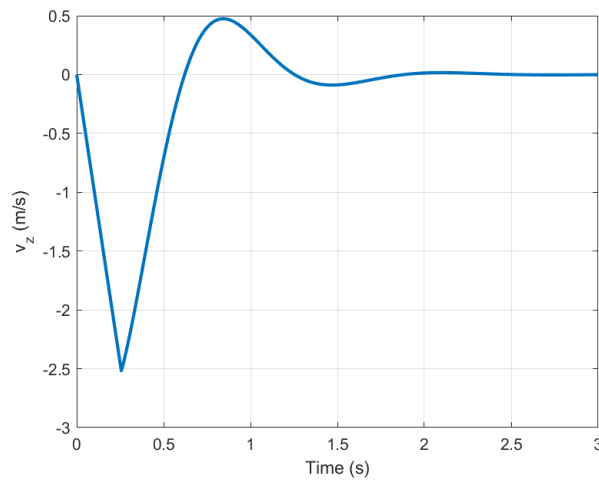


Figure 6.2: Vertical velocity of the sprung mass.

model, such as the inertial and, mainly, the equivalent damping and stiffness of the ensemble of suspension and structure of the landing gear.

The results of the dynamical equations are the shown in figures 6.1 and 6.2. As the landing gear structure works similarly to a vehicular suspension, it is expected that the z -coordinate of the sprung mass presents a damped oscillatory movement.

The angle θ , defined between the structure and the vertical axis, has a nonzero value initially and increases toward the maximum value when the wheel touches the ground and the tire force begins to actuate, producing a momentum that acts positively at this angle, as seen in Figure 6.3. The angle θ is limited by the stiffness of the structure and the suspension spring.

Since the dynamical equations of the landing gear are known, it is possible to write them as a matrix multiplication, such as presented on the Eq. (4-4), which is useful for the identification procedure:

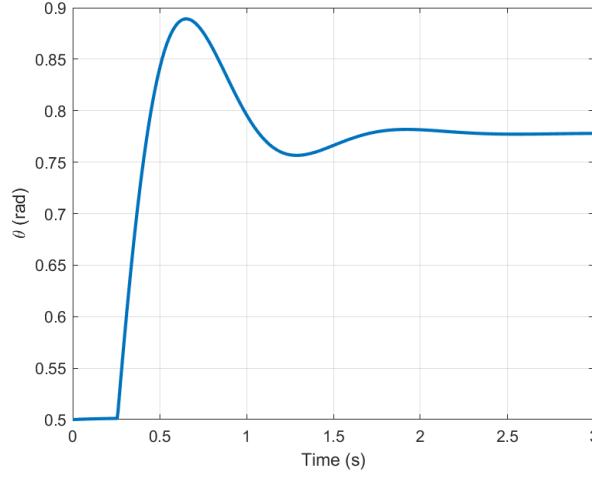


Figure 6.3: Angle between the vertical axis and the concentrated mass of the structure of landing gear.

$$\Phi = \begin{bmatrix} \ddot{x} & 0 & -\ddot{\theta} \cos \theta + \dot{\theta}^2 \sin \theta & 0 & 0 & 0 & 0 \\ \ddot{z} + g & 0 & -\ddot{\theta} \sin \theta + \dot{\theta}^2 \cos \theta & 0 & 0 & 0 & 0 \\ 0 & \ddot{\theta} & -\ddot{x} \cos \theta + \ddot{z} \sin \theta + g \sin \theta & \theta - \theta_0 & \dot{\theta} & 0 & 0 \\ 0 & 0 & 0 & 0 & 0 & \ddot{\phi} & \dot{\phi} \end{bmatrix} \quad (6-2)$$

$$\Theta = [M_1 \quad M_2 \quad M_3 \quad k \quad b \quad J \quad c]^T \quad (6-3)$$

$$F = \begin{bmatrix} 0 \\ F_z \\ F_z L \sin \theta + F_z \mu L \cos \theta \\ F_z \mu R - T \end{bmatrix} \quad (6-4)$$

Once it is supposed the vector on the right side is known, through measured or estimated variables, we may affirm that there are two decoupled systems, which are the sprung mass with suspension and the landing gear wheel. We may assume this because the parameters of each system do not affect the dynamics of the other, as observed in the matrix in Eq. (6-2). The parameters associated with the wheel are usually known or they may be easily measured, so that we may neglect the last equation and the parameters J and c in the identification process.

It is important to note that it is not possible to predict the mass, length and moment of inertia of each body, but only the combination of them, described by the parameters M_1 , M_2 and M_3 , in Eqs (3-37), (3-38) and (3-39). The set of estimated parameters should be as small as possible and any parameter should not be a linear combination of others.

We may also do a deduction related to the horizontal displacement of

the sprung mass. This variable remains so close to zero in all the simulation and the real drop test, because it is realized in a confined space. So, even if this variable is estimated, its value should be so small that could be lost in the associated noise, harming the identification process.

Consequently, the horizontal displacement of the wheel hub is also small, and the tire has a slip near to 1 in all the test. Given the above, the matrices described on Eqs (6-2), (6-3) and (6-4) may be adapted to:

$$\Phi = \begin{bmatrix} \ddot{z} + g & 0 & -\ddot{\theta} \sin \theta + \dot{\theta}^2 \cos \theta & 0 & 0 \\ 0 & \ddot{\theta} & -\ddot{x} \cos \theta + \ddot{z} \sin \theta + g \sin \theta & \theta - \theta_0 & \dot{\theta} \end{bmatrix} \quad (6-5)$$

$$\Theta = [M_1 \quad M_2 \quad M_3 \quad k \quad b]^T \quad (6-6)$$

$$F = \begin{bmatrix} F_z \\ F_z L \sin \theta + F_z \mu L \cos \theta \end{bmatrix} \quad (6-7)$$

Using all the data generated on the dynamics, the process of estimation becomes precise as the results show, reducing the error of estimation on both approaches. In the Kalman Filter estimation, the initial covariance matrix is defined as a diagonal matrix with 1E3 as entries. The estimated vector of parameters is initialized as zero. Table 6.1 presents the comparative analysis of the results, considering that there is no measurement noise.

Table 6.1: Estimation results without measurement noise.

Parameter (Unit)	Value	LS	LS Error (%)	KF	KF Error (%)
M_1 (ton)	10.2	10.2000	0.0002	10.2001	0.0005
M_2 (kg.m ²)	126	124.6235	-1.0925	124.6235	-1.0924
M_3 (kg.m)	150	151.8450	1.2300	151.8456	1.2304
k (kN/rad)	450	446.4083	-0.7981	446.4083	-0.7982
b (kN.s/rad)	90	89.8058	-0.2157	89.8058	-0.2157

The efficiency of the proposed method is evidenced by the small values of the errors of estimation. Since the main goal is to determine the angular stiffness of the ensemble suspension and structure, it is important to evaluate its error, which is less than 1% in terms of absolute value. The errors associated with inertial parameters are due to the approximations adopted in this methodology. However, as they are small, it may be affirmed that these approximations do not harm the estimation. It should be observed also that both approaches present similar results. So, the definition of which one must be used may follow criteria other than precision.

Considering that the measurement may be affected by noises, we present two additional results. In the first one, presented in Table 6.2, it is considered that the measured data has normal distribution with a standard deviation

of 0.1%. In the second one, presented on Table 6.3, the standard deviation adopted is 1%.

The errors associated with estimated parameters, including stiffness and damping of the landing gear, have the same magnitude as the case without noise. These errors are small and adequate, which denotes that the proposed methodology remains efficient, even if there are measure noises associated with the sensors.

Table 6.2: Estimation results with measurement noise of 0.1%.

Parameter (Unit)	Value	LS	LS Error (%)	KF	KF Error (%)
M_1 (ton)	10.2	10.2000	0.0002	10.2000	0.0005
M_2 (kg.m ²)	126	124.6341	-1.0841	124.6341	-1.0841
M_3 (kg.m)	150	151.9179	1.2786	151.9184	1.2790
k (kN/rad)	450	446.3996	-0.8001	446.3996	-0.8001
b (kN.s/rad)	90	89.8052	-0.2164	89.8052	-0.2164

Table 6.3: Estimation results with measurement noise of 1.0%.

Parameter (Unit)	Value	LS	LS Error (%)	KF	KF Error (%)
M_1 (ton)	10.2	10.2001	0.0008	10.2001	0.0011
M_2 (kg.m ²)	126	124.6797	-1.0478	124.6797	-1.0478
M_3 (kg.m)	150	156.4681	4.3121	156.4687	4.3125
k (kN/rad)	450	445.6982	-0.9560	445.6982	-0.9560
b (kN.s/rad)	90	89.7471	-0.2810	89.7471	-0.2810

It may be observed that in the second scenario the precision of the estimation of inertial parameters is worse than in the other cases, especially for the parameter M_3 , but the error is not considerable (less than 5%). However, the stiffness and damping of the suspension of the landing gear are estimated with errors of the same magnitude as the ones observed in the noise-free scenario, which leads to conclude that the methodology proposed is robust, even if the sensors have no measurement noise. These parameters are the main ones in the analysis of the gear walk phenomenon.

Figure 6.4 shows a comparison between the measured and simulated data for the angle of the structure, using parameters estimated presented in Table 6.3.

6.4 Discussion

This contribution presented a methodology that may be used in the identification of structural stiffness and damping parameters of landing gears, which is demonstrated to be effective even in scenarios with different scales

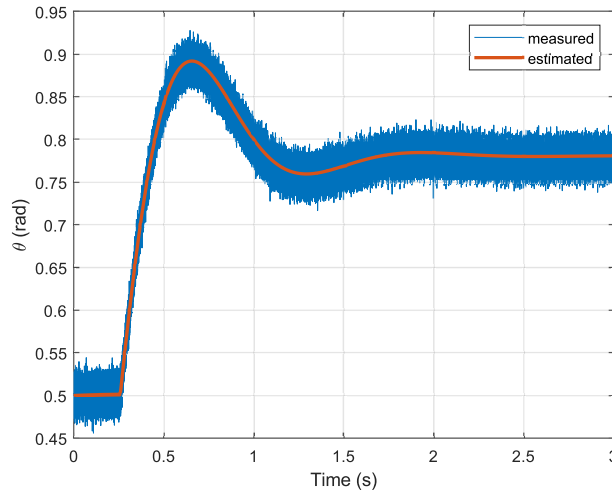


Figure 6.4: Comparison between measured and estimated angle of the landing gear structure.

of measurement noise. The errors presented are not harmful to the gear walk prediction, and, consequently to the application for braking systems design.

A possible improvement in the methodology is the association with state estimators, for observing the variables that are not measurable, which must enlarge its range of application and make viable the application with real drop test data.

Other future possibilities are related to using different modeling techniques, such as bond graphs [188], which enables modularity to dynamic modeling and makes easier the modeling and integration of systems with a high number of subsystems, such as aircraft.

Finally, it is important to mention that the accurate estimation of time-invariant parameters depends on the identifiability of the system, which assures that the set of parameters is unique for a given set of measurements [189]. In the case evaluated, as the results are accurate, we may infer that the system is identifiable. But for more complex systems, with a higher number of estimated parameters, this property must be previously evaluated.

7

Comparison of Nonlinear Receding-Horizon and Kalman Filter Strategies for Ground Vehicles Longitudinal Slip Estimation

Friction efforts are present in almost all mechanical applications, due to contact between bodies and there are many important situations, in which they must be properly controlled. Among these, there are tire contact forces, which are the focus of many studies in autonomous vehicles and control applications on vehicle systems, since the tire forces and moments are nonlinear and may be modeled as friction efforts. Any control synthesis focused to optimize its performance must be associated with state estimators, since efforts depend on slip variables, such as longitudinal slip and sideslip angle, and it is not possible to accurately measure them. So, in this contribution, three state estimation algorithms are evaluated: EKF, UKF and MHSE, which are applied to a quarter-car model for longitudinal dynamics. It is presented that, for both traction and braking phases, the MHSE is more accurate, since it takes explicitly into account the nonlinear model in the estimation process, independently of Jacobian sensitivities to discontinuities as is the case here, but UKF presents a good cost-benefit ratio, since their results are much better than EKF, with lower processing times. So, it is demonstrated that the developed estimators may be successfully associated with controllers with the objective of optimizing tire performance in traction and braking control.

7.1

Problem Definition

In many mechanical applications, friction interactions are commonly found, once there is usually contact between bodies. In most cases, these interactions have a nonlinear nature, which difficult any attempt to control the system performance or mitigate their effects, when harmful. Coulomb friction, tire-road forces in vehicles and bit-rock interaction in the perforation process are some examples of these effects.

However, in control applications, it is not commonly possible to measure all states or all controlled variables. In these situations, it is usually used a state observer, which has as function to estimate the states based on the measured variables. Among the state estimation algorithms, the Kalmar Filter

(KF) is one of the most known, such as its versions applied to nonlinear systems, the EKF and the UKF [17]. In the last decades, other algorithms have been developed, looking for more robustness and accuracy. The Moving Horizon Estimation (MHE) is one of these, defined by [22] as a powerful and robust approach, suitable in systems with modeling uncertainties and numerical errors. It was developed as a dual of Model Predictive Control and estimates the states variables using a defined horizon of recent information and measures. These algorithms are studied in many different applications [23], so that it is possible to clearly understand their power and robustness.

In vehicle systems, nonlinear observers are implemented on many control applications, but we may specially remark those dependents on tire dynamics, such as braking, traction and stability control. In most applications, the controlled variables, usually longitudinal slip, attitude angles, sideslip angle and others are impossible to measure, which justifies the implementation of observer-based control.

7.2

Simulation and Results

The quarter-car model, presented in Section 3.3, is simulated with the parameters of a typical passenger vehicle, moving on dry asphalt. To evaluate the system and the estimators, its dynamics is simulated considering an input torque defined with a proportional control law, so that the vehicle must track a reference speed of $20m/s$. Then the input traction torque is defined as:

$$T = k_p(v_{ref} - v) \quad (7-1)$$

In the simulations, we consider that the output variable, that is the wheel rotation, presented in Figure 7.1, is measured with a gaussian white noise (ξ_n). So, the main objective of the estimators is to obtain the states along the time, based on this measured one. In a first analysis, we consider that initial conditions are well-known and that there is a measurement noise (ξ_n) with normal distribution and standard deviation of 1%, and these results are demonstrated in Table 7.1. The results for longitudinal slip are presented on Figures 7.2 and 7.3. We may remark that the non-measured variables are estimated with good accuracy, especially the longitudinal slip, which is important in traction control and stability applications.

We must do two remarks about these results. The first one is related to slip estimation. As there is no relation between the definition of input torque and slip, the initial values of longitudinal slip are very high, which is represented by the situation of the wheel slipping on the road (Figure 7.1).

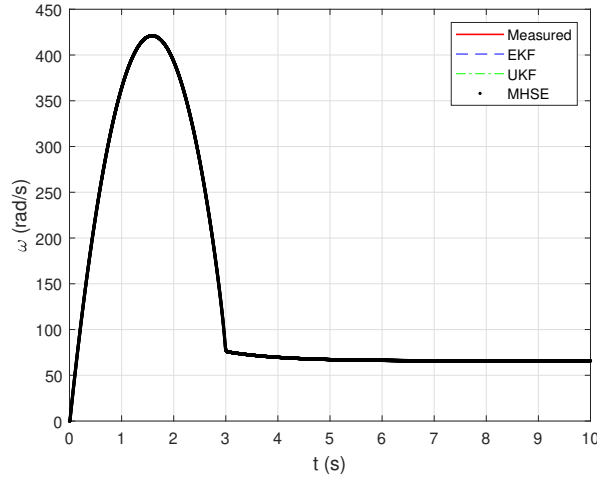


Figure 7.1: Estimated wheel rotation (rad/s).

Table 7.1: RMSE results with well-known initial conditions.

State	EKF	UKF	MHSE
λ	1.1005	0.8487	1.9675E-4
v	0.0233	0.0012	0.0022

In a second phase, the rotation falls, reducing the longitudinal slip to values between 0 and 1 (details in Figure 7.2).

The second remark is related to the Jacobians. The state equation related to the longitudinal slip presents many discontinuities points, mainly related to situations in which the velocity is zero. In this way, when this state is very low, the Jacobian F presents high values, harming the estimation process and also compromising the convergence of the Extended Kalman Filter. To prevent this situation, the same constraints applied to state variables are applied during the estimation process. As UKF and MHSE do not depend on derivatives, they are not affected by this situation and, so, their results are much better, presenting high relative reductions on RMSE. It is important to remark that the states are estimated based on a noisy signal and compared with the supposed real one, which is noiseless. It is remarkable also the nearest values presented by the MHSE result (details in Figure 7.3).

In other analysis, we may realize the estimation process with supposed unknown initial conditions, defined by uniformly distributed random values on the interval $[0, 1]$, many times. This way, it is possible to observe its tendency in more sampled data and to verify if the estimators are capable to correct states even if the initial conditions are badly defined or unknown.

Table 7.2 presents the evaluation of the mean and the standard deviation of the ARMSE for longitudinal slip (λ), which is one of the non-measured states and is used on control strategies. In this table are presented the

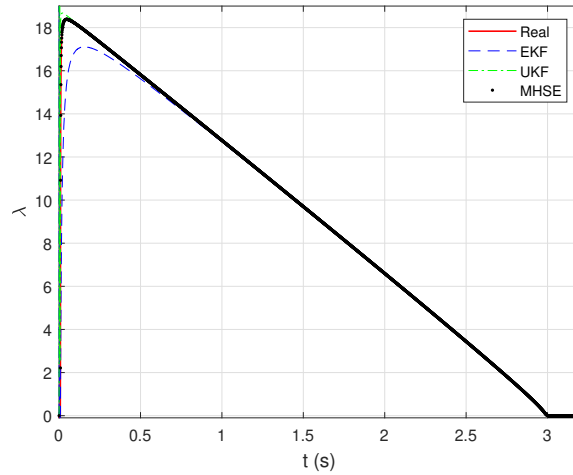


Figure 7.2: Estimated longitudinal slip.

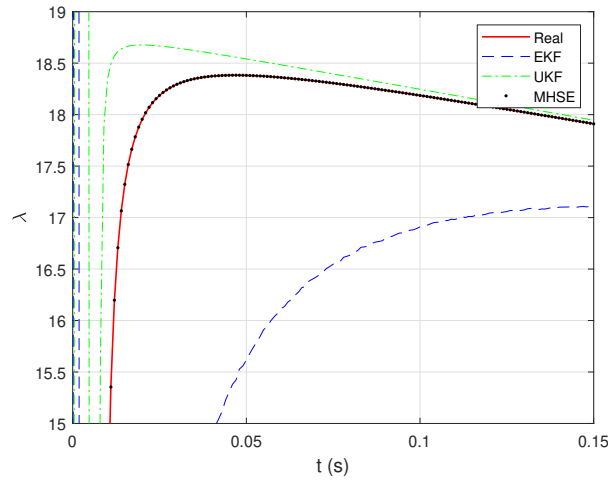


Figure 7.3: Estimated longitudinal slip, in detail.

simulation results for different noise standard deviations, after the convergence of $RMSE(t)$, previously defined as ARMSE (equation (4-47)).

We may observe in Table 7.2 that MHSE is more robust in the presence of white-noise, since its ARMSE mean and standard deviation are lower than the ones of EKF and UKF. Meantime, it is important to remark that UKF results are closer to MHSE ones than EKF ones, which leads us to understand that UKF algorithm may be used on applications in which high precision is not required, with a low processing time (Table 7.3). A more detailed analysis may be done interpreting the $RMSE(t)$, as defined by equation (4-46), and that is presented on Figure 7.4, Figure 7.5 for, respectively, standard deviations of 0.001 and 0.05 on the measurement noise.

The last analysis we may do concerns the elapsed time for each simulation process, which may be observed in Table 8.4.

We must remark that processing time is an advantage of Kalman filter

Table 7.2: ARMSE analysis for longitudinal slip (λ) estimation.

Algorithm		EKF	UKF	MHSE
$\xi_n = 0$	Mean	0.0137	4.8384E-7	6.9993E-16
	St Dev	1.3726E-4	3.3247E-9	2.8315E-18
$\xi_n = 0.001$	Mean	0.0075	6.0831E-5	3.3039E-5
	St Dev	2.2511E-4	3.4296E-5	1.8912E-5
$\xi_n = 0.01$	Mean	1.7319	6.0332E-4	3.2287E-4
	St Dev	0.8505	3.3201E-4	1.9260E-4
$\xi_n = 0.05$	Mean	0.0143	0.0033	0.0016
	St Dev	0.0024	0.0018	9.1652E-4
$\xi_n = 0.1$	Mean	0.9619	0.0082	0.0041
	St Dev	0.0773	0.0051	0.0027

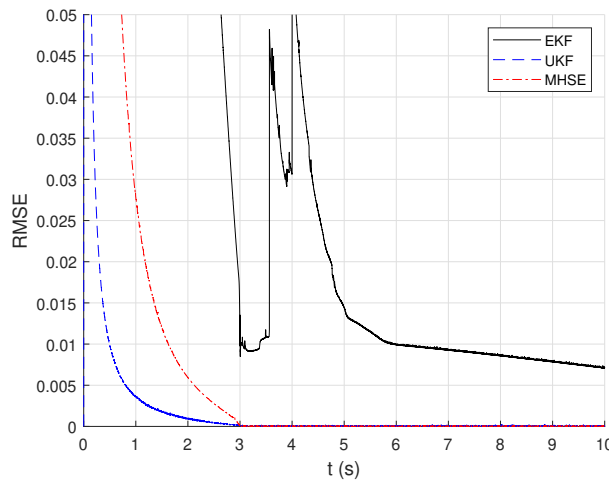


Figure 7.4: RMSE(t) for measurement noise of 0.1%.

strategies, since they depend only on model order and do not measure noise. MHSE processing time increases as the white-noise increases, but in KF approaches it remains similar. Due to white noise on measures, the states may change beyond the predicted by the mathematical model, harming the optimization process and time processing. These variations affect the KF algorithms only on the update of state estimation, which is performed by a matrix operation and does not affect elapsed time.

7.3 Discussion

We may observe, from the results, the efficiency of the MHSE, in comparison to EKF and UKF, for state estimation in nonlinear applications, especially with friction and discontinue efforts. In the studied case, all the algorithms estimate the non-measured states. However, when the system is subjected to measurement errors and uncertainties in its initial conditions, the

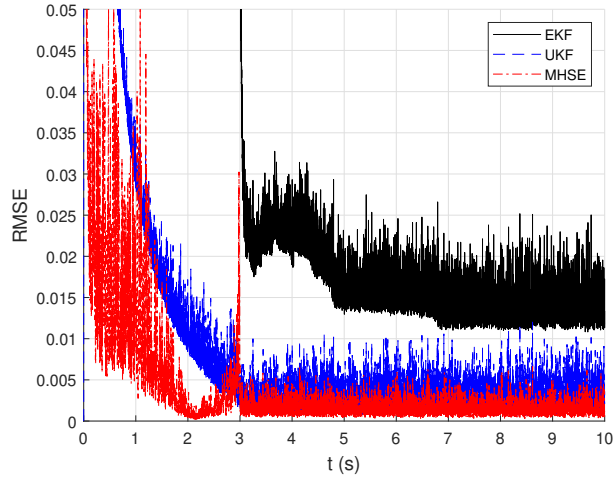


Figure 7.5: RMSE(t) for measurement noise of 5%.

Table 7.3: Mean time for simulation (s).

Case	EKF	UKF	MHSE
$\xi_n = 0$	0.1892	0.6080	12.2751
$\xi_n = 0.001$	0.1828	0.5888	24.2039
$\xi_n = 0.01$	0.1825	0.5875	25.9196
$\xi_n = 0.05$	0.1820	0.5874	28.5576
$\xi_n = 0.1$	0.1839	0.5910	30.3289

MHSE presents more accurate and robust results. It is important to remark that the results of UKF demonstrate its good cost-benefit ratio, since its results are relatively good, with lower processing time.

The main future possibilities derived from this contribution are related to the application of the MHSE in more complex vehicle systems, especially those comprising the lateral dynamics or with simultaneous time-varying parameters estimation.

Another possible research is the association of the MHSE observer with control laws for autonomous or highly automated vehicles. Due to its proven accuracy, the MHSE may be useful for control systems aiming for improved efficiency and safety, and reduced energy consumption.

Tire-road Friction Coefficient Estimation Using Nonlinear Receding-Horizon and Kalman Filter Strategies

In vehicle control applications, the use of estimation algorithms is necessary since some states and parameters are not measurable. Even on highly instrumented vehicles, tire-road interaction parameters must be estimated, once they may easily change and depend on road conditions and quality. For vehicle longitudinal control using model-based laws, such as model predictive control, optimal performance is related to informing accurate and current values of friction coefficient. In this way, this paper aims to evaluate nonlinear approaches for friction coefficient estimation, using an augmented states formulation for the vehicle model, not explored in the literature thus far. We compare three nonlinear observers: EKF, UKF and MHSE. The algorithms are evaluated with simulated and experimental data. In the former case, the results demonstrate the MHSE robustness, even under noisy measures. The latter case shows that all approaches can be applied with the augmented states proposed approach, though Kalman Filter ones have a more sensitive and difficult calibration, which makes their performance deteriorate, while MHSE has fewer design parameters and overall better results. We conclude that MHSE presents a high potential for application on vehicle control and estimation, with the use of the herein proposed augmented states formulation for friction and states joint estimation.

8.1

Problem Definition

In the present contribution, we propose a receding-horizon algorithm for the estimation of μ_p , based on the longitudinal dynamics of vehicles. The motion equations consider the friction efforts produced by tires, which are characterized by their nonlinearity and the discontinuity of derivatives and Jacobians. This parameter is hardly obtained by experiments and may change similarly to an uncontrolled disturbance in the system. Besides that, a current and proper value is required on model-based control laws, so that they may be optimized. In this way, an augmented states approach for the estimation algorithms may be useful, so that states and parameters are simultaneously

estimated.

Therefore, the possible solution presented is the application of nonlinear estimation algorithms, specially MHSE, which is expected to present better results, and be more robust and flexible, accordingly to the literature. The studied observers must be evaluated employing simulated and experimental datasets.

8.2 Dataset Description

The dataset used for the experimental analysis is made available by the authors of [116] and [190] and refers to an experimental vehicle developed at Bucknell University. This vehicle has rear traction, performed by two independent in-wheel electric motors and steerable wheels on the front axle. A schematic model of the vehicle, with the variables, is presented in Figure 8.1.

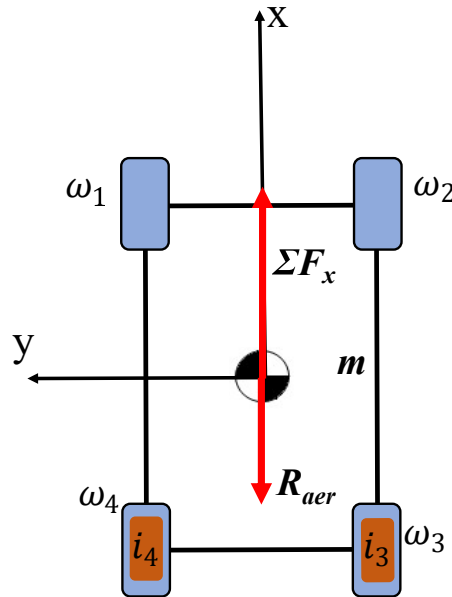


Figure 8.1: Schematic Model of the Vehicle.

The vehicle is also equipped with instruments, such as encoders on wheels hubs and steering motors, an inertial measurement unit (IMU), Global Positioning System (GPS) and force gauges. In this paper, only the variables related to longitudinal dynamics are used, since there are some maneuvers in which the initial path is a straight line.

The variables used in this paper are the angular velocity of the wheels, the longitudinal velocity of the vehicle (Figure 8.2) and the current on the wheel traction motors (Figure 8.3). These data are preprocessed, so that they are filtered and treated, for application on the estimation algorithms. Besides that, a clipping of the data is taken, so that the vehicle longitudinal velocity

is positive, but near to zero and the input current is different to zero. This is necessary to ensure the observability of the system on the first samples.

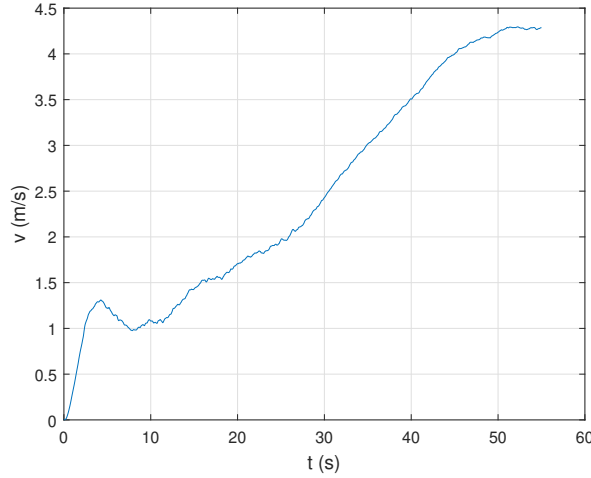


Figure 8.2: Longitudinal velocity of the vehicle (m/s).

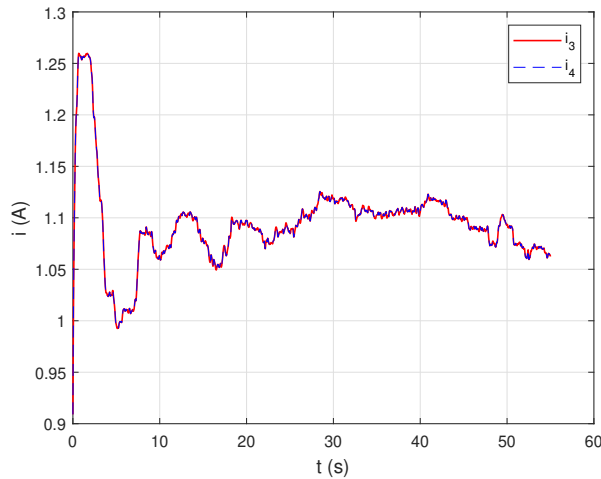


Figure 8.3: Current at electric motors (A).

Remarkably, most of the vehicle parameters are known, but the tire-road friction coefficient is not known and may be easily changed because of many circumstances. Therefore, this parameter and states are intended to be estimated, as presented in Section 8.3.

8.3 Proposed Approach

Using equations (3-23) and (3-24), and considering the peak value of friction coefficient μ_p as a state, with slower dynamics related to other ones, we obtain the continuous-time nonlinear state-space equations of the system.

$$\mathbf{x} = [v_x \ \omega_1 \ \omega_2 \ \omega_3 \ \omega_4 \ \mu_p]^T \quad (8-1)$$

$$\mathbf{u} = [i_1 \quad i_2 \quad i_3 \quad i_4]^T \quad (8-2)$$

$$\dot{\mathbf{x}} = \mathbf{f}(x, u) = \begin{bmatrix} \frac{1}{m} \sum_{i=1}^4 \mu_p p(\lambda_i) F_{z_i} - cv^2 \\ \frac{K_t i_1}{J} - (\mu_p p(\lambda_1) + f_R) \frac{r F_{z_1}}{J} \\ \frac{K_t i_2}{J} - (\mu_p p(\lambda_2) + f_R) \frac{r F_{z_2}}{J} \\ \frac{K_t i_3}{J} - (\mu_p p(\lambda_3) + f_R) \frac{r F_{z_3}}{J} \\ \frac{K_t i_4}{J} - (\mu_p p(\lambda_4) + f_R) \frac{r F_{z_4}}{J} \\ 0 \end{bmatrix} \quad (8-3)$$

$$\mathbf{z} = \mathbf{h}(x) = [v_x \quad \omega_1 \quad \omega_2 \quad \omega_3 \quad \omega_4]^T \quad (8-4)$$

Note that the augmented states formulation assumes that the dynamics of the unknown changes of μ_p occur slowly concerning the rest of the system states. As a further simplification of the physical phenomenon, it is a necessary step as the changes in friction are independent of other states. It will affect the estimation process assuming that the friction coefficient does not vary within the prediction horizon, which for small enough sampling rates is reasonable. This is however not detrimental as the estimator can be tuned to respond quickly to such changes and by using the augmented states formulation we can use the aforementioned nonlinear state estimation methods to obtain the resulting friction that better fits the state evolution in time.

8.4 Results

In this section, we present the results of the use of the aforementioned observers for friction coefficient estimation. The parameters used on the estimation algorithms, for both simulation and experimental analysis, are presented in Table 8.1. The algorithms are implemented and executed on MATLAB, using a Windows PC with 32 GB RAM and i7 processor with 2.6 GHz.

Table 8.1: Vehicle Parameters.

Parameter	Value
m	1724 kg
r	0.3 m
c	0.5 m ⁻¹
f_R	0.01
J	2.5 N.m/s ²
K_t	50 N.m/A
C_2	2.5
C_3	6
C_4	1

In the simulation environment, the results presented are the RMSE error of states and parameter estimation, besides the ARMSE of multiple simulations with unknown initial conditions and measurement noise, for evaluating the robustness and convergence of the estimation. For an experimental dataset of an EV, the results are the RMSE for state estimation and a comparison of the friction coefficient estimated by each algorithm.

8.4.1 Simulation Environment Estimation Results

The longitudinal dynamic model is simulated with the same parameters of the vehicle subjected to experimental tests presented on the Subsection 8.4.2 [116, 190]. For evaluating correctly the methodology, the inputs of the simulated system are the same as the experimental data, presented in Figure 8.3 and the initial velocity of the vehicle is defined as $1m/s$, while the wheels are supposed to be in free rolling. It is important to note that the front wheels are not motorized, so that their input currents are null.

We must also observe that the continuous-time system equations must be transformed into a discrete-time ones. For this purpose, a 4th-order Runge-Kutta algorithm is used for calculating one-step predictions of the state equation, aiming to improve the accuracy of the integration.

The first step of all algorithms is the calibration of the initialization parameters, such as covariance matrices P , Q and R of Kalman Filter approaches, the window size N and the weighting matrices of the MHSE. For EKF and UKF algorithms, many researches are focused on this task, as well as in adaptive approaches. In this paper, after exhaustively trying to find the best set of parameters through trial-and-error, we have selected the following initialization matrices for EKF:

$$P = \text{diag}([1E + 5 \quad 1E + 3]) \quad (8-5)$$

$$Q = \text{diag}([1E + 3 \quad 1E + 3]) \quad (8-6)$$

$$R = \text{diag}([1E + 4 \quad 1E + 4 \quad 1E + 4 \quad 1E + 4 \quad 1E + 4]) \quad (8-7)$$

Using the same methodology, the calibrated matrices for UKF algorithm are defined as presented below:

$$P = \text{diag}([5E - 1 \quad 5E - 1]) \quad (8-8)$$

$$Q = \text{diag}([1E - 5 \quad 1E - 5]) \quad (8-9)$$

$$R = \text{diag}([1E - 4 \quad 1E - 4 \quad 1E - 4 \quad 1E - 4 \quad 1E - 4]) \quad (8-10)$$

As a first analysis with simulated data, the MHSE is calibrated without different weights for each portion, considering that the measures are accurate. So, the matrices P and Q of MHSE cost function (Eq. (4-38)) are defined as identity. Besides that, we define that the size of the observing horizon is of 10 samples.

To demonstrate the correct estimation of the peak value of the friction coefficient, we simulate a situation in which the vehicle drives through a region with a time-varying friction coefficient. The result of the estimation of this parameter is presented in Figure 8.4.

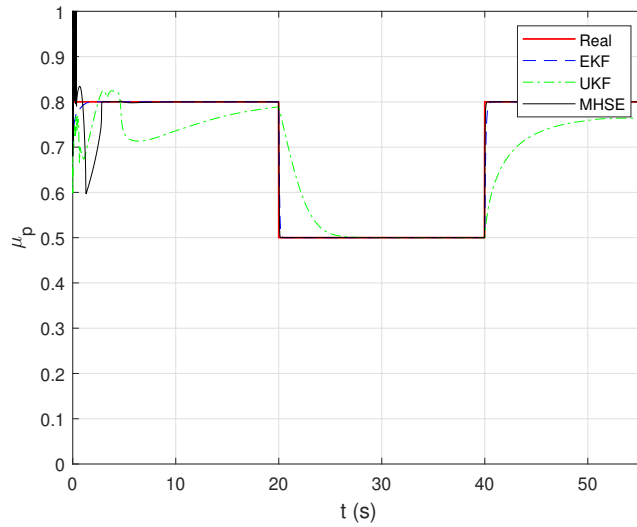


Figure 8.4: Peak value of coefficient of adherence (μ_p , dimensionless).

It is possible to identify that EKF and MHSE have adequate results, but with different convergence times. The UKF results may indicate a possible use, but its convergence is slower. MHSE presents an accurate and quick result, both in the beginning and in road condition changes on simulations, which indicates its efficiency.

Another interesting remark we must do is about the range of the longitudinal slip during the simulation. We observe that this variable, presented in Figure 8.5 remains in lower values, near to zero, in a region in which the observability may be harmed. However, the simulation results indicate that the proposed observer can correctly estimate the friction coefficient even under this

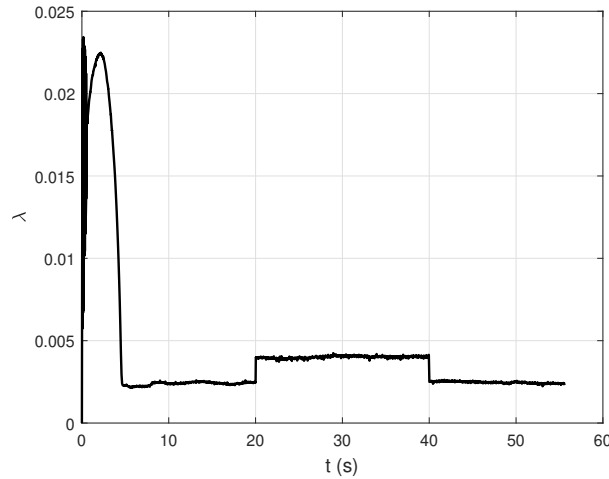


Figure 8.5: Longitudinal slip of the wheel 4, on simulation environment.

condition. This result is important, because the experimental vehicle operates in low velocities, and consequently, with low longitudinal slip.

These results may be also analyzed by employing the RMSE and ARMSE. Some results of RMSE may be misinterpreted, due to oscillations during the time elapsed until convergence. In this case, the ARMSE analysis may be more appropriate, since it evaluates the error after a defined time. The results of ARMSE are presented on Table 8.2. It is important to observe that all estimators present accurate results, but MHSE is the better one. Only the results for the 4th wheel are presented in this section, but they reflect the results of other wheels.

Table 8.2: ARMSE results for simulated data, considering no noise.

State	EKF	UKF	MHSE
v	2.9837E-17	1.4320E-04	1.3433E-05
ω_4	7.3171E-17	0.0021	2.8622E-04
μ_p	9.2328E-16	0.0428	4.5201E-05

In a second analysis, we simulate that system outputs are measured data with a gaussian white-noise, for evaluating the robustness of all algorithms. The kind of vehicle on which this research is based is usually equipped with encoders on wheels, so that the angular velocities measures are relatively accurate. On the other hand, vehicle velocities are estimated through GPS and IMU-based measures, which may be inaccurate.

For evaluating the robustness of each algorithm against different measure errors on the velocity, the simulations are performed with gaussian noises associated with vehicle longitudinal velocity measures. These simulations are executed many times, so that we may analyze the RMSE for each sample and

also the ARMSE, in the convergence region. As we suggest that there is an error on velocity measures, the matrix Q of the MHSE (Eq. (4-38)) must be changed, to penalize this output. So, in these simulations, it is defined as:

$$Q = \text{diag}([1E - 1 \quad 1 \quad 1 \quad 1 \quad 1]) \quad (8-11)$$

The results on all evaluated cases are presented in table 8.3. When no noise is associated with the vehicle velocity, the ARMSE mean of EKF is better than the MHSE one, but this is acceptable and adequate, due to its small value. Meantime, when measurement errors are associated with vehicle velocity, the estimation of μ_p performed by MHSE is better than EKF, demonstrating its capacity and robustness under unfavorable situations. Both mean and standard deviation of MHSE results are better, which demonstrates that the convergence of MHSE is more appropriate, besides its accuracy.

Table 8.3: ARMSE analysis for friction coefficient (μ_p) estimation.

Algorithm		EKF	UKF	MHSE
$\xi_n = 0$	Mean	1.3112E-15	0.0360	5.6082E-05
	St Dev	1.6324E-15	1.6373E-04	9.7575E-06
$\xi_n = 0.001$	Mean	2.0421E-04	0.0331	6.1443E-05
	St Dev	1.1845E-04	2.3971E-04	3.2034E-05
$\xi_n = 0.01$	Mean	0.0046	0.0585	3.6487E-04
	St Dev	0.0020	0.0128	1.7865E-04
$\xi_n = 0.05$	Mean	0.1019	0.2331	0.0019
	St Dev	0.0239	0.0861	0.0010

Regarding processing time (Table 8.4), we may observe that MHSE has its computational cost as a disadvantage, when compared with Kalman Filter approaches. Comparing the values to the sampling time of the data (0.002s), we note that EKF and UKF may be used on online applications. The MHSE, however, must be performed on better processors, enabling its real application in high-performance control and estimation.

Table 8.4: Mean time for sample on simulations (s).

Case	EKF	UKF	MHSE
$\xi_n = 0$	3.9275E-04	9.3092E-04	0.0127
$\xi_n = 0.001$	4.8989E-04	9.8426E-04	0.0126
$\xi_n = 0.01$	4.3793E-04	0.0011	0.0131
$\xi_n = 0.05$	3.8692E-04	8.4768E-04	0.0136

8.4.2

EV Estimation Results

The previously presented is also evaluated with experimental data. These data are made available in [116, 191] and the algorithms are applied, to estimate the friction coefficient of the road the vehicle has passed. For the experimental vehicle, data used in this analysis are the current on in-wheel electric motors (inputs of the system) and the wheel rotation and the longitudinal velocity of the vehicle (outputs), measured, respectively by encoders and inertial measurement units. The vehicle presents traction only on the rear wheels, such as the vehicle model presented in Section 8.2.

In this way, the model presented in simulation results may be validated with the previously mentioned experimental data. Due to the characteristics of the signals and looking for better performance, it is important to adjust the initialization of the matrices and parameters of MHSE. So, for EKF, initialization matrices are:

$$P = \text{diag}([1\text{E} + 6 \quad 1\text{E} + 5 \quad 1\text{E} + 5 \quad 1\text{E} + 5 \quad 1\text{E} + 5 \quad 1\text{E} + 4]) \quad (8-12)$$

$$Q = \text{diag}([1\text{E} + 3 \quad 1\text{E} + 3]) \quad (8-13)$$

$$R = \text{diag}([1\text{E} + 4 \quad 1\text{E} + 4 \quad 1\text{E} + 4 \quad 1\text{E} + 4 \quad 1\text{E} + 4]) \quad (8-14)$$

The calibrated matrices for UKF are defined as:

$$P = \text{diag}([1 \quad 1 \quad 1 \quad 1 \quad 1 \quad 1]) \quad (8-15)$$

$$Q = \text{diag}([1\text{E} - 4 \quad 1\text{E} - 4]) \quad (8-16)$$

$$R = \text{diag}([1\text{E} - 3 \quad 1\text{E} - 3 \quad 1\text{E} - 3 \quad 1\text{E} - 3 \quad 1\text{E} - 3]) \quad (8-17)$$

Due to the usage of experimental data, and the inaccuracy of the longitudinal velocity measurements, based on GPS and IMU devices. The first weight matrix must be designed considering the reliability of the dynamic model and to avoid high oscillations in the friction coefficient estimation. So, the selected weight matrix is defined as:

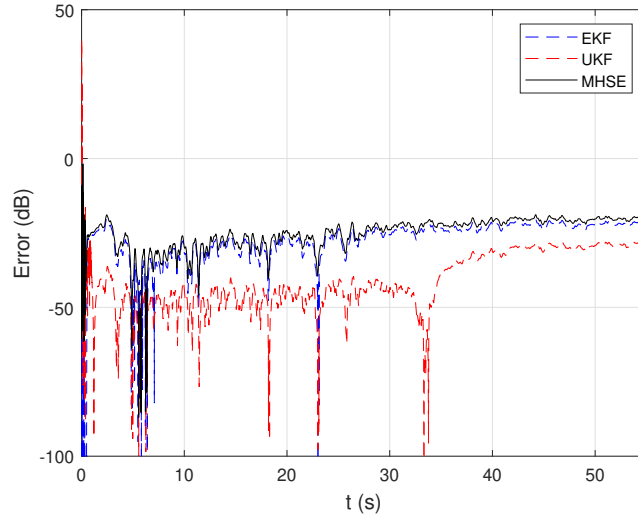


Figure 8.6: RMSE(t) of estimation of longitudinal velocity of the vehicle (dB).

$$P = \text{diag}([1 \quad 1 \quad 1 \quad 1 \quad 1 \quad 1E + 2]) \quad (8-18)$$

About the second weight matrix, it must be defined so that higher values are associated with the most reliable measures. In this case, the higher entries must be associated with the angular velocities and a lower one to the longitudinal velocity. Therefore, the second matrix Q is defined as:

$$Q = \text{diag}([1E - 1 \quad 1 \quad 1 \quad 1 \quad 1]) \quad (8-19)$$

The estimation process may be evaluated by the RMSE of the states that are also outputs of the system. So, the estimation errors, in dB, of longitudinal vehicle and rotation of the wheel 4 are presented on Figures 8.6 and 8.7.

We observe that all algorithms present relatively good convergence to the outputs, but it is remarkable that the MHSE presents the best result for the angular velocity, which is desirable due to the accuracy of this measure. Although the convergence to the longitudinal velocity, we note that its result is worse, which, in this case, indicates that the algorithms can bypass the errors in the measures, improving the accuracy of the friction coefficient estimation.

The friction coefficient μ_p estimation result is presented in Figure 8.8. We should note that the algorithms do not present the same value on each sample, but have similar magnitudes. We remark that there is no reference value for this result since this parameter is unknown on the experimental dataset used in this estimation. Different from the Kalman-based algorithms, the MHSE result is smoother and without oscillations, which is more appropriate for control applications.

We may also note that the experimental vehicle used for data obtaining travels with reduced velocity and acceleration, which indicates relatively low

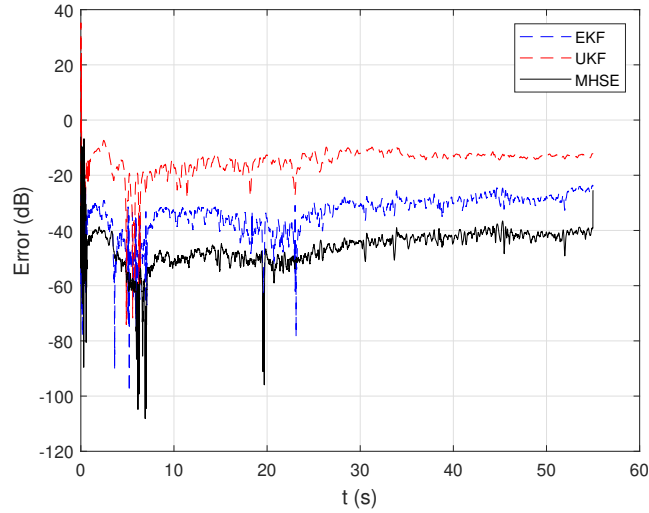


Figure 8.7: RMSE(t) of estimation of angular velocity of the wheel 4 (dB).

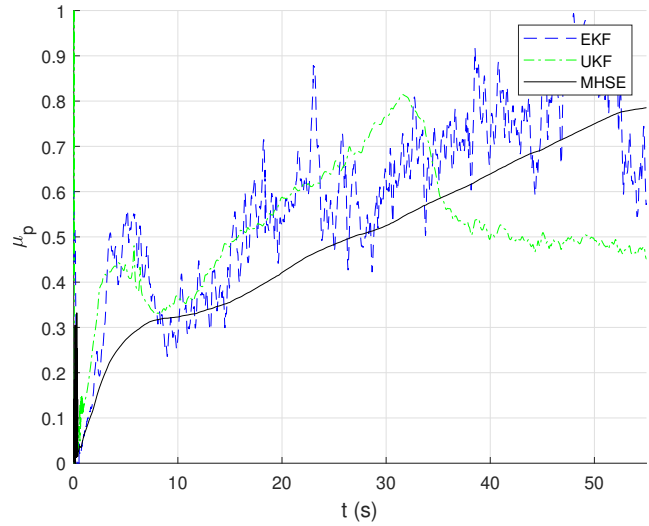


Figure 8.8: Estimated value of coefficient of adherence.

longitudinal slip. Meantime, as the outputs present convergence, we may deduce that the values presented are suitable according to road conditions and employing them on mathematical models should present accurate results for some tasks such as traction and braking control and path tracking. Besides that, The lower RMSE values of states estimation indicate that MHSE results for friction coefficient must be considered most reliable. It is important to note, that, augmented states are limited to physical bounds, so that the parameter estimation is saturated at its maximum value on the last third of simulation time.

8.4.3

Discussion

From the results presented in the previous subsections, we must elaborate on some observations about the research. The first one is related to the efficiency of the proposed algorithms. We may observe that all can present adequate estimation results, but EKF and UKF are more susceptible to covariance matrices initialization, besides the discontinuities on Jacobians and derivatives, in the first algorithm, which becomes EKF more difficult to employ. This constitutes an advantage of MHSE, which presents easier calibration and fewer initialization parameters.

The ARMSE results for multiple simulations with inaccurate initial conditions and measurement noise demonstrate the robustness of MHSE, in comparison with KF algorithms. These results indicate that the receding-horizon approach trends to be more adequate for parameter estimation in nonlinear systems with noisy data or unknown initial conditions.

The evaluation of the estimators with experimental data demonstrates that, with an adjustment of the initialization parameters and matrices, the algorithms converge accurately on the estimation of the states, which are also outputs of the system. In this way, we may infer that all algorithms can identify values of friction coefficient which leads to accurate values of the states. We remark that MHSE presents a more accurate state estimation, which indicates a more accurate friction coefficient estimation.

Nonlinear Receding-horizon Filter Approximation with Neural Networks for Fast State of Charge Estimation of Lithium-Ion Batteries

An important component of electric vehicles that allows optimizing their autonomy is the Battery Management System (BMS), whose primary goal is to monitor the State of Charge (SOC) of the battery. The SOC may be estimated using filtering algorithms and, in this context, higher accuracy and computational complexity are of great importance. The present paper aims at proposing receding-horizon strategies, namely Moving-Horizon State Estimation (MHSE) and Neural Network Moving-Horizon Estimation (NNMHE), for SOC estimation. Simulated results demonstrate that the unknown lumped parameters of the battery model are may be jointly estimated with the states using an augmented states formulation, through the first algorithm. The accuracy of MHSE on the process is high enough to use their results for training the NNMHE, so that a machine learning based solution, with reduced processing time is found. This approach is evaluated with an experimental dataset, achieving a coefficient of determination of almost 99% and about 10 times faster, which proves that it is effective and can be readily employed in an embedded systems application requiring less computational resources.

9.1

Problem Definition

The main purpose of this research is the evaluation of receding-horizon observers for simultaneous estimation of the battery states and lumped parameters of an ECM. In this way, an augmented formulation of the discrete-time battery model is adopted, in which unknown parameters are supposed to have slow-varying dynamics relative to regular states.

Based on the literature review, we evaluate the application of MHSE and NNMHE for SOC estimation, since they are appointed as potential algorithms for observing tasks [22, 42].

9.2

Dataset Description

The dataset used for experimental analysis is provided by NASA Ames Prognostics Center of Excellence Datasets [131], and presents data measured on cycling tests with randomly generated current profiles at room temperature [192]. The battery is a 18650-size one with nominal capacity of 2.1002 Ah [130, 193].

For experimental analysis, a clipping is taken for evaluation, which contains approximately 9 hours of data, with a sample time of 10 seconds. An extract of the electrical current measured on the battery, i in Figure 3.5, is presented on Figure 9.1. The sign of the current denotes when the battery is charging (negative) or providing power (positive). For this time window, the voltage measured on battery terminals is presented in Figure 9.2. We have not presented all the range used in experimental analysis for easier visualization.

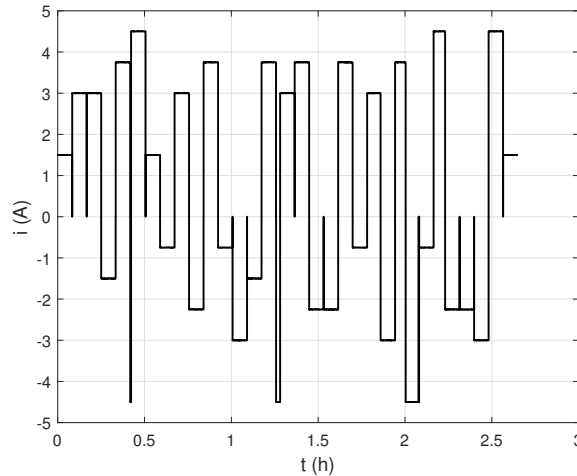


Figure 9.1: Electrical current measured on battery on experimental test bench, in A.

9.3

Proposed Approach

To perform simultaneous estimation of states and parameters, we use an augmented states formulation, in which it is supposed that unknown parameters are also states, with slow dynamics within the receding-horizon window. So, based on equation (4-1), we may define input, output and states vectors, respectively, as $u = i, z = U_t, \mathbf{x} = [U_p \quad SOC \quad R_s \quad R_p \quad C_p]^T$. The resulting discrete-time equations of the system are presented in Eqs. (3-33)–(3-35) using the state space formalism can be then obtained. The state transition functions for a sampling time T_s are

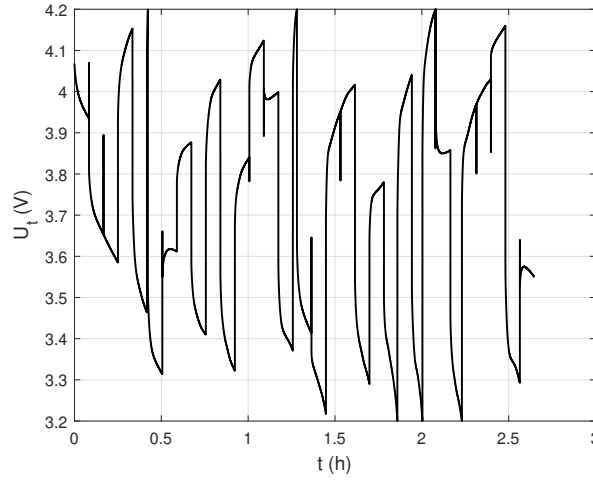


Figure 9.2: Voltage on battery terminals measured on experimental test bench, in V.

$$f_1(x_{k-1}, u_{k-1}) = x_{1,k-1} \exp\left(-\frac{T_s}{x_{4,k-1} x_{5,k-1}}\right) + \dots + u_{k-1} x_{4,k-1} \left[1 - \exp\left(-\frac{T_s}{x_{4,k-1} x_{5,k-1}}\right)\right] \quad (9-1a)$$

$$f_2(x_{k-1}, u_{k-1}) = x_{2,k-1} - \frac{\eta T_s u_{k-1}}{C_n} \quad (9-1b)$$

$$f_3(x_{k-1}, u_{k-1}) = x_{3,k-1} \quad (9-1c)$$

$$f_4(x_{k-1}, u_{k-1}) = x_{4,k-1} \quad (9-1d)$$

$$f_5(x_{k-1}, u_{k-1}) = x_{5,k-1} \quad (9-1e)$$

while the output equation can be defined as

$$z = h(\mathbf{x}_k) = p(x_{2,k}) - x_{1,k} - u_k x_{3,k} \quad (9-2)$$

where function $p(\cdot)$ has been defined in (3-32) (note that the open-circuit voltage at each sample $U_{OC,k}$ depends on SOC, or $x_{2,k}$, on state space formalism). For that, measured data about the low current discharge must be used for a polynomial fitting, using for that end a 12th order polynomial as in [130]. Using the experimental data described in the previous subsection, the coefficients K_i for the best polynomial fitting are presented on Tab. 9.1, while the fitting results can be found in Figure 9.3.

It is important to remark that the 3rd to 5th states are time-varying parameters of the battery, which are jointly estimated with the states. This is what we call an augmented states formulation for joint states and parameter estimation, so it is possible to employ off-the-shelf state estimation methods for SOC prediction considering an unknown battery model. To write the

Table 9.1: Parameters for polynomial fitting of OCV-SOC measured data.

K_i	Value
K_0	3.2364
K_1	19.0076
K_2	-373.8293
K_3	4.1383E+03
K_4	-2.7800E+04
K_5	1.2078E+05
K_6	-3.5341E+05
K_7	7.1078E+05
K_8	-9.8489E+05
K_9	9.2391E+05
K_{10}	-5.6025E+05
K_{11}	1.9811E+05
K_{12}	-3.1015E+04

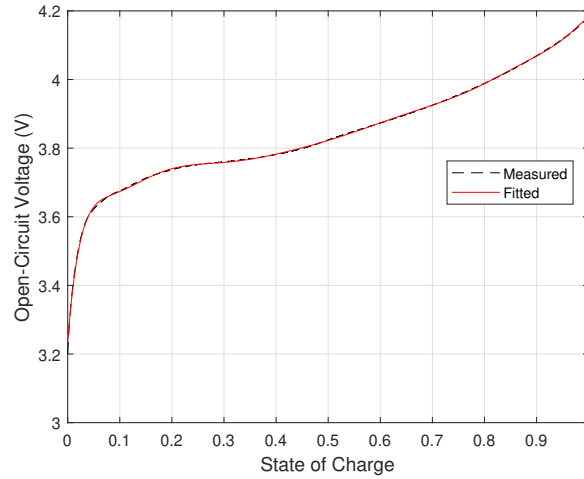


Figure 9.3: Polynomial fitting of OCV-SOC measured data on test bench.

state equations related to variables, we consider that the system dynamics is considerably faster than the parameter change within the moving-horizon window, which is quite reasonable. There will be errors in this approach when the moving-horizon window does contain samples with different parameters and the parameter ρ implies slow enough dynamics for the filter, which is possible to tune.

In the following section, we describe the results for state estimation of battery SOC.

9.4 Results

In this section, we present the results of the application of the proposed receding-horizon algorithms for SOC estimation, namely the EKF, MHSE and

NNMHE. The datasets used for both simulation and experimental results are detailed in Section 9.2.

The results are presented to allow quantitative comparison. Firstly, we compare the performance of the MHSE against the classical formulation of EKF, using the simulated data of a Thévenin ECM. For this purpose, we compare the RMSE and R^2 along the simulation time of the estimation of SOC , U_t and the model parameters. In this case, we show the influence on the joint estimation of states and parameters, as well as of the prediction of system output, made by the receding window size, as well as on the observability property of the system with augmented states. Additionally, we present a robustness analysis of the algorithms performed under uncertain initial conditions.

Once demonstrated the efficiency and accuracy of MHSE, we present the results of NNMHE, in which an ANN is trained by MHSE results of experimental data. We present the calibration of the ANN with different numbers of neurons, through the evaluation of the resulting RMSE and R^2 of validation data.

The battery configuration and dataset used are those used in [130] and made available by the authors of [192] on [131]. All the codes used in this paper are implemented on MATLAB®. Data is freely available on the internet, and the source code of the filtering procedure is made available for the interested reader¹.

9.4.1 Simulation Results

A simulation with the input shown in Figure 9.1, extracted from the experimental data, is used for generating data. The goal is to compare the real simulated states with the estimated ones, so that it is possible to evaluate the applicability and accuracy of the MHSE, and empirically assess whether in the simulated states envelope the error is bounded. As such, we may then employ the same parameters to estimate the states using real experimental data.

The lumped parameters of the battery are defined as time-varying, so that we may evaluate the capacity of each methodology in changes detection. As these parameters are supposed to be unknown along the estimation process, the initial condition of vector states defined for all algorithms is $x_0 = [0 \ 0.9 \ 0.05 \ 0.05 \ 500]^T$. The MHSE is defined using the formulation presented on Eq. (4-36), with a window of $N = 20$ samples and different weights are associated with augmented states, using $\rho = [1E-8 \ 1E+1 \ 1E-$

¹<https://github.com/helonayala/SOCestimation>

$8 \cdot 10^{-8} \quad 10^{-8}]$. The use of a vector weight allows differentiating the influence of each state on the cost function, which trends to improve the accuracy of one at the expense of others.

The EKF must be initialized by 3 matrices P , Q and R , which are, respectively, the estimate covariance matrix, the covariance of the process noise and the covariance of the observation noise [17]. After some trial and error, these matrices are defined as

$$P = \text{diag}([10^{-1} \quad 10^{-2} \quad 10^{-5} \quad 10^{-5} \quad 10^4]), \quad (9-3)$$

$$Q = \text{diag}([10^{-2} \quad 10^{-12} \quad 10^{-6} \quad 10^{-6} \quad 10^{-2}]), \quad (9-4)$$

$$R = \text{diag}([10^{-3}]). \quad (9-5)$$

The results of the estimation of states and parameters, as well as of the output are presented on Tab. 9.2. We may note that the results of all states and the output are much better using the MHSE, when compared to EKF. It is important to note that EKF has worse results for parameters estimation, which are relatively more accurately estimated by the receding-horizon algorithm.

Table 9.2: Results for simulated data.

Method	Variable	RMSE	R ²
EKF	U_p	2.9412E-4	0.9015
	SOC	1.0555E-4	0.9993
	R_s	9.7159E-5	0.7867
	R_p	1.3664E-4	0.3464
	C_p	3.7130	0
	U_t	1.5036E-4	0.9994
MHSE	U_p	1.3099E-4	0.9805
	SOC	6.8222E-6	1
	R_s	4.9125E-5	0.9455
	R_p	5.4835E-5	0.8947
	C_p	1.2851	0.6400
	U_t	6.2428E-5	0.9999

Evaluating these simulation results, we may observe that MHSE has superior results in all analysis, especially on those related to parameter estimation. The main cause of this difference is the observability of the system in each case. The EKF worst result for estimation with augmented states formulation indicates that the system is not fully observable with the single sample window used. On the other hand, the receding-horizon algorithm presents better results for both states and parameters estimation, indicating that the system is full-observable in the window defined on the algorithm or presents more observable states [180].

We may evaluate the rank of the observability matrix of the system with augmented states during the simulation, as defined in [180] for receding-horizon state estimation methods. In this analysis, we note that with a window of 1 sample, used on EKF estimation, the rank of the observability matrix remains at 1 along all simulation time, which implies that the system is not observable. Meanwhile, for a window size of 20 samples, the system has a rank equal to 5 on the most simulation time, indicating it is fully observable in a considerable range. This result is important to understand the model parameters estimation results and shows that by increasing the window size we improve the observability property without the need of adding sensors to gather additional measurements.

To evaluate the robustness and convergence of the observers, many simulations are executed with different initial conditions, which are presented in Table 9.3. In this table, we see the error related metrics and also the mean time needed to perform the estimation on each sample. It is thus possible to verify if each observer can correctly estimate the state trajectory under different operating envelopes. We note that MHSE presents the best ARMSE mean, denoting its robustness, since its result is more accurate and less oscillatory.

Table 9.3: ARMSE analysis results.

Method	Mean Time for Sample (s)	Variable	ARMSE Mean	ARMSE Std Dev
EKF	9.1322E-5	SOC	7.7879E-11	1.8564E-10
		U_t	9.5049E-4	0.0093
MHSE	0.0385	SOC	3.1294E-17	6.9975E-16
		U_t	1.1355E-10	6.2754E-10

It is important to note that, despite the high processing time, they could be used on online applications of SOC estimation, since each step requires approximately 0.0385s, while the sample time is 10s, when run in a Windows PC with 32 GB RAM and i7 processor with 2.6 GHz. We note, however, that in most cases moving-horizon estimation or control are run in real-time in resource-constrained hardware and demand algorithmic optimization [194], as the ones provided herein with NNs [195].

The simulation results allow us to infer that MHSE is accurate enough to produce high fidelity data that may be used for training an ANN able to be used instead of MHSE, which is proved to be less computationally costly [42]. The solution presented herein offers a way of obtaining a compromise between precision and computational complexity with machine learning as we shall also

confirm next when experimental data is employed for training and validation of the NNMHE.

9.4.2 Experimental Results

As demonstrated in the previous subsection, the MHSE may be, with a relatively high computational cost, accurately used for SOC estimation. To associate the accuracy of MHSE with a lower computational effort, the NNMHE is proposed. The input of the ANN used on it is the information vector containing the measured inputs and outputs along the receding horizon defined for MHSE. As output, the NN gives the estimated SOC on the current sample, that is, on the end of the observing window. This process is illustrated in Figure 9.4.

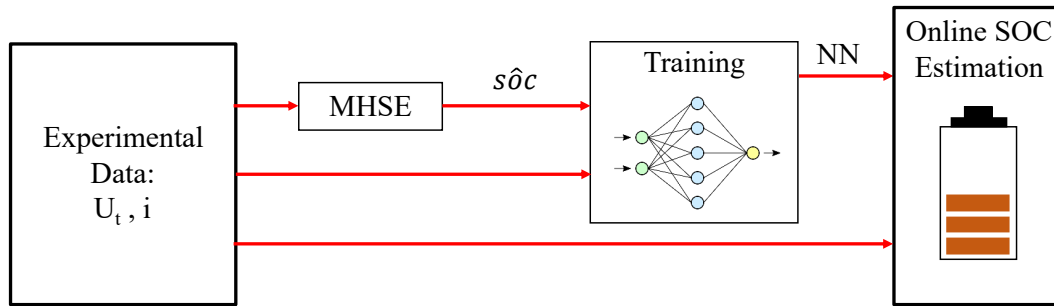


Figure 9.4: Flowchart of NNMHE. This filter is trained offline using the SOC estimated of experimental data, so that a NN that maps the information vector to the SOC estimated by MHSE is built.

For this, the MHSE with the same configuration presented on Simulation Results is applied over a large data extracted from the dataset described on Sec. 9.2, with 32667 samples. The first 20114 samples are used for the NN training process, while the remaining are used for validation. It is important to note that the beginning of each data extract must be a sample with a null current, for which the SOC is precisely defined by the U_{OC} (Eq. (3-35)). Using this information, the initial condition of each process is defined.

The NN selected for the NNMHE is a feed-forward one, with two hidden layers, and the first step in its implementation is the definition of the number of neurons employed. Some attempts are done, and their results are presented on Tab. 9.4. For both RMSE and R^2 coefficients, we note that a better performance of the network with 10 neurons, achieving an R^2 of 0.9847. This indicates that the results are close to the validating data, that is the SOC estimated through MHSE.

The resulting R^2 for both training and test of NN with 10 neurons is presented in Figure 9.6. We may note that the R^2 on the test phase (0.98466) is

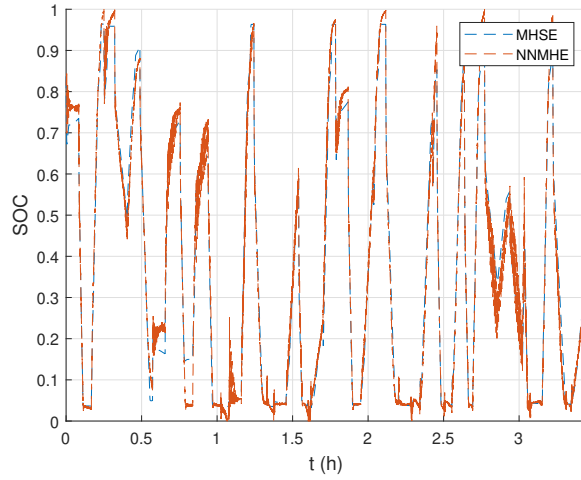


Figure 9.5: Estimation of the SOC, with experimental data, using MHSE and the ANN with 10 neurons.

Table 9.4: Validation results of the ANN trained with MHSE.

Neurons	Mean Time for sample (s)	RMSE	R ²
10	0.0043	3.4173E-4	0.98466
20	0.0042	4.8560E-4	0.96903
30	0.0042	4.3652E-4	0.97497
40	0.0042	10.8460E-4	0.84548
50	0.0043	6.7308E-3	0.94049

high and close to the training one (0.99811), which demonstrates the efficiency of the NNMHE. The results demonstrate also the better computational efficiency of the NNMHE, since the mean time for each sample is 0.0043s, while the MHSE requires almost 10 times higher.

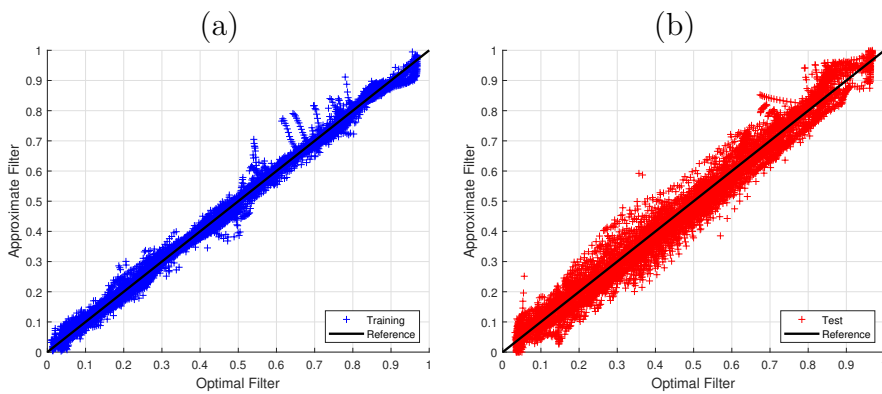


Figure 9.6: R² for SOC estimated by NNMHE with 10 neurons in the (a) training process and the (b) test with the resulting NN.

9.5

Discussion

From the results presented in previous subsections, we may mention that MHSE is robust and accurate, which makes it proper and adequate for SOC estimation, as denoted by the quantitative error metrics shown. The computational cost is greater, however, when compared to classical filtering methods. We must also remark that it has simple calibration and relative ease of implementation. Besides that, we may predict that the augmented states discrete-time system of the battery has full observability or a high number of observable states for the receding window defined in the algorithm. This is an important feature of moving-horizon filters, as they allow to improve the observability condition without adding sensors and thus avoiding costs by smarter algorithmic decisions.

Once demonstrated that MHSE has more accurate performance than EKF and that the receding window of time allows to improve observability, it may be used for training the NNMHE, so that it may perform, with considerably less computational effort, the estimation of SOC.

Finally, we demonstrate that the computations cost of the optimal MHSE can be alleviated by using NNMHE, which is an approximate version of the filter. It is an important filter option for systems with lower sampling times and limited hardware resources. It allows lower samplings times at a price tag of less accurate estimation. Better accuracy may be achieved as the results herein presented are non-exhaustive, as the filter construction is dependent on precise data generation for training, spanning the full operating envelope for SOC, or still by performing architecture search [196].

The results demonstrate also that the approximated solution based on ANN is perfectly tailored for hardware implementation. Our recent work shows that it is possible to embed conveniently ANN with relatively complex structures on FPGA getting very fast responses (in the order of microseconds) [195]. We note, however, that it is very time-consuming to obtain ad-hoc hardware solutions for implementing ANN on FPGA and thus further research is encouraged in exploring new hardware solutions, such as the Nvidia Jetson platform [197].

Hierarchical Nonlinear Model Predictive Control for Path Tracking of In-Wheel Motor Drive Electric Vehicles

The rising use of electric vehicles with different levels of automation leads to the development of novel control strategies, aiming for better performance with safety and driveability. Researches about MPC indicates its advanced performance for different systems, which is penalized with a high processing time. In this context, this contribution aims to propose a hierarchical framework for the control of electric vehicles with independent in-wheel motors, which is applied for velocity and path tracking. The hierarchical framework is composed of a novel structure, in which the upper layer is performed by MPC, aiming to define the reference forces on the vehicle chassis. Through static relations, these forces are related to wheel angular velocity and steering angles references, which are the inputs of the low-level controller. We demonstrate, through a velocity tracking analysis, the effectiveness and advantages of the hierarchical approach, compared to a nonlinear MPC law. The path tracking case study is used for presenting the application of the hierarchical control law on a coupled longitudinal-lateral dynamic model, using different sample times for MPC layer and the open-loop simulations, which enlarges the prediction window and reduces considerably the computational efforts. An experimentally obtained tire dataset is used on the open-loop simulations, which includes effects do not predicted in mathematical models and, thus, approaching the results to real situations.

10.1

Dataset Description and Parameters Estimation

For evaluation of the hierarchical framework proposed, an experimental dataset of tire variables is used for the open-loop simulations, approaching real situations. The dataset is made available on [198] and includes information about longitudinal and lateral forces, under different conditions, such as internal pressure and normal load.

In this contribution, we extract the data concerning the vehicle model and the tire force is defined through a look-up table. For the NMPC algorithm, the dataset is used for obtaining approximate Magic Formula parameters, which

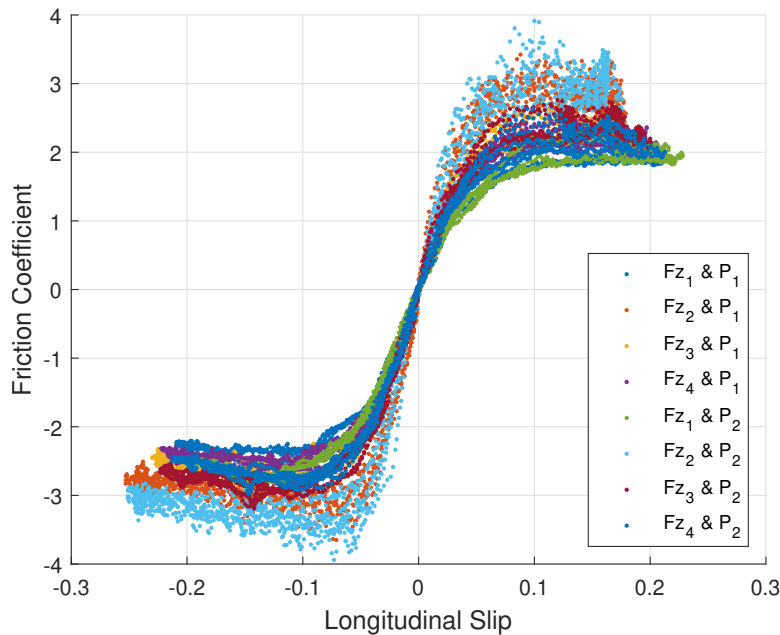


Figure 10.1: Available experimental data about longitudinal force.

may be employed properly in the optimization algorithm. The Figure 10.1 demonstrate the diversity of data for longitudinal force measurements.

The friction coefficient data is obtained by dividing the traction force by the normal load of each sample. The data indicate that normal load may affect the friction coefficient value. For the open-loop simulations, we identify the parameters using the data related to an internal pressure of 82 kPa and the maximum normal load of 1100 kN, which are the nearest of the vehicle model used on the contribution, whose parameters are presented in Table 8.1.

The data related to the used configuration is extracted through the k-means clustering algorithm. Using a classical formulation of Particle Swarm Optimization (PSO), we may find the Magic Formula parameters (Table 10.1). The friction coefficient data and the fitted curve is presented in Figure 10.2.

A similar optimization problem is used for finding approximate lateral force magic formula parameters, which is used for calculating the cornering stiffness of each wheel, since this parameter is the derivative of lateral force near zero. The cornering stiffness of the front and rear wheel are different since they are dependent on normal loads. The parameter a_y is calculated using the aligning moment and lateral forces values.

All the estimated parameters are demonstrated on Table 10.1.

10.2 Hierarchical Framework for EV Control

The proposed hierarchical framework is presented in Figure 10.3. Usually, for path tracking, only information about the position related to the global

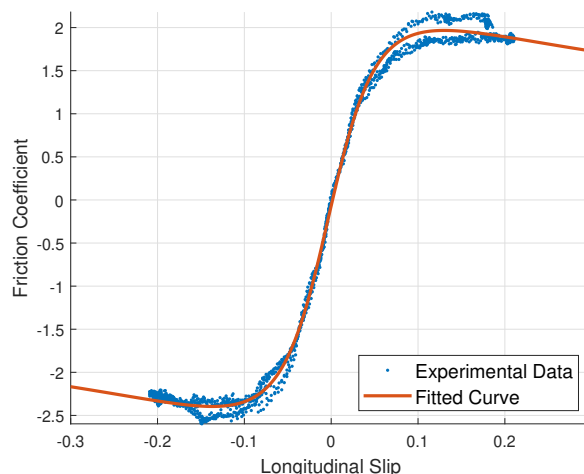


Figure 10.2: Fitted curve for longitudinal friction coefficient.

Table 10.1: Identified tire parameters.

Parameter	Value
A_x	2.1815
B_x	1.7245
C_x	11.6041
D_x	0.4738
S_{H_x}	0.0034
S_{V_x}	-0.2145
C_α^*	33.7928
S_{H_y}	-0.0056
S_{V_y}	-0.0756
a_y	0.0143

frame is available, but, for more accuracy, we may calculate the consequent attitude angle and its rate and the velocities related to the body frame, which are evaluated on the Newton-Euler equations. These data are the main information used on the NMPC layer, in comparison to the current values of the state variables.

The symbols adopted on the Figure 10.3 are explained on the Table 10.2. The index d indicates that it is the desired variable and i indicates the i -th wheel of the vehicle model.

The NPMC layer has as output the set of longitudinal and lateral forces, written on the vehicle body frame, that is, the forces of the wheels on the chassis that allow achieving the references of the vehicle states.

The second layer of the framework is not a control task, but a static relation among the forces on the vehicle body frame and the angular velocities on wheels and steering angle. Its first step is to define the longitudinal force on the wheel frame and the steering angle, which is an argument of the lateral force on the wheel frame. The relation among the forces written on the wheel

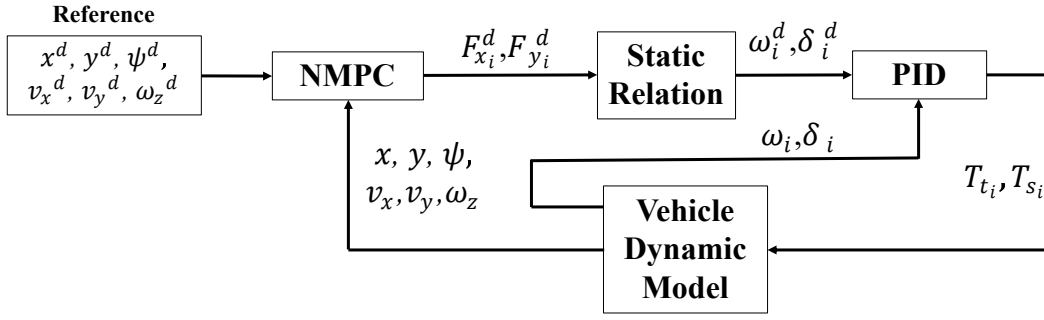


Figure 10.3: Proposed Hierarchical Framework.

Table 10.2: Description of the symbols used on the framework.

Symbol	Description
x	Longitudinal displacement on vehicle body frame
y	Lateral displacement on vehicle body frame
ψ	Yaw angle
v_x	Longitudinal velocity on vehicle body frame
v_y	Lateral velocity on vehicle body frame
ω_z	Angular velocity of the vehicle
F_x	Force along x-axis on vehicle chassis
F_y	Force along y-axis on vehicle chassis
ω	Angular velocity of the wheel
δ	Steering angle of the wheel
T_t	Traction torque
T_s	Steering torque

frame and vehicle body frame may be established by the following equations system:

$$\begin{cases} F_{w_{x_i}}^d \cos \delta_i^d - F_{w_{y_i}}^d \sin \delta_i^d = F_{x_i}^d \\ F_{w_{x_i}}^d \sin \delta_i^d - F_{w_{y_i}}^d \cos \delta_i^d = F_{y_i}^d \end{cases} \quad (10-1)$$

As the lateral force on the wheel frame depends on the sideslip angle (Eq. (3-8)), which depends on the steering angle (Eq. (3-5)), the system above has, actually, only two variables, that are the longitudinal force and the steering angle, as follows:

$$\begin{cases} F_{w_{x_i}}^d \cos \delta_i^d - C_{\alpha_i}(\delta_i^d - \beta_i) \sin \delta_i^d = F_{x_i}^d \\ F_{w_{x_i}}^d \sin \delta_i^d - C_{\alpha_i}(\delta_i^d - \beta_i) \cos \delta_i^d = F_{y_i}^d \end{cases} \quad (10-2)$$

So, the first step of static relation is to solve the nonlinear equations system (Eq. (10-2)). Once defined the desired value of longitudinal force on the wheel frame, the second step may be performed. It consists on to define the wheel angular velocity that produces the desired force.

In this way, we must note that, for a part of the domain of the slip-force function (Eq. (3-3)), there are two possible values of longitudinal slip for a given traction force (Figure 10.4), on the stable and unstable regions.

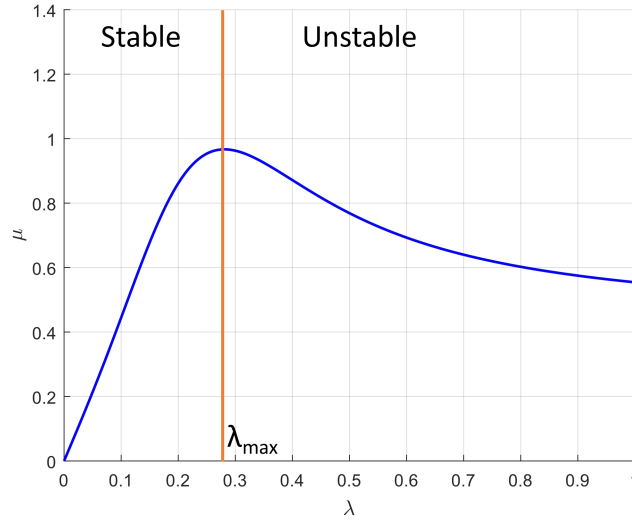


Figure 10.4: Stable and unstable regions of tire curve.

Then, in the static relation phase, we must adopt the slip reference inside the stable region, assuring safety and driveability for the vehicle. Once defined the slip reference, we may find the angular velocity desired, which is directly related to the slip, for a given longitudinal velocity, according to Eq. (3-2).

$$\omega_i^d = \frac{v_{x_i}}{R} (1 + \mu_x^{-1}(F_{w_{x_i}}^d)) \quad (10-3)$$

Note that the inverse function μ_x^{-1} has its range limited to $[-\lambda_{max}, \lambda_{max}]$, in which λ_{max} is the longitudinal slip for maximum friction force.

The last step of the Hierarchical Framework is the PID control as a low-level controller, in which the traction and steering torques are defined as a function of error and its derivative and integer, such defined in classical literature.

10.3 Results

The results of this contribution are presented in this section. Firstly, the hierarchical framework is applied to a quarter-car model (Section 3.3), for longitudinal velocity control. Through this case study, we demonstrate the effectiveness of the hierarchical control, compared to a pure NMPC algorithm. The main advantage presented is related to the computational effort, which is considerably smaller.

In the sequence, the application of the hierarchical control is evaluated for path tracking, using a single-track model (Section 3.4). In this case, we evaluate

the velocity and path tracking during a double-lane change maneuver, as well as the efficiency of the low-level controller. In this case study, different time samples are used for NMPC and open-loop simulations and the tire forces are defined using experimentally obtained data, to evaluate the effectiveness of the control under tire model inaccuracies.

10.3.1 Longitudinal Vehicle Control Results

As a simpler model, the single-corner or quarter-car model may be effectively used for validating the hierarchical framework proposed. In this case, the HMPC is compared to NMPC, in which the torque applied on the wheel is defined directed by the optimization problem. In this first result analysis, both MPC algorithms are used with the same sampling time, so that the optimization problem is performed at each sample. In this way, we intend to demonstrate that the hierarchical framework improves the processing time.

In this first analysis, we do not consider different sample times for simulation, so that a sampling rate of $10^2 Hz$ is adopted for both simulations. The MPC parameters initialization, which are scalar and not matrix in this situation, are defined as $Q = 1E4$, $R = 0$ and $S = 1E - 3$.

In the single-corner model, the only output considered is the velocity, whose result of the simulation is presented in Figure 10.5.

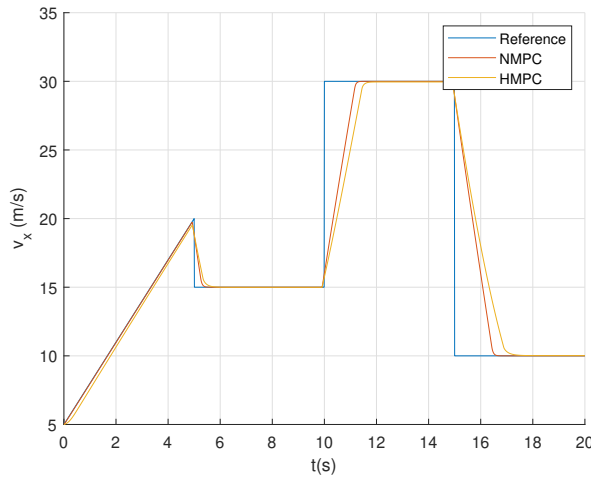


Figure 10.5: Vehicle velocity for NMPC and HMPC.

Firstly, it is important to note that the hierarchical algorithm presents a slightly worse result at the beginning of the simulation, due to the settling time of the low-level controller. The performance of both strategies is harmed on high variations of velocity reference, on 10s and 15s, which is due to friction force limits. That is, the acceleration or deceleration required is not feasible for the given tire-road conditions.

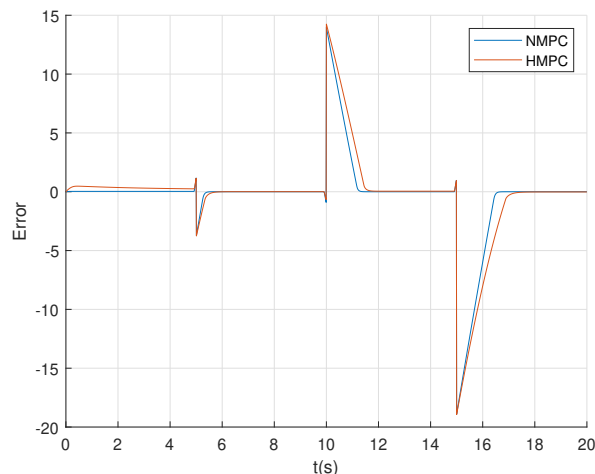


Figure 10.6: Vehicle velocity for NMPC and HMPC.

We may also note these observations in Figure 10.6, in which the errors related to reference velocity are presented. It is possible to note that the errors due to velocity variation are similar in both cases. As for the error due to settling time, the error of HMPC is small and negligible when compared to absolute values.

Regarding driveability and safety, we may note in Figure 10.7 that both controllers can keep the longitudinal slip inside the stable region. Considering that the $\lambda_{max} = 0.1481$, we may note that for both NMPC and HMPC, the tire slip is inside the stable region, which ensures that the driving conditions are suitable.

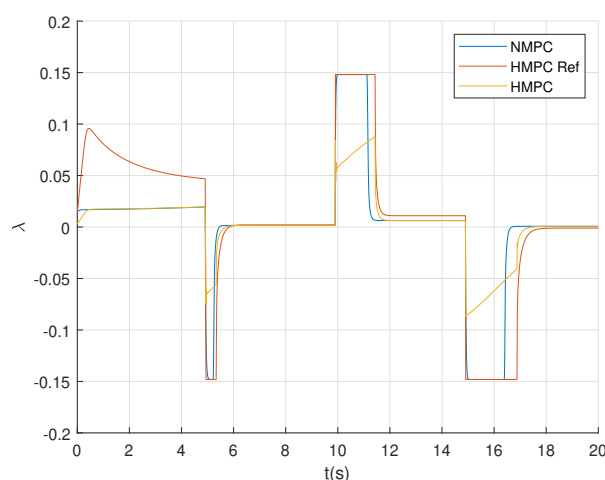


Figure 10.7: Longitudinal slip for NMPC and HMPC.

Nonetheless, the processing time of HMPC is much smaller than the presented by NMPC, as we may observe in Figure 10.8. It is possible to note that NMPC, as proposed, is not able to be used online, since it is higher than the defined sample time of $0.01s$. Meanwhile, the processing time of HMPC

is lower than this value, denoting it may be used on online applications and reinforcing its superior performance.

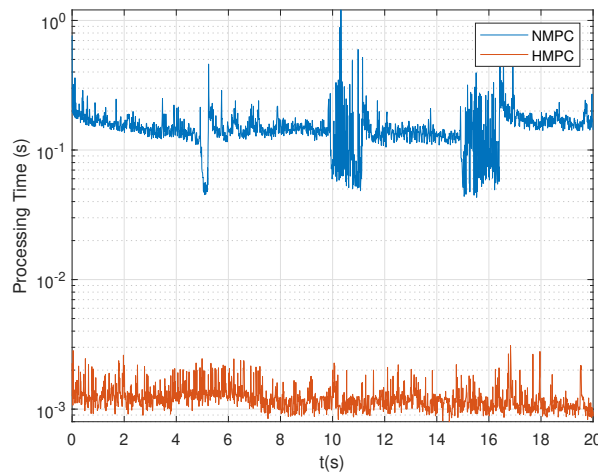


Figure 10.8: Processing Times, in seconds, for NMPC and HMPC.

Evaluating the differences between the torque on wheels (Figure 10.9), we may note that on most of the simulation time, the defined inputs for both algorithms are close. That is, the HMPC achieves values close to NMPC, with more efficiency.

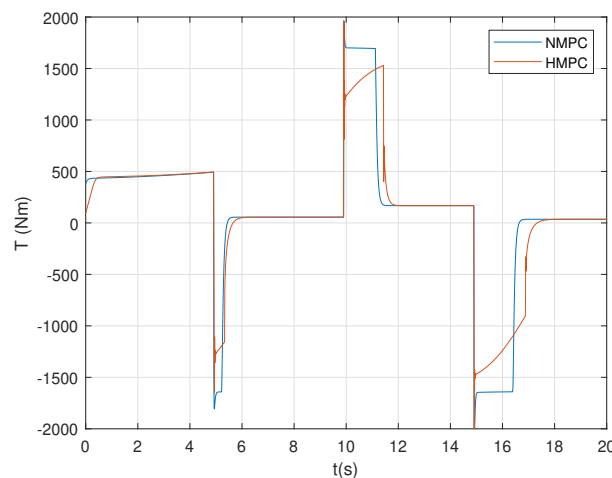


Figure 10.9: Torque defined by NMPC and HMPC.

10.3.2 Path Tracking Results with Experimental Data of Tires

On the single-track model simulations, we adopt a novel feature, compared to the one presented in the first case study, that is different sample times for MPC and PID controllers. We may observe that a higher sample time for the MPC algorithm enlarges the window time of prediction, which trends to anticipate changes on references to the controller and, then, require inputs with

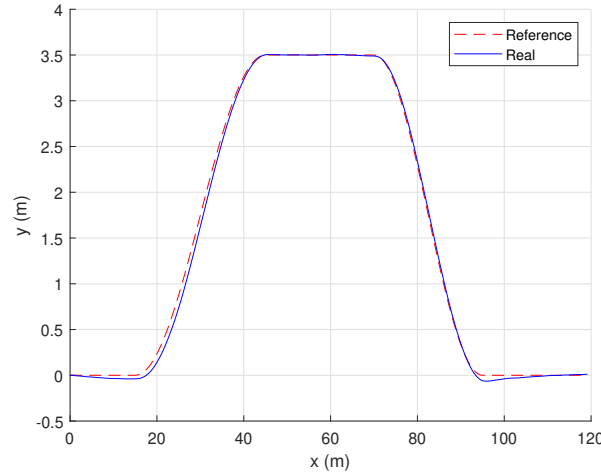


Figure 10.10: Path tracking results comparison.

smoother variations. In the simulations, we adopt a sampling rate of $1E+03Hz$ for the vehicle dynamic system, and consequently for the low-level controller, and one of $2E+01Hz$ for the NPMC layer.

As PID is faster for processing, its sample time is the same employed in the open-loop simulation of the dynamical model. Besides that, we adopt experimental data for tire dynamics modeling [198] and, so, the longitudinal and lateral forces on the tires are defined through a lookup table with the experimental data. In the wheel controller algorithm, these data are used for fitting the longitudinal (Eq. (3-3)) and lateral (Eq. (3-8)) force curves, as commented on Section 10.1.

The reference path for control is a double lane change [199], which we consider that must be executed in a maximum time of 10s, with approximately constant longitudinal velocity. So, the initial reference is the position (X, Y) in the fixed frame and the time vector. As consequence, we define, by approximations, the yaw angle ψ , the yaw rate $\omega_z = \dot{\psi}$ and the components of the velocity v_x and v_y , related and written in the body frame.

As the first result, we may observe the path tracking result (Figure 10.10), which compares the reference path of the vehicle CG and the obtained using the hierarchical framework.

Despite the errors presented, we may evaluate that the proposed controller is effective, since the error is negligible when compared to vehicle dimensions and path width. The requirements of execution time and stability are also assured, since the longitudinal velocity (Figure 10.11) and the yaw angle (Figure 10.12) of the vehicle are correctly tracked, with negligible errors.

Concerning low-level controller, we may note that it is also effective. The traction control allows achieving the references for wheel angular velocity after a few seconds of simulation, which is sustained throughout the maneuver, as

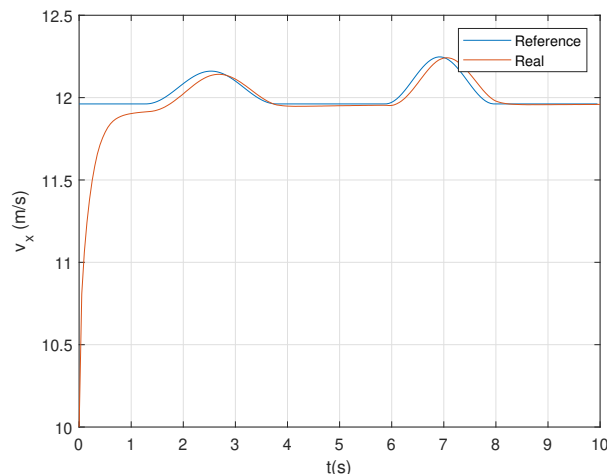


Figure 10.11: Longitudinal velocity of the vehicle.

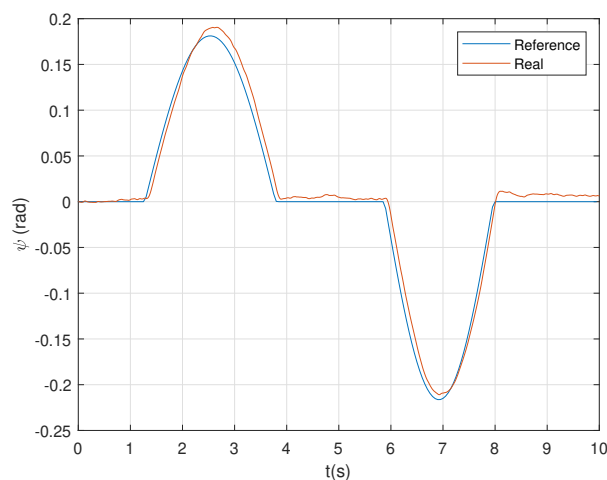


Figure 10.12: Yaw angle of the vehicle.

observed in Figure 10.13.

The steering control presents faster convergence and we may observe in Figure 10.14 that the controller can track the references of steering angles for both wheels along with all the simulation.

Regarding processing time, we note that the NMPC layer has a considerably higher processing time, about 100 times the low-level one. As the NMPC layer is only executed every 50 samples of the dynamic system, we may conclude that the total computational effort is quite reduced.

10.4 Discussion

The results of single corner simulations, presented in Subsection 10.3.1, demonstrate the efficiency of the proposed hierarchical framework, reducing considerably the processing time, ensuring the safety and the velocity tracking suggested as the objective of the longitudinal control. As a simpler model

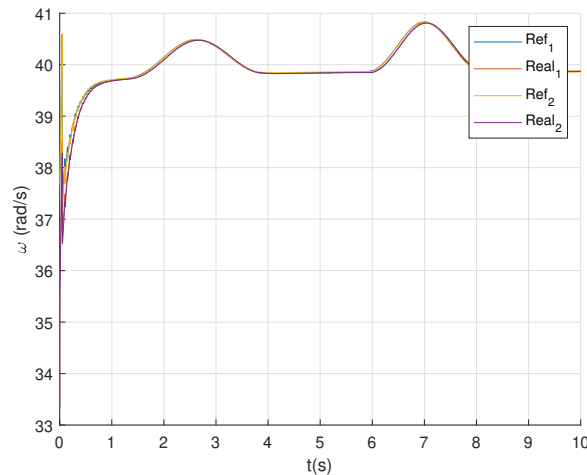


Figure 10.13: Reference and real wheel angular velocities.

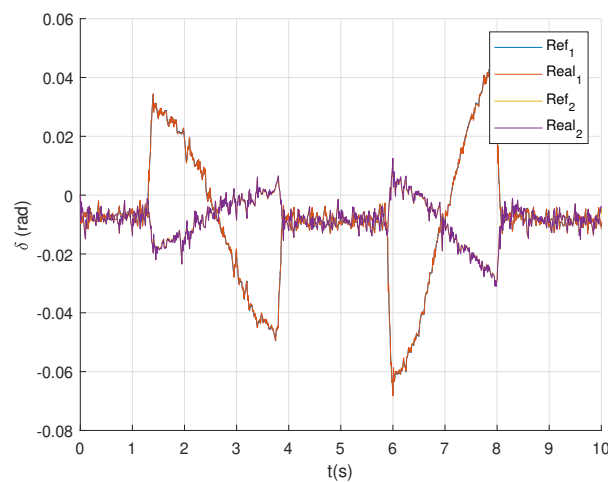


Figure 10.14: Reference and real steering angles.

with a similar hierarchical control structure, this case study demonstrates the capacity of the proposed framework in reducing the controller processing time. Further researches may be conducted using this model and the hierarchical controller proposed, especially evaluating strategies that ally good performance with efficient energy consumption, which is an issue of large interest in recent researches [200, 201].

About the path tracking tasks, we observe that a simulation performed using the single-track model allows us to correctly evaluate and calibrate the control laws, reducing the order of the system. Thus, we perform reliable simulations with reduced computational efforts. The use of the experimental tire dataset approaches the simulations to real conditions, since effects not always predicted on mathematical formulations are consequently involved.

The results for the single-track model demonstrate that the hierarchical framework can correctly control the vehicle path and the proposed division of tasks is suitable. As the NMPC layer is restricted to the rigid-body motion of

the vehicle, the optimization problem is executed with a lower order, improving its performance. The static relation takes advantage of the mathematical model of the vehicular systems and defines the reference of the low-level controller, which is properly executed with a classical PID.

We note also that the use of different sampling rates for NMPC and the complete dynamic model is an effective solution for the commonly high computational efforts required for MPC-based systems. A higher sample time for NMPC enlarges the time window of prediction, which allows previewing changes on references in advance. Besides that, it allows the execution of many samples for the low-level controller for each NMPC execution, reducing considerably the processing time.

Part IV

Final Remarks

11

Conclusions

In an overall conclusion, we may observe on the results of all contributions presented that the proposed objectives have been achieved, and the estimation and control algorithms are demonstrated to be efficient, through simulated and/or experimental data. Hereafter, the specific conclusions are commented on.

Firstly, the methodology proposed for grey-box identification of time-invariant parameters is effectively applied to the estimation of structural parameters of landing gears. Even in scenarios with a large scale of measurement noise, the stiffness and damping of landing gear structure are predicted with small deviations, which do not affect the gear walk simulation. Since the simulated data was obtained from a complete model, which considers even the tire dynamics, we presume that the methodology may be applied to real drop test data. This application is important for the practical robust control design of aircraft braking systems.

Regarding the state estimation on vehicle and tire dynamics, we may conclude about the efficiency and superiority of the MHSE in comparison to EKF and UKF on state estimation for nonlinear applications, especially with friction and discontinuous efforts. In the studied case, all algorithms estimate the non-measured states. However, in the performance analysis, the MHSE presents better and more robust results, followed by UKF, especially when it is considered the measurement errors and uncertainties in the initial conditions of the system. We remark that UKF presents a good cost-benefit ratio, since its results are considerably good, with low processing time.

These algorithms are also evaluated for friction coefficient estimation for vehicle control applications. Augmented states formulation is demonstrated as suitable for estimation tasks on vehicle dynamics and it may be useful even when states and parameters must be simultaneously estimated.

We observe that all nonlinear observers present adequate results, but Kalman Filter based approaches are highly harmed when the calibration is not suitable, which does not occur easily in MHSE.

Regarding accuracy and convergence, we note that MHSE presents the best performance since it is more robust under noisy measures and inaccurate

information about initial conditions. This robustness is identified through ARMSE results for multiple simulations.

Despite many advantages, the MHSE has as its main disadvantage the processing time, which is higher than the presented by EKF and UKF. Anyway, the use of better processors and faster programming languages may become possible online applications of MHSE in observing tasks [202].

Finally, the application of the nonlinear estimator on experimentally obtained data demonstrates that outputs observed converge with the proposed nonlinear estimators. The lower levels of errors on state estimation presented by MHSE indicate that the friction coefficient estimated by it must be nearest to real values, and, consequently, more reliable.

The receding-horizon algorithms present also adequate results for simultaneous states and parameters estimation for BMS applications, specifically SOC estimation. Comparing the EKF with the MHSE results unveils that using a window for estimation, instead of only the most recent data, increases the accuracy and also is necessary for achieving full observability of augmented states and parameters discrete-time system.

Simulation results demonstrate that the MHSE estimates accurately and simultaneously the battery SOC as well as unknown lumped model parameters. Having proper processing time for an online application, it is possible to readily employ it. Nonetheless, as a faster solution, we present the NNMHE for SOC estimation, which presents suboptimal results with considerably less complexity and processing cost. The experimental results demonstrate that its methodology may be successfully employed on BMS, since it presents suitable evaluation metrics, achieving a R2 of almost 99% on validation tests.

Regarding control of electric vehicles with independent in-wheel motors, we may conclude that the NMPC is an effective control law for vehicle control, and it can predict optimal control inputs for the system. Meantime, as the vehicle systems are usually complex and present nonlinear phenomena, such as friction, the NMPC applied for the complete dynamic model may require high computational effort, as demonstrated.

In this way, the HMPC results have demonstrated that, without losing reliability and performance, the control task may be divided, earning on processing time. So, the rigid-body dynamics, which is the more relevant to a path and velocity tracking, is controlled by the MPC layer, defining the proper longitudinal and lateral forces for the proposed task. On the other hand, the classical PID controller may achieve good results for the low-level control, since the dynamics of the systems are relatively simpler.

12 Future Works

From all results and discussions of each contribution, it is possible to list some future possible researches that may be conducted from those presented in this work.

About the grey-box identification of time-invariant parameters, there are two main future possibilities. The first one is the application of the identification process with the formulation provided by different methods of dynamic modeling, especially bond graphs. This technique allows the integration of models of the different systems, by the coupling of power inputs and outputs [188]. So, it is possible to construct and identify parameters of an entire aircraft, as well as associate predictive control algorithms for its automation.

The second one is the improvement of the identification process. In complex systems, with many parameters, it is important to demonstrate and understand which ones are identifiable, and then, apply an identification process focused on these. The identifiability analysis enables one to infer whether the estimation of the parameters based on measurements is unique, thus granting greater confidence in the parameters estimates concerning fitting error amplitudes. In other words, the identifiability property holds if a set of model parameters will map to a different set of measurements [189]. In the case of landing gear modeling, it is important to have such theoretical confirmation as this model is used to certificate aircraft.

Related to the second contribution, it is suggested the application of the estimation algorithm in complete vehicle models, considering all wheels and the lateral dynamics, in which it is possible to evaluate the estimator behavior on different maneuvers. In this sense, all tire longitudinal slip and sideslip angles must be accurately estimated, which possibilities suitable control strategies for agile, stable and high-speed path tracking.

Another future possible work is the association of the estimators to complex control strategies, intending to achieve prescribed velocities with optimized longitudinal slip. We must remark that in autonomous vehicle applications, state observers allow the possibility to define a suitable controller for path tracking, agility, or stability.

It is also suggested the application of the developed estimators in other mechanical applications in which the friction efforts must be mitigated or estimated properly, especially on discontinuous systems, as, for example, with Coulomb friction, in which MHSE must present better performance compared to Kalman Filter approaches, since its robustness is demonstrated on the results section.

The friction coefficient estimation contribution may be continued with an observability analysis of the augmented states formulations for vehicle dynamics, which may lead to an adapted algorithm for MHSE. Another possible contribution is the proposal of hierarchical frameworks for MHSE, that may reduce processing times and facilitate the online application of this algorithm for vehicle control, as well as proposed for MPC control laws [49, 50, 169]. Finally, we suggest that the same methodology may be applied to the lateral dynamics of the vehicle, so that cornering stiffness and other tire-road parameters may also be estimated. Despite their relevance to reliable controllers, these parameters are hardly obtainable, which justifies the use of estimation processes.

It was demonstrated that NN may be an effective alternative to MHSE, but its results can be improved by using experimental data obtained on a highly instrumented test bench, in which it is possible to measure SOC and the filter thus constructed used online. Additionally, we would like to develop more complex lumped parameters battery models in addition to MHSE, to improve filter accuracy and evaluate its impact on real-time computational time. Another possibility is the evaluation of state estimation dependent on temperature. This problem may be dealt with time-varying parameters, as we have used, or state-dependent parameters, which can be conveniently solved with receding-horizon approaches, but requires more complex battery models [34].

Moreover, we may use different NN model construction procedures by leveraging a larger amount of data in a receding-horizon fashion bypassing the MHSE procedure, which will still use the known first principles for battery SOC estimation while permitting a full NN solution with well-known software frameworks [203] also on heterogeneous platforms [197, 204]. Finally, this methodology may be also tested with different machine learning techniques, since its use for approximating control and estimation laws is a recent topic of research [205].

In the advanced control field, we suggest the investigation of other controllers for the low-level layer, as alternatives for the classical PID, which requires an exhaustive task of trial and error for calibration. Another future

possibility is the integration of the hierarchical controller to the Battery Management System (BMS), ensuring an optimized energy consumption of the electric motors [206].

Bibliography

- [1] KUMAR, R. R.; ALOK, K.. **Adoption of electric vehicle: A literature review and prospects for sustainability.** *Journal of Cleaner Production*, 253:119911, 2020.
- [2] ANGELINE, P. S.; RAJKUMAR, M. N.. **Evolution of electric vehicle and its future scope.** *Materials Today: Proceedings*, 33:3930–3936, 2020.
- [3] TSAKALIDIS, A.; KRAUSE, J.; JULEA, A.; PEDUZZI, E.; PISONI, E.; THIEL, C.. **Electric light commercial vehicles: Are they the sleeping giant of electromobility?** *Transportation Research Part D: Transport and Environment*, 86:102421, 2020.
- [4] LI, Z.; KHAJEPOUR, A. ; SONG, J.. **A comprehensive review of the key technologies for pure electric vehicles.** *Energy*, 182:824–839, 2019.
- [5] PAVIĆ, I.; PANDŽIĆ, H. ; CAPUDER, T.. **Electric vehicle based smart e-mobility system—definition and comparison to the existing concept.** *Applied Energy*, 272:115153, 2020.
- [6] YANG, B.; WANG, J.; CAO, P.; ZHU, T.; SHU, H.; CHEN, J.; ZHANG, J. ; ZHU, J.. **Classification, summarization and perspectives on state-of-charge estimation of lithium-ion batteries used in electric vehicles: A critical comprehensive survey.** *Journal of Energy Storage*, 39:102572, 2021.
- [7] RATHOR, S. K.; SAXENA, D.. **Energy management system for smart grid: An overview and key issues.** *International Journal of Energy Research*, 44(6):4067–4109, 2020.
- [8] ELLIS, M.; DURAND, H. ; CHRISTOFIDES, P. D.. **A tutorial review of economic model predictive control methods.** *Journal of Process Control*, 24(8):1156–1178, 2014.
- [9] ELLIS, M.; LIU, J. ; CHRISTOFIDES, P. D.. **Economic Model Predictive Control: Theory, Formulations and Chemical Process Applications.** Springer, 1st edition, 2018.

- [10] HALVGAARD, R.; POULSEN, N. K.; MADSEN, H.; JØRGENSEN, J. B.; MARRA, F. ; BONDY, D. E. M.. **Electric vehicle charge planning using economic model predictive control**. In: 2012 IEEE INTERNATIONAL ELECTRIC VEHICLE CONFERENCE, p. 1–6, 2012.
- [11] HUSSAIN, S.; EL-BAYEH, C. Z.; LAI, C. ; EICKER, U.. **Multi-level energy management systems toward a smarter grid: A review**. IEEE Access, 9:71994–72016, 2021.
- [12] ILIADIS, P.; NTOMALIS, S.; ATSONIOS, K.; NESIADIS, A.; NIKOLOPOULOS, N. ; GRAMMELIS, P.. **Energy management and techno-economic assessment of a predictive battery storage system applying a load levelling operational strategy in island systems**. International Journal of Energy Research, 45(2):2709–2727, 2021.
- [13] MURATA, S.. **Innovation by in-wheel-motor drive unit**. Vehicle System Dynamics, 50(6):807–830, 2012.
- [14] VDOVIC, H.; BABIC, J. ; PODOBNIK, V.. **Automotive software in connected and autonomous electric vehicles: A review**. IEEE Access, 7:166365–166379, 2019.
- [15] MARTÍNEZ-DÍAZ, M.; SORIGUERA, F. ; PÉREZ, I.. **Autonomous driving: a bird’s eye view**. IET Intelligent Transport Systems, 13(4):563–579, 2019.
- [16] LENG, B.; JIN, D.; XIONG, L.; YANG, X. ; YU, Z.. **Estimation of tire-road peak adhesion coefficient for intelligent electric vehicles based on camera and tire dynamics information fusion**. Mechanical Systems and Signal Processing, 150:107275, 2021.
- [17] SIMON, D.. **Optimal state estimation: Kalman, H_∞ and nonlinear approaches**. John Wiley & Sons, Hoboken, New Jersey, 2006.
- [18] SINGH, K. B.; ARAT, M. A. ; TAHERI, S.. **Literature review and fundamental approaches for vehicle and tire state estimation**. Vehicle System Dynamics, 57(11):1643–1665, 2019.
- [19] ZAREIAN, A.; AZADI, S. ; KAZEMI, R.. **Estimation of road friction coefficient using extended kalman filter, recursive least square, and neural network**. Proceedings of the Institution of Mechanical Engineers, Part K: Journal of Multi-body Dynamics, 230(1):52–68, 2016.

- [20] HONG, S.; LEE, C.; BORRELLI, F. ; HEDRICK, J. K.. **A novel approach for vehicle inertial parameter identification using a dual kalman filter.** *IEEE Transactions on Intelligent Transportation Systems*, 16(1):151–161, 2014.
- [21] HEIDFELD, H.; SCHÜNEMANN, M. ; KASPER, R.. **Ukf-based state and tire slip estimation for a 4wd electric vehicle.** *Vehicle System Dynamics*, 58(10):1479–1496, 2020.
- [22] ALESSANDRI, A.; BAGLIETTO, M. ; BATTISTELLI, G.. **Moving-horizon state estimation for nonlinear discrete-time systems: New stability results and approximation schemes.** *Automatica*, 44(7):1753–1765, 2008.
- [23] BREMBECK, J.. **Nonlinear constrained moving horizon estimation applied to vehicle position estimation.** *Sensors*, 19(10):2276, 2019.
- [24] GHARBI, M.; EBENBAUER, C.. **A proximity moving horizon estimator for a class of nonlinear systems.** *International Journal of Adaptive Control and Signal Processing*, 34(6):721–742, 2020.
- [25] HUANG, D.; CHEN, Z.; ZHENG, C. ; LI, H.. **A model-based state-of-charge estimation method for series-connected lithium-ion battery pack considering fast-varying cell temperature.** *Energy*, 185:847–861, 2019.
- [26] LI, Y.; WANG, C. ; GONG, J.. **A combination kalman filter approach for state of charge estimation of lithium-ion battery considering model uncertainty.** *Energy*, 109:933–946, 2016.
- [27] SHEN, P.; OUYANG, M.; LU, L.; LI, J. ; FENG, X.. **The co-estimation of state of charge, state of health, and state of function for lithium-ion batteries in electric vehicles.** *IEEE Transactions on Vehicular Technology*, 67(1):92–103, 2017.
- [28] YANG, K.; TANG, Y. ; ZHANG, Z.. **Parameter identification and state-of-charge estimation for lithium-ion batteries using separated time scales and extended kalman filter.** *Energies*, 14(4):1054, 2021.
- [29] BIAN, X.; WEI, Z.; HE, J.; YAN, F. ; LIU, L.. **A two-step parameter optimization method for low-order model-based state-of-**

- charge estimation. *IEEE Transactions on Transportation Electrification*, 7(2):399–409, 2020.
- [30] YANG, S.; ZHOU, S.; HUA, Y.; ZHOU, X.; LIU, X.; PAN, Y.; LING, H.; WU, B.. **A parameter adaptive method for state of charge estimation of lithium-ion batteries with an improved extended kalman filter.** *Scientific reports*, 11:5805, 2021.
- [31] KHAN, H. F.; HANIF, A.; ALI, M. U. ; ZAFAR, A.. **A lagrange multiplier and sigma point kalman filter based fused methodology for online state of charge estimation of lithium-ion batteries.** *Journal of Energy Storage*, 41:102843, 2021.
- [32] ZHENGXIN, J.; QIN, S.; YUJIANG, W.; HANLIN, W.; BINGZHAO, G. ; LIN, H.. **An immune genetic extended kalman particle filter approach on state of charge estimation for lithium-ion battery.** *Energy*, 230:120805, 2021.
- [33] HU, L.; HU, X.; CHE, Y.; FENG, F.; LIN, X. ; ZHANG, Z.. **Reliable state of charge estimation of battery packs using fuzzy adaptive federated filtering.** *Applied Energy*, 262:114569, 2020.
- [34] SEO, M.; SONG, Y.; KIM, J.; PAEK, S. W.; KIM, G.-H. ; KIM, S. W.. **Innovative lumped-battery model for state of charge estimation of lithium-ion batteries under various ambient temperatures.** *Energy*, 226:120301, 2021.
- [35] LING, L.; WEI, Y.. **State-of-charge and state-of-health estimation for lithium-ion batteries based on dual fractional-order extended kalman filter and online parameter identification.** *IEEE Access*, 9:47588–47602, 2021.
- [36] ZHANG, Z.; JIANG, L.; ZHANG, L. ; HUANG, C.. **State-of-charge estimation of lithium-ion battery pack by using an adaptive extended kalman filter for electric vehicles.** *Journal of Energy Storage*, 37:102457, 2021.
- [37] NIAN, P.; SHUZHI, Z. ; XIONGWEN, Z.. **Co-estimation for capacity and state of charge for lithium-ion batteries using improved adaptive extended kalman filter.** *Journal of Energy Storage*, 40:102559, 2021.
- [38] BEELEN, H.; BERGVELD, H. J. ; DONKERS, M.. **Joint estimation of battery parameters and state of charge using an extended**

- kalman filter: a single-parameter tuning approach. *IEEE Transactions on Control Systems Technology*, 29(3):1087, 2021.
- [39] ZHU, R.; DUAN, B.; ZHANG, J.; ZHANG, Q. ; ZHANG, C.. **Co-estimation of model parameters and state-of-charge for lithium-ion batteries with recursive restricted total least squares and unscented kalman filter.** *Applied Energy*, 277:115494, 2020.
- [40] ZHU, Q.; XU, M.; LIU, W. ; ZHENG, M.. **A state of charge estimation method for lithium-ion batteries based on fractional order adaptive extended kalman filter.** *Energy*, 187:115880, 2019.
- [41] LINGHU, J.; KANG, L.; LIU, M.; LUO, X.; FENG, Y. ; LU, C.. **Estimation for state-of-charge of lithium-ion battery based on an adaptive high-degree cubature kalman filter.** *Energy*, 189:116204, 2019.
- [42] ALESSANDRI, A.; BAGLIETTO, M.; BATTISTELLI, G. ; GAGGERO, M.. **Moving-horizon state estimation for nonlinear systems using neural networks.** *IEEE Transactions on Neural Networks*, 22(5):768–780, 2011.
- [43] GRÜNE, L.; PANNEK, J.. **Nonlinear model predictive control.** In: *NONLINEAR MODEL PREDICTIVE CONTROL*, p. 45–69. Springer, 2017.
- [44] ATAEI, M.; KHAJEPOUR, A. ; JEON, S.. **Model predictive control for integrated lateral stability, traction/braking control, and rollover prevention of electric vehicles.** *Vehicle System Dynamics*, 58(1):49–73, 2020.
- [45] YUAN, L.; ZHAO, H.; CHEN, H. ; REN, B.. **Nonlinear mpc-based slip control for electric vehicles with vehicle safety constraints.** *Mechatronics*, 38:1–15, 2016.
- [46] GUO, H.; LIU, J.; CAO, D.; CHEN, H.; YU, R. ; LV, C.. **Dual-envelop-oriented moving horizon path tracking control for fully automated vehicles.** *Mechatronics*, 50:422–433, 2018.
- [47] CUI, Q.; DING, R.; WEI, C. ; ZHOU, B.. **Path-tracking and lateral stabilisation for autonomous vehicles by using the steering angle envelope.** *Vehicle System Dynamics*, 59(11):1672–1696, 2021.
- [48] CHENG, S.; LI, L.; GUO, H.-Q.; CHEN, Z.-G. ; SONG, P.. **Longitudinal collision avoidance and lateral stability adaptive control system**

- based on mpc of autonomous vehicles. *IEEE Transactions on Intelligent Transportation Systems*, 21:2376–2385, 2020.
- [49] CAO, H.; ZHAO, S.; SONG, X.; BAO, S.; LI, M.; HUANG, Z. ; HU, C.. **An optimal hierarchical framework of the trajectory following by convex optimisation for highly automated driving vehicles.** *Vehicle System Dynamics*, 57(9):1287–1317, 2019.
- [50] NOVI, T.; LINIGER, A.; CAPITANI, R. ; ANNICCHIARICO, C.. **Real-time control for at-limit handling driving on a predefined path.** *Vehicle System Dynamics*, 58(7):1007–1036, 2020.
- [51] PRITCHARD, J.. **Overview of landing gear dynamics.** *Journal of aircraft*, 38(1):130–137, 2001.
- [52] KRÜGER, W.; BESSELINK, I.; COWLING, D.; DOAN, D.; KORTÜM, W. ; KRABACHER, W.. **Aircraft landing gear dynamics: simulation and control.** *Vehicle System Dynamics*, 28(2-3):119–158, 1997.
- [53] SINOUE, J.-J.; DEREURE, O.; MAZET, G.-B.; THOUVEREZ, F. ; JEZEQUEL, L.. **Friction-induced vibration for an aircraft brake system - part 1: experimental approach and stability analysis.** *International Journal of Mechanical Sciences*, 48(5):536–554, 2006.
- [54] LUO, H.-T.; ZHAO, J.-S.. **Synthesis and kinematics of a double-lock overconstrained landing gear mechanism.** *Mechanism and Machine Theory*, 121:245–258, 2018.
- [55] VAN SLAGMAAT, M.. **Tire models in aircraft landing gear simulation.** *Vehicle System Dynamics*, 21(S1):108–115, 1992.
- [56] YADAV, D.; SINGH, C.. **Landing response of aircraft with optimal anti-skid braking.** *Journal of Sound and Vibration*, 181(3):401–416, 1995.
- [57] GUALDI, S.; MORANDINI, M. ; GHIRINGHELLI, G. L.. **Anti-skid induced aircraft landing gear instability.** *Aerospace Science and Technology*, 12(8):627–637, 2008.
- [58] D'AVICO, L.; TANELLI, M.; SAVARESI, S.; AIROLDI, M. ; RAPICANO, G.. **A deceleration-based algorithm for anti-skid control of aircraft.** *IFAC-PapersOnLine*, 50(1):14168–14173, 2017.

- [59] D'AVICO, L.; TANELLI, M. ; SAVARESI, S.. **Experimental validation of landing-gear dynamics for anti-skid control design.** In: 2018 EUROPEAN CONTROL CONFERENCE (ECC), p. 2751–2756, Limassol, Cyprus, 2018. IEEE.
- [60] YIN, Q.; JIANG, J. Z.; NEILD, S. A. ; NIE, H.. **Investigation of gear walk suppression while maintaining braking performance in a main landing gear.** *Aerospace Science and Technology*, 91:122–135, 2019.
- [61] JIAO, Z.; SUN, D.; SHANG, Y.; LIU, X. ; WU, S.. **A high efficiency aircraft anti-skid brake control with runway identification.** *Aerospace Science and Technology*, 91:82–95, 2019.
- [62] CHEN, M. Q.; LIU, W. S.; MA, Y. Z.; WANG, J.; XU, F. R. ; WANG, Y. J.. **Mixed slip-deceleration pid control of aircraft wheel braking system.** *IFAC-PapersOnLine*, 51(4):160–165, 2018.
- [63] TOURAJIZADEH, H.; ZARE, S.. **Robust and optimal control of shimmy vibration in aircraft nose landing gear.** *Aerospace Science and Technology*, 50:1–14, 2016.
- [64] SOMAKUMAR, R.; CHANDRASEKHAR, J.. **Intelligent anti-skid brake controller using a neural network.** *Control Engineering Practice*, 7(5):611–621, 1999.
- [65] WANG, H.; WU, D.; WANG, F. ; REN, H.. **A method for determining the horizontal impact load based on the rotational speed of the aircraft's wheel in a landing gear drop test.** *International Journal of Crashworthiness*, 23(6):627–634, 2018.
- [66] XUE, C.; WANG, Y.; SUN, B. ; XU, F.. **Optimization of the cushion properties of amphibious aircraft landing gear by simulation and drop test.** *Journal of Vibration and Control*, 19(11):1753–1760, 2013.
- [67] SHIXING, Z.; PENG, W. ; JING, T.. **Experimental research on aircraft landing gear drop test based on mrf damper.** *Procedia Engineering*, 15:4712–4717, 2011.
- [68] LI, F.; WEI, G.; QI, W. ; XINHE, X.. **Modeling and adaptive control of magneto-rheological buffer system for aircraft landing gear.** *Applied Mathematical Modelling*, 39(9):2509–2517, 2015.

- [69] WEI, X.; LIU, C.; LIU, X.; NIE, H. ; SHAO, Y.. **Improved model of landing-gear drop dynamics**. *Journal of Aircraft*, 51(2):695–700, 2014.
- [70] FALLAH, M.; LONG, S.; XIE, W. ; BHAT, R.. **Robust model predictive control of shimmy vibration in aircraft landing gears**. *Journal of Aircraft*, 45(6):1872–1880, 2008.
- [71] PYTKA, J.; JÓZWIK, J.; BUDZYŃSKI, P.; ŁYSZCZYK, T.; TOFIL, A.; GNAPOWSKI, E. ; LASKOWSKI, J.. **Wheel dynamometer system for aircraft landing gear testing**. *Measurement*, 148:106918, 2019.
- [72] BATILL, S.; BACARRO, J.. **Modeling and identification of nonlinear dynamic systems with application to aircraft landing gear**. In: 29TH STRUCTURES, STRUCTURAL DYNAMICS AND MATERIALS CONFERENCE, p. 2315, Williamsburg, VA, U.S.A, 1988.
- [73] WU, J.; WANG, J. ; YOU, Z.. **An overview of dynamic parameter identification of robots**. *Robotics and Computer-Integrated Manufacturing*, 26(5):414–419, 2010.
- [74] OLIVIERS, M.; CAMPION, G.. **Identification methodology of a robot with flexible arms**. *IFAC Proceedings Volumes*, 30(20):125–130, 1997.
- [75] DÍAZ-RODRÍGUEZ, M.; MATA, V.; VALERA, A. ; PAGE, A.. **A methodology for dynamic parameters identification of 3-dof parallel robots in terms of relevant parameters**. *Mechanism and Machine Theory*, 45(9):1337–1356, 2010.
- [76] BAHLOUL, A.; TLIBA, S. ; CHITOUR, Y.. **Dynamic parameters identification of an industrial robot with and without payload**. *Ifac-Papersonline*, 51(15):443–448, 2018.
- [77] GAO, G.; SUN, G.; NA, J.; GUO, Y. ; WU, X.. **Structural parameter identification for 6 dof industrial robots**. *Mechanical Systems and Signal Processing*, 113:145–155, 2018.
- [78] KAYACAN, E.; YOUNG, S. N.; PESCHEL, J. M. ; CHOWDHARY, G.. **High-precision control of tracked field robots in the presence of unknown traction coefficients**. *Journal of Field Robotics*, 35(7):1050–1062, 2018.
- [79] LI, L.; JIA, G.; RAN, X.; SONG, J. ; WU, K.. **A variable structure extended kalman filter for vehicle sideslip angle estimation on a low friction road**. *Vehicle System Dynamics*, 52(2):280–308, 2014.

- [80] SUN, F.; LOLENKO, K. ; RUDOLPH, J.. **Nonlinear observer design for state estimation during antilock braking**. Proceedings of the Institution of Mechanical Engineers, Part I: Journal of Systems and Control Engineering, 228(2):78–86, 2014.
- [81] BOADA, B. L.; GARCIA-POZUELO, D.; BOADA, M. J. L. ; DIAZ, V.. **A constrained dual kalman filter based on pdf truncation for estimation of vehicle parameters and road bank angle: Analysis and experimental validation**. IEEE Transactions on Intelligent Transportation Systems, 18(4):1006–1016, 2016.
- [82] NA, J.; CHEN, A. S.; HERRMANN, G.; BURKE, R. ; BRACE, C.. **Vehicle engine torque estimation via unknown input observer and adaptive parameter estimation**. IEEE Transactions on Vehicular Technology, 67(1):409–422, 2017.
- [83] JO, K.; LEE, M. ; SUNWOO, M.. **Road slope aided vehicle position estimation system based on sensor fusion of gps and automotive onboard sensors**. IEEE Transactions on Intelligent Transportation Systems, 17(1):250–263, 2015.
- [84] HSIAO, T.. **Robust estimation and control of tire traction forces**. IEEE Transactions on Vehicular Technology, 62(3):1378–1383, 2012.
- [85] NILSSON, J.; FREDRIKSSON, J. ; ÖDBLÖM, A. C.. **Reliable vehicle pose estimation using vision and a single-track model**. IEEE Transactions on Intelligent Transportation Systems, 15(6):2630–2643, 2014.
- [86] CHEN, Y.; WANG, J.. **Adaptive vehicle speed control with input injections for longitudinal motion independent road frictional condition estimation**. IEEE Transactions on Vehicular Technology, 60(3):839–848, 2011.
- [87] SINGH, K. B.; ALI ARAT, M. ; TAHERI, S.. **An intelligent tire based tire-road friction estimation technique and adaptive wheel slip controller for antilock brake system**. Journal of Dynamic Systems, Measurement, and Control, 135(3), 2013.
- [88] HSU, Y.-H. J.; LAWS, S. M. ; GERDES, J. C.. **Estimation of tire slip angle and friction limits using steering torque**. IEEE Transactions on Control Systems Technology, 18(4):896–907, 2009.
- [89] DU, H.; LAM, J.; CHEUNG, K.-C.; LI, W. ; ZHANG, N.. **Side-slip angle estimation and stability control for a vehicle with a non-linear**

- tyre model and a varying speed. Proceedings of the Institution of Mechanical Engineers, Part D: Journal of Automobile Engineering, 229(4):486–505, 2015.
- [90] LI, B.; DU, H.; LI, W. ; ZHANG, B.. **Non-linear tyre model-based non-singular terminal sliding mode observer for vehicle velocity and side-slip angle estimation.** Proceedings of the Institution of Mechanical Engineers, Part D: Journal of Automobile Engineering, 233(1):38–54, 2019.
- [91] ZHAO, L.; LIU, Z.. **Vehicle velocity and roll angle estimation with road and friction adaptation for four-wheel independent drive electric vehicle.** Mathematical Problems in Engineering, 2014, 2014.
- [92] FENG, Y.; CHEN, H.; ZHAO, H. ; ZHOU, H.. **Road tire friction coefficient estimation for four wheel drive electric vehicle based on moving optimal estimation strategy.** Mechanical Systems and Signal Processing, 139:106416, 2020.
- [93] JEON, S.-Y.; CHUNG, R. ; LEE, D.. **Tire force estimation of dynamic wheeled mobile robots using tire-model based constrained kalman filtering.** In: 2018 IEEE/RSJ INTERNATIONAL CONFERENCE ON INTELLIGENT ROBOTS AND SYSTEMS (IROS), p. 2470–2477, Madrid, Spain, 2018. IEEE.
- [94] PACEJKA, H. B.; BAKKER, E.. **The magic formula tyre model.** Vehicle System Dynamics, 21(S1):1–18, 1992.
- [95] JALALI, M.; HASHEMI, E.; KHAJEPOUR, A.; CHEN, S.-K. ; LITKOUHI, B.. **Integrated model predictive control and velocity estimation of electric vehicles.** Mechatronics, 46:84–100, 2017.
- [96] KOU, S. R.; ELLIOTT, D. L. ; TARN, T. J.. **Observability of nonlinear systems.** Information and Control, 22(1):89–99, 1973.
- [97] KATRINIOK, A.; ABEL, D.. **Adaptive ekf-based vehicle state estimation with online assessment of local observability.** IEEE Transactions on Control Systems Technology, 24(4):1368–1381, 2015.
- [98] CHEN, T.; CAI, Y.; CHEN, L.; XU, X.; JIANG, H. ; SUN, X.. **Design of vehicle running states-fused estimation strategy using kalman filters and tire force compensation method.** IEEE Access, 7:87273–87287, 2019.

- [99] LIU, Y.; FAN, X.; LV, C.; WU, J.; LI, L. ; DING, D.. **An innovative information fusion method with adaptive Kalman filter for integrated INS/GPS navigation of autonomous vehicles.** *Mechanical Systems and Signal Processing*, 100:605–616, 2018.
- [100] BOADA, M. J. L.; BOADA, B. L. ; ZHANG, H.. **Event-triggering h_∞ -based observer combined with NN for simultaneous estimation of vehicle sideslip and roll angles with network-induced delays.** *Nonlinear Dynamics*, 103(3):2733–2752, 2021.
- [101] VIEHWEGER, M.; VASEUR, C.; VAN AALST, S.; ACOSTA, M.; REGOLIN, E.; ALATORRE, A.; DESMET, W.; NAETS, F.; IVANOV, V.; FERRARA, A. ; OTHERS. **Vehicle state and tyre force estimation: demonstrations and guidelines.** *Vehicle System Dynamics*, 59(5):675–702, 2021.
- [102] REINA, G.; PAIANO, M. ; BLANCO-CLARACO, J.-L.. **Vehicle parameter estimation using a model-based estimator.** *Mechanical Systems and Signal Processing*, 87:227–241, 2017.
- [103] REINA, G.; MESSINA, A.. **Vehicle dynamics estimation via augmented extended kalman filtering.** *Measurement*, 133:383–395, 2019.
- [104] BOADA, B.; BOADA, M. ; ZHANG, H.. **Sensor fusion based on a dual kalman filter for estimation of road irregularities and vehicle mass under static and dynamic conditions.** *IEEE/ASME Transactions on Mechatronics*, 24(3):1075–1086, 2019.
- [105] KIM, D.; MIN, K.; KIM, H. ; HUH, K.. **Vehicle sideslip angle estimation using deep ensemble-based adaptive kalman filter.** *Mechanical Systems and Signal Processing*, 144:106862, 2020.
- [106] XIA, X.; XIONG, L.; LU, Y.; GAO, L. ; YU, Z.. **Vehicle sideslip angle estimation by fusing inertial measurement unit and global navigation satellite system with heading alignment.** *Mechanical Systems and Signal Processing*, 150:107290, 2021.
- [107] SHAO, L.; JIN, C.; LEX, C. ; EICHBERGER, A.. **Robust road friction estimation during vehicle steering.** *Vehicle System Dynamics*, 57(4):493–519, 2019.
- [108] LIU, Y.; JI, X.; YANG, K.; HE, X.; NA, X. ; LIU, Y.. **Finite-time optimized robust control with adaptive state estimation algorithm**

- for autonomous heavy vehicle. *Mechanical Systems and Signal Processing*, 139, 2020.
- [109] RODRIGUEZ, A.; SANJURJO, E.; PASTORINO, R. ; NAYA, M.. **State, parameter and input observers based on multibody models and kalman filters for vehicle dynamics.** *Mechanical Systems and Signal Processing*, 155, 2021.
- [110] HIRSCHBERG, W.; RILL, G. ; WEINFURTER, H.. **Tire model tmeasy.** *Vehicle System Dynamics*, 45(Sup1):101–119, 2007.
- [111] ZHANG, W.; WANG, Z.; ZOU, C.; DRUGGE, L. ; NYBACKA, M.. **Advanced vehicle state monitoring: evaluating moving horizon estimators and unscented kalman filter.** *IEEE Transactions on Vehicular Technology*, 68(6):5430–5442, 2019.
- [112] MADHUSUDHANAN, A. K.; CORNO, M.; ARAT, M. A. ; HOLWEG, E.. **Load sensing bearing based road-tyre friction estimation considering combined tyre slip.** *Mechatronics*, 39:136–146, 2016.
- [113] ALIGIA, D. A.; MAGALLAN, G. A. ; DE ANGELO, C. H.. **Ev traction control based on nonlinear observers considering longitudinal and lateral tire forces.** *IEEE Transactions on Intelligent Transportation Systems*, 19(8):2558–2571, 2018.
- [114] SHARIFZADEH, M.; SENATORE, A.; FARNAM, A.; AKBARI, A. ; TIMPONE, F.. **A real-time approach to robust identification of tyre–road friction characteristics on mixed- μ roads.** *Vehicle System Dynamics*, 57(9):1338–1362, 2019.
- [115] BONFITTO, A.; FERACO, S.; TONOLI, A. ; AMATI, N.. **Combined regression and classification artificial neural networks for sideslip angle estimation and road condition identification.** *Vehicle System Dynamics*, 58(11):1766–1787, 2020.
- [116] BEAL, C. E.. **Rapid road friction estimation using independent left/right steering torque measurements.** *Vehicle System Dynamics*, 58(3):377–403, 2020.
- [117] TRAN, M.-K.; DACOSTA, A.; MEVAWALLA, A.; PANCHAL, S. ; FOWLER, M.. **Comparative study of equivalent circuit models performance in four common lithium-ion batteries: Lfp, nmc, lmo, nca.** *Batteries*, 7(3):51, 2021.

- [118] LI, X.; HUANG, Z.; TIAN, J. ; TIAN, Y.. **State-of-charge estimation tolerant of battery aging based on a physics-based model and an adaptive cubature kalman filter.** *Energy*, 220:119767, 2021.
- [119] HU, M.; LI, Y.; LI, S.; FU, C.; QIN, D. ; LI, Z.. **Lithium-ion battery modeling and parameter identification based on fractional theory.** *Energy*, 165:153–163, 2018.
- [120] PANCHAL, S.; RASHID, M.; LONG, F.; MATHEW, M.; FRASER, R. ; FOWLER, M.. **Degradation testing and modeling of 200 ah lifepo 4 battery.** Technical report, SAE Technical Paper, 2018.
- [121] TRAN, M.-K.; PANCHAL, S.; CHAUHAN, V.; BRAHMBHATT, N.; MEVAWALLA, A.; FRASER, R. ; FOWLER, M.. **Python-based scikit-learn machine learning models for thermal and electrical performance prediction of high-capacity lithium-ion battery.** *International Journal of Energy Research*, 46(2), 2021.
- [122] DUAN, J.; ZHAO, J.; LI, X.; PANCHAL, S.; YUAN, J.; FRASER, R. ; FOWLER, M.. **Modeling and analysis of heat dissipation for liquid cooling lithium-ion batteries.** *Energies*, 14(14):4187, 2021.
- [123] ZHANG, C.; ALLAFI, W.; DINH, Q.; ASCENCIO, P. ; MARCO, J.. **Online estimation of battery equivalent circuit model parameters and state of charge using decoupled least squares technique.** *Energy*, 142:678–688, 2018.
- [124] HOU, J.; YANG, Y. ; GAO, T.. **A variational bayes based state-of-charge estimation for lithium-ion batteries without sensing current.** *IEEE Access*, 9, 2021.
- [125] FAN, Y.; SHI, H.; WANG, S.; FERNANDEZ, C.; CAO, W. ; HUANG, J.. **A novel adaptive function—dual kalman filtering strategy for online battery model parameters and state of charge co-estimation.** *Energies*, 14:2268, 2021.
- [126] LI, X.; XU, J.; HONG, J.; TIAN, J. ; TIAN, Y.. **State of energy estimation for a series-connected lithium-ion battery pack based on an adaptive weighted strategy.** *Energy*, 214:118858, 2021.
- [127] LIU, X.; LI, K.; WU, J.; HE, Y. ; LIU, X.. **An extended kalman filter based data-driven method for state of charge estimation of lithium batteries.** *Journal of Energy Storage*, 40:102655, 2021.

- [128] YU, M. J.; BERNSTEIN, D. S.. **Combined state and parameter estimation and identifiability of state space realizations**. In: 2016 IEEE 55TH CONFERENCE ON DECISION AND CONTROL (CDC), p. 3054–3059, Las Vegas, NV, USA, 2016. IEEE.
- [129] BACKI, C. J.; GRAVDAHL, J. T. ; SKOGESTAD, S.. **Combined state and parameter estimation for not fully observable dynamic systems**. IFAC Journal of Systems and Control, 13:100103, 2020.
- [130] SUN, D.; YU, X.; WANG, C.; ZHANG, C.; HUANG, R.; ZHOU, Q.; AMIETSAJEW, T. ; BHAGAT, R.. **State of charge estimation for lithium-ion battery based on an intelligent adaptive extended kalman filter with improved noise estimator**. Energy, 214:119025, 2021.
- [131] BOLE, B.; KULKARNI, C. S. ; DAIGLE, M.. **Randomized battery usage data set**. Dataset, NASA Ames Research Center, Moffett Field, United States, 2014.
- [132] HU, L.; HU, X.; CHE, Y.; FENG, F.; LIN, X. ; ZHANG, Z.. **Reliable state of charge estimation of battery packs using fuzzy adaptive federated filtering**. Applied Energy, 262:114569, 2020.
- [133] BABAEIYAZDI, I.; REZAEI-ZARE, A. ; SHOKRZADEH, S.. **State of charge prediction of ev li-ion batteries using eis: A machine learning approach**. Energy, 223:120116, 2021.
- [134] XIONG, W.; MO, Y. ; YAN, C.. **Online state-of-health estimation for second-use lithium-ion batteries based on weighted least squares support vector machine**. IEEE Access, 9:1870–1881, 2020.
- [135] OUYANG, T.; XU, P.; CHEN, J.; LU, J. ; CHEN, N.. **An online prediction of capacity and remaining useful life of lithium-ion batteries based on simultaneous input and state estimation algorithm**. IEEE Transactions on Power Electronics, 36(7):8102, 2021.
- [136] YE, M.; GUO, H.; XIONG, R. ; YU, Q.. **A double-scale and adaptive particle filter-based online parameter and state of charge estimation method for lithium-ion batteries**. Energy, 144:789–799, 2018.
- [137] HUANG, C.-S.; CHOW, M.-Y.. **Robust state-of-charge estimation for lithium-ion batteries over full soc range**. IEEE Journal of Emerging and Selected Topics in Industrial Electronics, 2(3):305–313, 2021.

- [138] KIM, W.-Y.; LEE, P.-Y.; KIM, J. ; KIM, K.-S.. A robust state of charge estimation approach based on nonlinear battery cell model for lithium-ion batteries in electric vehicles. *IEEE Transactions on Vehicular Technology*, 70(6):5638–5647, 2021.
- [139] OUYANG, T.; XU, P.; CHEN, J.; SU, Z.; HUANG, G. ; CHEN, N.. A novel state of charge estimation method for lithium-ion batteries based on bias compensation. *Energy*, 226:120348, 2021.
- [140] CHEN, J.; FENG, X.; JIANG, L. ; ZHU, Q.. State of charge estimation of lithium-ion battery using denoising autoencoder and gated recurrent unit recurrent neural network. *Energy*, 227:120451, 2021.
- [141] YANG, F.; ZHANG, S.; LI, W. ; MIAO, Q.. State-of-charge estimation of lithium-ion batteries using lstm and ukf. *Energy*, 201:117664, 2020.
- [142] BIAN, C.; HE, H. ; YANG, S.. Stacked bidirectional long short-term memory networks for state-of-charge estimation of lithium-ion batteries. *Energy*, 191:116538, 2020.
- [143] ZHANG, Z.; DONG, Z.; LIN, H.; HE, Z.; WANG, M.; HE, Y.; GAO, X. ; GAO, M.. An improved bidirectional gated recurrent unit method for accurate state-of-charge estimation. *IEEE Access*, 9:11252–11263, 2021.
- [144] CHEN, Z.; ZHAO, H.; SHU, X.; ZHANG, Y.; SHEN, J. ; LIU, Y.. Synthetic state of charge estimation for lithium-ion batteries based on long short-term memory network modeling and adaptive h-infinity filter. *Energy*, 228:120630, 2021.
- [145] XIA, B.; CUI, D.; SUN, Z.; LAO, Z.; ZHANG, R.; WANG, W.; SUN, W.; LAI, Y. ; WANG, M.. State of charge estimation of lithium-ion batteries using optimized levenberg-marquardt wavelet neural network. *Energy*, 153:694–705, 2018.
- [146] WANG, Q.; GU, H.; YE, M.; WEI, M. ; XU, X.. State of charge estimation for lithium-ion battery based on narx recurrent neural network and moving window method. *IEEE Access*, 9:83364, 2021.
- [147] WEI, Z.; HU, J.; HE, H.; LI, Y. ; XIONG, B.. Load current and state-of-charge co-estimation for current sensor-free lithium-

- ion battery. *IEEE Transactions on Power Electronics*, 36(10):10970–10975, 2021.
- [148] ZHANG, Z.; XUE, B. ; FAN, J.. **Noise adaptive moving horizon estimation for state-of-charge estimation of li-ion battery.** *IEEE Access*, 9:5250–5259, 2020.
- [149] CHEN, Y.; LI, C.; CHEN, S.; REN, H. ; GAO, Z.. **A combined robust approach based on auto-regressive long short-term memory network and moving horizon estimation for state-of-charge estimation of lithium-ion batteries.** *International Journal of Energy Research*, 45(9):12838–12853, 2021.
- [150] PAN, H.; LÜ, Z.; LIN, W.; LI, J. ; CHEN, L.. **State of charge estimation of lithium-ion batteries using a grey extended kalman filter and a novel open-circuit voltage model.** *Energy*, 138:764–775, 2017.
- [151] ZHENG, L.; ZHU, J.; WANG, G.; LU, D. D.-C. ; HE, T.. **Differential voltage analysis based state of charge estimation methods for lithium-ion batteries using extended kalman filter and particle filter.** *Energy*, 158:1028–1037, 2018.
- [152] CASS, S.. **Nvidia makes it easy to embed ai: The jetson nano packs a lot of machine-learning power into diy projects-[hands on].** *IEEE Spectrum*, 57(7):14–16, 2020.
- [153] AL-GABALAWY, M.; HOSNY, N. S. ; ABDEL-HAMID, S. A.. **Model predictive control for a basic adaptive cruise control.** *International Journal of Dynamics and Control*, 9:1132—1143, 2021.
- [154] BAKIBILLAH, A.; KAMAL, M. A. S.; TAN, C. P.; HAYAKAWA, T. ; IMURA, J.-I.. **Fuzzy-tuned model predictive control for dynamic eco-driving on hilly roads.** *Applied Soft Computing*, 99:106875, 2021.
- [155] WALZ, F.; HOHMANN, S.. **Model predictive longitudinal motion control for low velocities on known road profiles.** *Vehicle System Dynamics*, 58(8):1310–1328, 2020.
- [156] SUN, X.; WU, P.; CAI, Y.; WANG, S. ; CHEN, L.. **Piecewise affine modeling and hybrid optimal control of intelligent vehicle longitudinal dynamics for velocity regulation.** *Mechanical Systems and Signal Processing*, 162:108089, 2022.

- [157] SUNUSI, I. I.; ZHOU, J.; SUN, C.; WANG, Z.; ZHAO, J. ; WU, Y.. **Development of online adaptive traction control for electric robotic tractors.** *Energies*, 14(12):3394, 2021.
- [158] WANG, Q.; ZHAO, Y.; LIN, F.; ZHANG, C. ; DENG, H.. **Integrated control for distributed in-wheel motor drive electric vehicle based on states estimation and nonlinear mpc.** *Proceedings of the Institution of Mechanical Engineers, Part D: Journal of Automobile Engineering*, 236(5):893–906, 2021.
- [159] LI, S. E.; CHEN, H.; LI, R.; LIU, Z.; WANG, Z. ; XIN, Z.. **Predictive lateral control to stabilise highly automated vehicles at tire-road friction limits.** *Vehicle System Dynamics*, 58(5):768–786, 2020.
- [160] BERNTORP, K.; QUIRYNEN, R.; UNO, T. ; DI CAIRANO, S.. **Trajectory tracking for autonomous vehicles on varying road surfaces by friction-adaptive nonlinear model predictive control.** *Vehicle System Dynamics*, 58(5):705–725, 2020.
- [161] JALALI, M.; HASHEMI, E.; KHAJEPOUR, A.; CHEN, S.-K. ; LITKOUHI, B.. **A combined-slip predictive control of vehicle stability with experimental verification.** *Vehicle System Dynamics*, 56(2):319–340, 2018.
- [162] BASRAH, M. S.; SIAMPIS, E.; VELENIS, E.; CAO, D. ; LONGO, S.. **Wheel slip control with torque blending using linear and nonlinear model predictive control.** *Vehicle System Dynamics*, 55(11):1665–1685, 2017.
- [163] LIU, J.; JAYAKUMAR, P.; STEIN, J. L. ; ERSAL, T.. **A study on model fidelity for model predictive control-based obstacle avoidance in high-speed autonomous ground vehicles.** *Vehicle System Dynamics*, 54(11):1629–1650, 2016.
- [164] LIU, J.; JAYAKUMAR, P.; STEIN, J. L. ; ERSAL, T.. **A nonlinear model predictive control formulation for obstacle avoidance in high-speed autonomous ground vehicles in unstructured environments.** *Vehicle System Dynamics*, 56(6):853–882, 2018.
- [165] YUAN, H.; SUN, X. ; GORDON, T.. **Unified decision-making and control for highway collision avoidance using active front steer and individual wheel torque control.** *Vehicle System Dynamics*, 57(8):1188–1205, 2019.

- [166] ATTIA, R.; ORJUELA, R. ; BASSET, M.. **Nonlinear cascade strategy for longitudinal control in automated vehicle guidance**. *Control Engineering Practice*, 29:225–234, 2014.
- [167] CHENG, S.; MEI, M.-M.; GUO, S.-Y.; LI, L.; LIU, C.-Z.; CHEN, X. ; WU, X.-H.. **A novel coupling strategy for automated vehicle's longitudinal dynamic stability**. *Proceedings of the Institution of Mechanical Engineers, Part D: Journal of Automobile Engineering*, 235(10-11):2753–2763, 2021.
- [168] NGUYEN, B.-M.; TROVAO, J. P. F.; TA, M. C. ; KAWANISHI, M.. **Longitudinal motion control of electric vehicles: Glocal model and design using passivity**. *IEEE Vehicular Technology Magazine*, 16(3):75–86, 2021.
- [169] ZHU, J.; WANG, Z.; ZHANG, L. ; DORRELL, D. G.. **Braking/steering coordination control for in-wheel motor drive electric vehicles based on nonlinear model predictive control**. *Mechanism and Machine Theory*, 142:103586, 2019.
- [170] REN, B.; CHEN, H.; ZHAO, H. ; YUAN, L.. **Mpc-based yaw stability control in in-wheel-motored ev via active front steering and motor torque distribution**. *Mechatronics*, 38:103–114, 2016.
- [171] JAZAR, R. N.. **Vehicle dynamics: theory and application**. Springer, Cham, Switzerland, 2017.
- [172] LOPES, E. D. R.; PINTO, A. F. A.; VALENTIM, M. X. G.; PEIXOTO, P. S. ; NETO, R. T. D. C.. **Extended model for calculation of soil-wheel contact area parameters in rigid soil-deformable tyre approximation**. *International Journal of Vehicle Systems Modelling and Testing*, 13(4):358–372, 2019.
- [173] SAVARESI, S. M.; TANELLI, M.; CANTONI, C.; CHARALAMBAKIS, D.; PREVIDI, F. ; BITTANTI, S.. **Slip-deceleration control in anti-lock braking systems**. *IFAC Proceedings Volumes*, 38(1):103–108, 2005.
- [174] PACEJKA, H.. **Tire and vehicle dynamics**. Elsevier, Oxford, 2006.
- [175] CHANG, W.-Y.. **The state of charge estimating methods for battery: A review**. *International Scholarly Research Notices*, 2013, 2013.
- [176] ZHENG, F.; XING, Y.; JIANG, J.; SUN, B.; KIM, J. ; PECHT, M.. **Influence of different open circuit voltage tests on state of**

- charge online estimation for lithium-ion batteries. *Applied Energy*, 183:513–525, 2016.
- [177] HARIFI, A.; AGHAGOLZADEH, A.; ALIZADEH, G. ; SADEGHI, M.. **Designing a sliding mode controller for slip control of antilock brake systems**. *Transportation Research Part C: Emerging Technologies*, 16(6):731–741, 2008.
- [178] SÖDERSTRÖM, T.; STOICA, P.. **System identification**. Prentice-Hall International, Hemel Hempstead, 1989.
- [179] BILLINGS, S. A.. **Nonlinear system identification: NARMAX methods in the time, frequency, and spatio-temporal domains**. John Wiley & Sons, West Sussex, United Kingdom, 2013.
- [180] HANBA, S.. **On the “uniform” observability of discrete-time nonlinear systems**. *IEEE Transactions on Automatic Control*, 54(8):1925–1928, 2009.
- [181] ANDERSSON, J. A.; GILLIS, J.; HORN, G.; RAWLINGS, J. B. ; DIEHL, M.. **Casadi: a software framework for nonlinear optimization and optimal control**. *Mathematical Programming Computation*, 11(1):1–36, 2019.
- [182] ALESSIO, A.; BEMPORAD, A.. **A survey on explicit model predictive control**. In: *NONLINEAR MODEL PREDICTIVE CONTROL*, p. 345–369. Springer, 2009.
- [183] RAWLINGS, J. B.; MAYNE, D. Q. ; DIEHL, M.. **Model predictive control: theory, computation, and design**. Nob Hill Publishing Madison, WI, Santa Barbara, California, 2 edition, 2017.
- [184] BEMPORAD, A.; MORARI, M. ; RICKER, N. L.. **Model predictive control toolbox user’s guide**. The mathworks, 2010.
- [185] NOCEDAL, J.; WRIGHT, S. J.. **Numerical optimization**. Springer, New York, NY, 2006.
- [186] RAHMANI, M.; BEHDINAN, K.. **Interaction of torque link freeplay and coulomb friction nonlinearities in nose landing gear shimmy scenarios**. *International Journal of Non-Linear Mechanics*, 119:103338, 2020.

- [187] RAHMANI, M.; BEHDINAN, K.. **On the effectiveness of shimmy dampers in stabilizing nose landing gears.** *Aerospace Science and Technology*, 91:272–286, 2019.
- [188] KARNOPP, D. C.; MARGOLIS, D. L. ; ROSENBERG, R. C.. **System dynamics: modeling, simulation, and control of mechatronic systems.** John Wiley & Sons, Hoboken, New Jersey, 2012.
- [189] GREWAL, M.; GLOVER, K.. **Identifiability of linear and nonlinear dynamical systems.** *IEEE Transactions on Automatic Control*, 21(6):833–837, 1976.
- [190] BEAL, C. E.; BRENNAN, S.. **Modeling and friction estimation for automotive steering torque at very low speeds.** *Vehicle System Dynamics*, 59(3):458–484, 2021.
- [191] BEAL, C. E.; BOYD, C.. **Coupled lateral-longitudinal vehicle dynamics and control design with three-dimensional state portraits.** *Vehicle System Dynamics*, 57(2):286–313, 2019.
- [192] BOLE, B.; KULKARNI, C. S. ; DAIGLE, M.. **Adaptation of an electrochemistry-based li-ion battery model to account for deterioration observed under randomized use.** In: ANNUAL CONFERENCE OF THE PROGNOSTICS AND HEALTH MANAGEMENT SOCIETY, p. 502–510, Fort Worth, Texas, 2014.
- [193] SAHA, B.; GOEBEL, K.; POLL, S. ; CHRISTOPHERSEN, J.. **Prognostics methods for battery health monitoring using a bayesian framework.** *IEEE Transactions on Instrumentation and Measurement*, 58(2):291–296, 2008.
- [194] STELLATO, B.; GEYER, T. ; GOULART, P. J.. **High-speed finite control set model predictive control for power electronics.** *IEEE Transactions on Power Electronics*, 32(5):4007–4020, 2017.
- [195] AYALA, H. V. H.; MUÑOZ, D. M.; LLANOS, C. H. ; DOS SANTOS COELHO, L.. **Efficient hardware implementation of radial basis function neural network with customized-precision floating-point operations.** *Control Engineering Practice*, 60:124–132, 2017.
- [196] BALDEON CALISTO, M.; LAI-YUEN, S. K.. **Adaen-net: An ensemble of adaptive 2d–3d fully convolutional networks for medical image segmentation.** *Neural Networks*, 126:76–94, 2020.

- [197] TABANI, H.; MAZZOCCHETTI, F.; BENEDICTE, P.; ABELLA, J. ; CAZORLA, F. J.. **Performance analysis and optimization opportunities for nvidia automotive gpus.** *Journal of Parallel and Distributed Computing*, 152:21–32, 2021.
- [198] MATHWORKS STUDENT COMPETITIONS TEAM. **Analyzing tire test data.** Dataset, MATLAB Central File Exchange, 2021.
- [199] INTERNATIONAL ORGANIZATION FOR STANDARDIZATION. **Passenger cars – test track for a severe lane-change manoeuvre – part 1: Double lane-change.** Standard ISO 3888-1:2018, Geneva, Switzerland, 2018.
- [200] WEI, H.; AI, Q.; ZHAO, W. ; ZHANG, Y.. **Modelling and experimental validation of an ev torque distribution strategy towards active safety and energy efficiency.** *Energy*, 239:121953, 2022.
- [201] WANG, J.; GAO, S.; WANG, K.; WANG, Y. ; WANG, Q.. **Wheel torque distribution optimization of four-wheel independent-drive electric vehicle for energy efficient driving.** *Control Engineering Practice*, 110:104779, 2021.
- [202] ABDOLLAHPOURI, M.; TAKÁCS, G. ; ROHAL'-ILKIV, B.. **Real-time moving horizon estimation for a vibrating active cantilever.** *Mechanical Systems and Signal Processing*, 86:1–15, 2017.
- [203] ABADI, M.; BARHAM, P.; CHEN, J.; CHEN, Z.; DAVIS, A.; DEAN, J.; DEVIN, M.; GHEMAWAT, S.; IRVING, G.; ISARD, M.; KUDLUR, M.; LEVENBERG, J.; MONGA, R.; MOORE, S.; MURRAY, D. G.; STEINER, B.; TUCKER, P.; VASUDEVAN, V.; WARDEN, P.; WICKE, M.; YU, Y. ; ZHENG, X.. **TensorFlow: A system for large-scale machine learning**, 2016.
- [204] MITTAL, S.. **A survey on optimized implementation of deep learning models on the nvidia jetson platform.** *Journal of Systems Architecture*, 97:428–442, 2019.
- [205] LOQUERCIO, A.; KAUFMANN, E.; RANFTL, R.; MÜLLER, M.; KOLTUN, V. ; SCARAMUZZA, D.. **Learning high-speed flight in the wild.** *Science Robotics*, 6(59), 2021.
- [206] WEI, H.; FAN, L.; AI, Q.; ZHAO, W.; HUANG, T. ; ZHANG, Y.. **Optimal energy allocation strategy for electric vehicles based on the**

real-time model predictive control technology. Sustainable Energy Technologies and Assessments, 50:101797, 2022.